US010672113B2

(12) **United States Patent**
Patriarche

(10) **Patent No.: US 10,672,113 B2**
(45) **Date of Patent: Jun. 2, 2020**

(54) **METHODS AND SYSTEMS FOR NORMALIZING IMAGES**

(71) Applicant: **AI ANALYSIS, INC.**, Bellevue, WA (US)

(72) Inventor: **Julia Patriarche**, Bellevue, WA (US)

(73) Assignee: **AI Analysis, Inc.**, Bellevue, WA (US)

(*) Notice: Subject to any disclaimer, the term of this patent is extended or adjusted under 35 U.S.C. 154(b) by 0 days.

(21) Appl. No.: **16/251,412**

(22) Filed: **Jan. 18, 2019**

(65) **Prior Publication Data**

US 2019/0156470 A1 May 23, 2019

Related U.S. Application Data

(62) Division of application No. 15/347,681, filed on Nov. 9, 2016, now Pat. No. 10,192,295.

(51) **Int. Cl.**

G06T 5/00	(2006.01)
G06T 5/50	(2006.01)
G06T 7/00	(2017.01)

(52) **U.S. Cl.**

CPC ***G06T 5/009*** (2013.01); ***G06T 5/008*** (2013.01); ***G06T 5/50*** (2013.01); ***G06T 7/97*** (2017.01); *G06T 2207/10024* (2013.01); *G06T 2207/20008* (2013.01); *G06T 2207/20012* (2013.01)

(58) **Field of Classification Search**

CPC G06T 5/008; G06T 5/007; G06T 5/50; G06T 5/009; G06T 7/0022; G06T 7/97; G06T 2207/20008; G06T 2207/20012; G06T 2207/20208; G06T 2207/20228; H04N 19/176; H04N 19/186; H04N 19/157

See application file for complete search history.

(56) **References Cited**

U.S. PATENT DOCUMENTS

8,873,812	B2 *	10/2014	Larlus-Larrondo	G06K 9/00 382/103
8,934,697	B2 *	1/2015	Wiemker	G06T 11/60 382/132
9,025,880	B2 *	5/2015	Perazzi	H04N 19/117 382/190
9,218,651	B2 *	12/2015	Zhao	H04N 1/6027
9,691,140	B2 *	6/2017	Seshadrinathan	G06T 5/50
10,235,344	B2 *	3/2019	Moutafis	G06F 17/17

(Continued)

Primary Examiner — Michael S Osinski

(74) *Attorney, Agent, or Firm* — Olympic Patent Works PLLC

(57) **ABSTRACT**

The current document is directed to digital-image-normalization methods and systems that generate accurate intensity mappings between the intensities in two digital images. The intensity mapping generated from two digital images is used to normalize or adjust the intensities in one image in order to produce a pair of normalized digital images to which various types of change-detection methodologies can be applied in order to extract differential data. In one approach, a mapping model is selected to provide a basis for statistically meaningful intensity normalization. In this implementation, a genetic optimization approach is used to determine and refine model parameters. The implementation produces a hybrid intensity mapping that includes both intensity mappings calculated by application of the mapping model and intensity mappings obtained directly from comparison of the images.

6 Claims, 49 Drawing Sheets

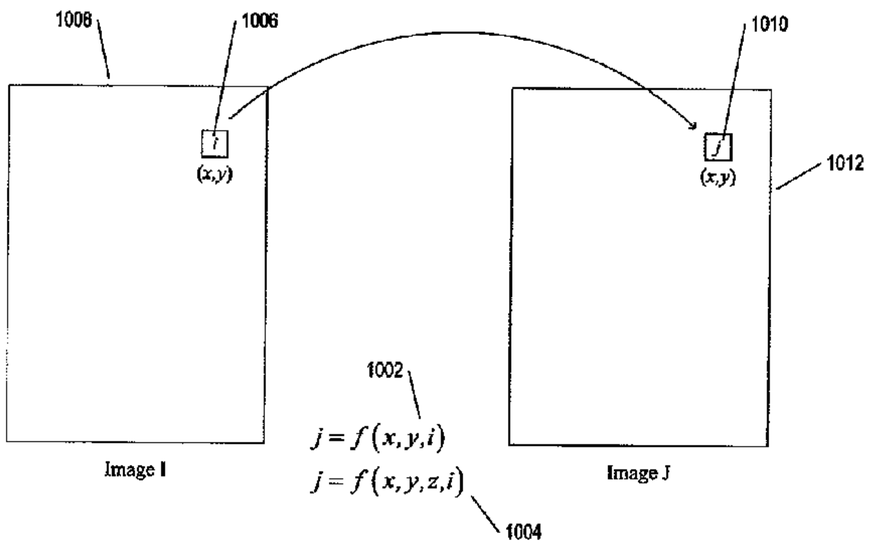

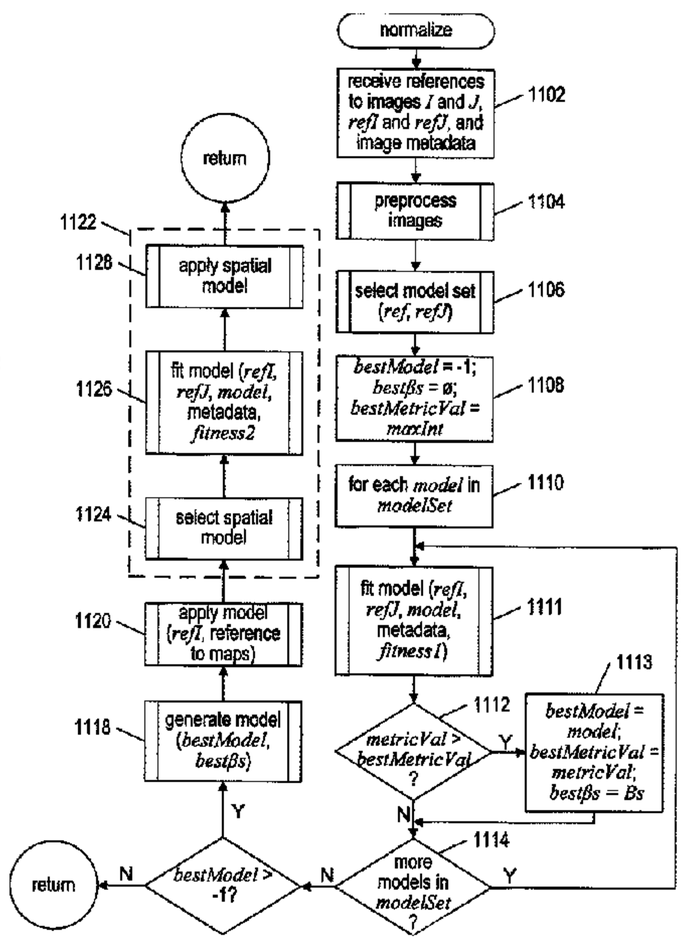

(56) **References Cited**

U.S. PATENT DOCUMENTS

10,375,534	B2 *	8/2019	Rezvani	H04W 4/14
2004/0208396	A1 *	10/2004	Gunther	G01C 11/04 382/294
2006/0004275	A1 *	1/2006	Vija	A61B 6/00 600/407
2008/0131016	A1 *	6/2008	Kokemohr	G06T 5/009 382/254
2010/0158332	A1 *	6/2010	Rico	A61B 5/4312 382/128
2010/0189363	A1 *	7/2010	Riley	G06T 5/50 382/209
2011/0292246	A1 *	12/2011	Brunner	G06T 5/009 348/231.99
2012/0327243	A1 *	12/2012	Rezvani	H04N 7/12 348/158
2013/0287296	A1 *	10/2013	Li	H04N 5/2355 382/167
2015/0117791	A1 *	4/2015	Mertens	H04N 19/17 382/239
2015/0248746	A1 *	9/2015	Bordes	G06T 5/40 382/170
2016/0055634	A1 *	2/2016	Bystrov	G06T 5/50 382/128
2016/0117975	A1 *	4/2016	Kang	G09G 3/2003 345/694
2016/0127616	A1 *	5/2016	Seshadrinathan	G06T 5/50 348/241
2016/0381363	A1 *	12/2016	Tao	G06T 5/009 375/240.03
2017/0078706	A1 *	3/2017	Van Der Vleuten	G06T 5/009
2017/0163999	A1 *	6/2017	Li	H04N 19/105
2017/0302936	A1 *	10/2017	Li	H04N 19/142
2017/0330529	A1 *	11/2017	Van Mourik	H04N 19/85
2017/0345130	A1 *	11/2017	Wang	G06T 3/4046
2018/0082454	A1 *	3/2018	Sahu	G06T 7/90
2019/0043176	A1 *	2/2019	Li	G06T 5/40
2019/0080441	A1 *	3/2019	Guo	G06T 5/40
2019/0208173	A1 *	7/2019	Kadu	G06T 5/009
2019/0281201	A1 *	9/2019	Stauder	H04N 5/235

* cited by examiner

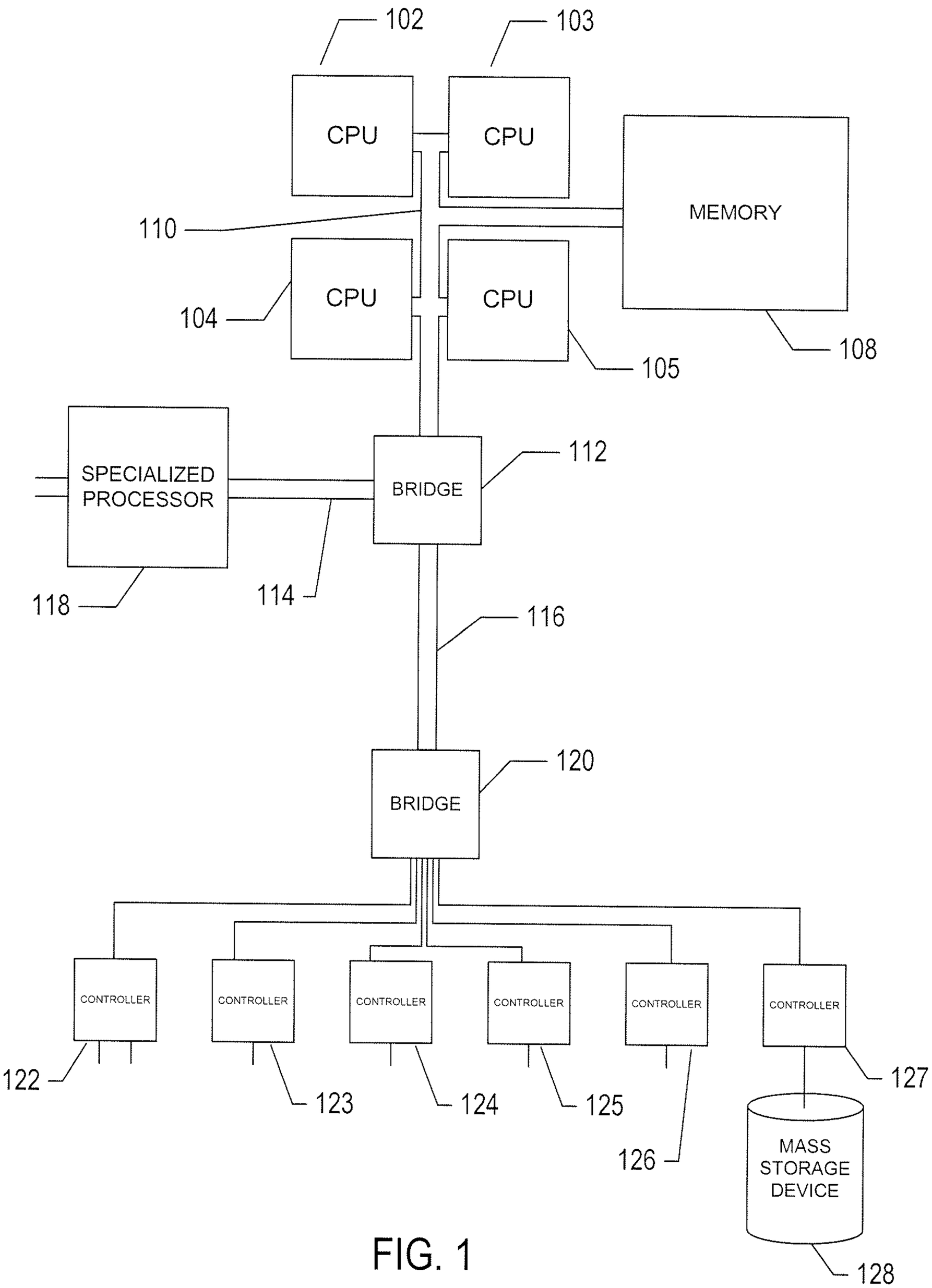
102
103
CPU
CPU
MEMORY
110
CPU
CPU
104
108
105
SPECIALIZED PROCESSOR
BRIDGE
112
118
114
116
BRIDGE
120
CONTROLLER
CONTROLLER
CONTROLLER
CONTROLLER
CONTROLLER
CONTROLLER
122
123
124
125
126
127
MASS STORAGE DEVICE
128

FIG. 1

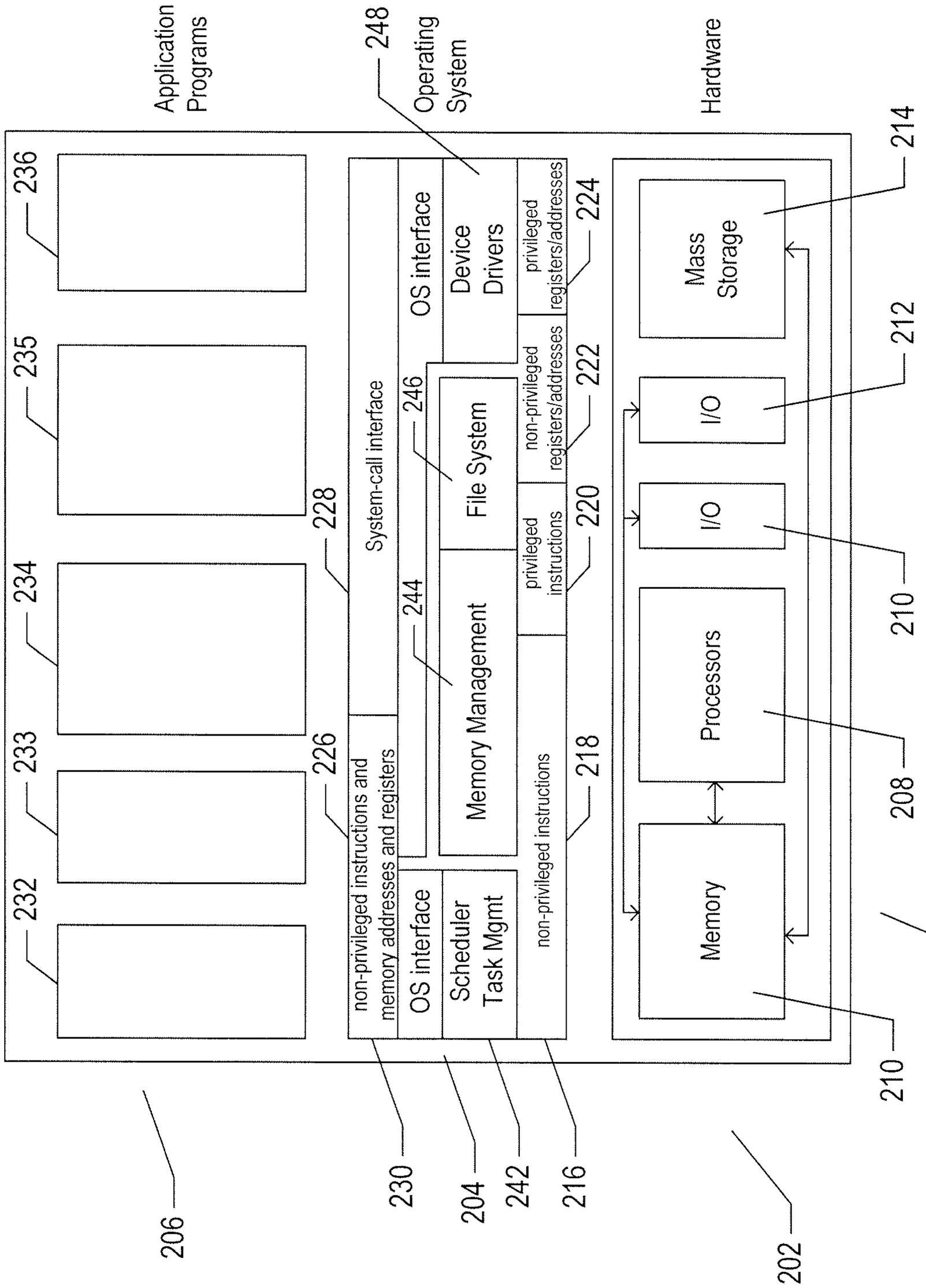
Application Programs
Operating System
Hardware
236
235
234
233
232
228
226
System-call interface
OS interface
Device Drivers
privileged registers/addresses
224
non-privileged registers/addresses
222
privileged instructions
220
non-privileged instructions and memory addresses and registers
218
246
244
File System
Memory Management
OS interface
Scheduler Task Mgmt
non-privileged instructions
Mass Storage
214
I/O
212
I/O
210
Processors
208
Memory
210
206
230
204
242
216
202
200

FIG. 2

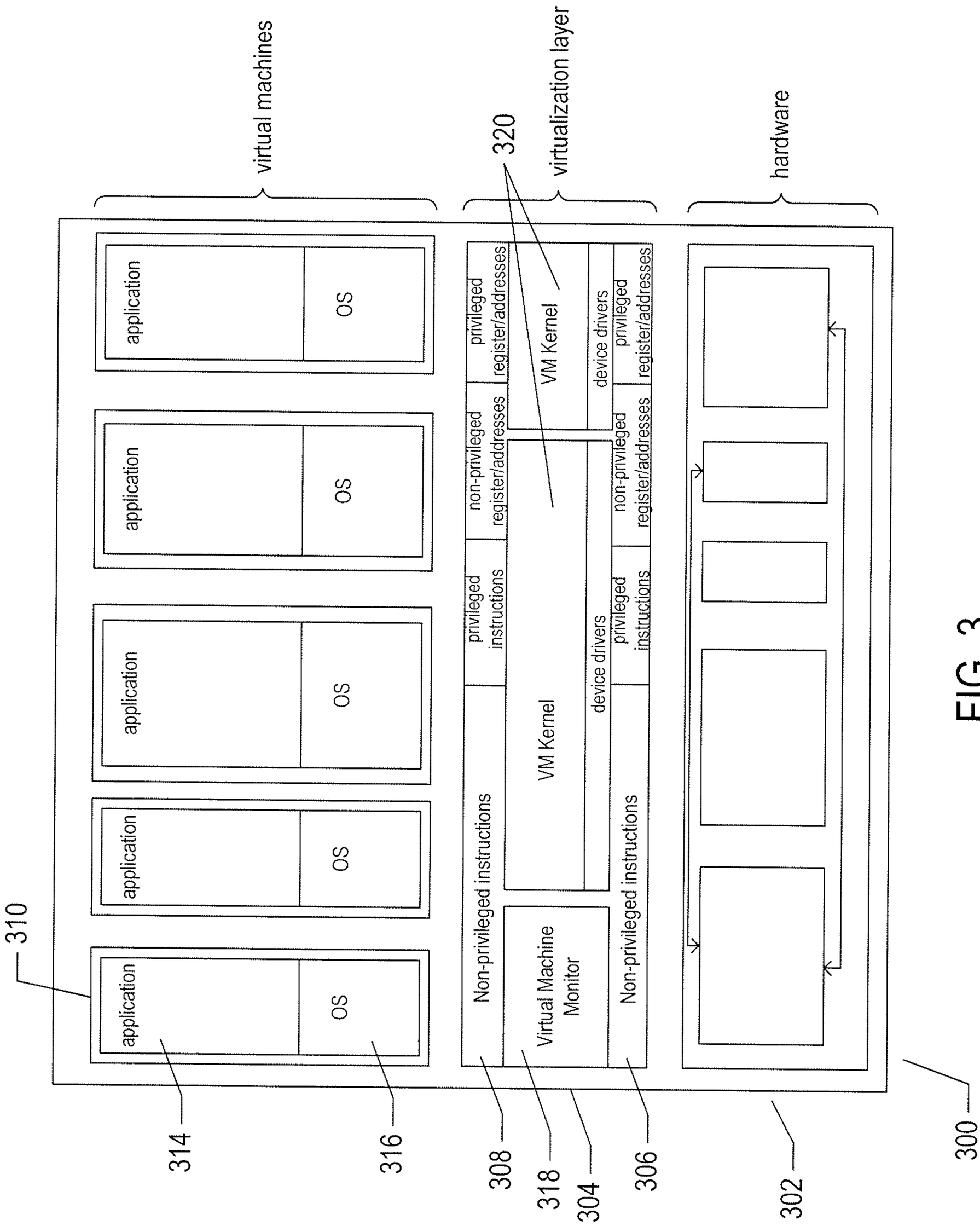
virtual machines
320
virtualization layer
hardware
application
OS
application
OS
application
OS
application
OS
application
OS
privileged instructions
non-privileged register/addresses
VM Kernel
device drivers
privileged instructions
non-privileged register/addresses
privileged instructions
VM Kernel
device drivers
privileged instructions
non-privileged register/addresses
Non-privileged instructions
Virtual Machine Monitor
Non-privileged instructions
310
314
316
308
318
304
306
302
300

FIG. 3

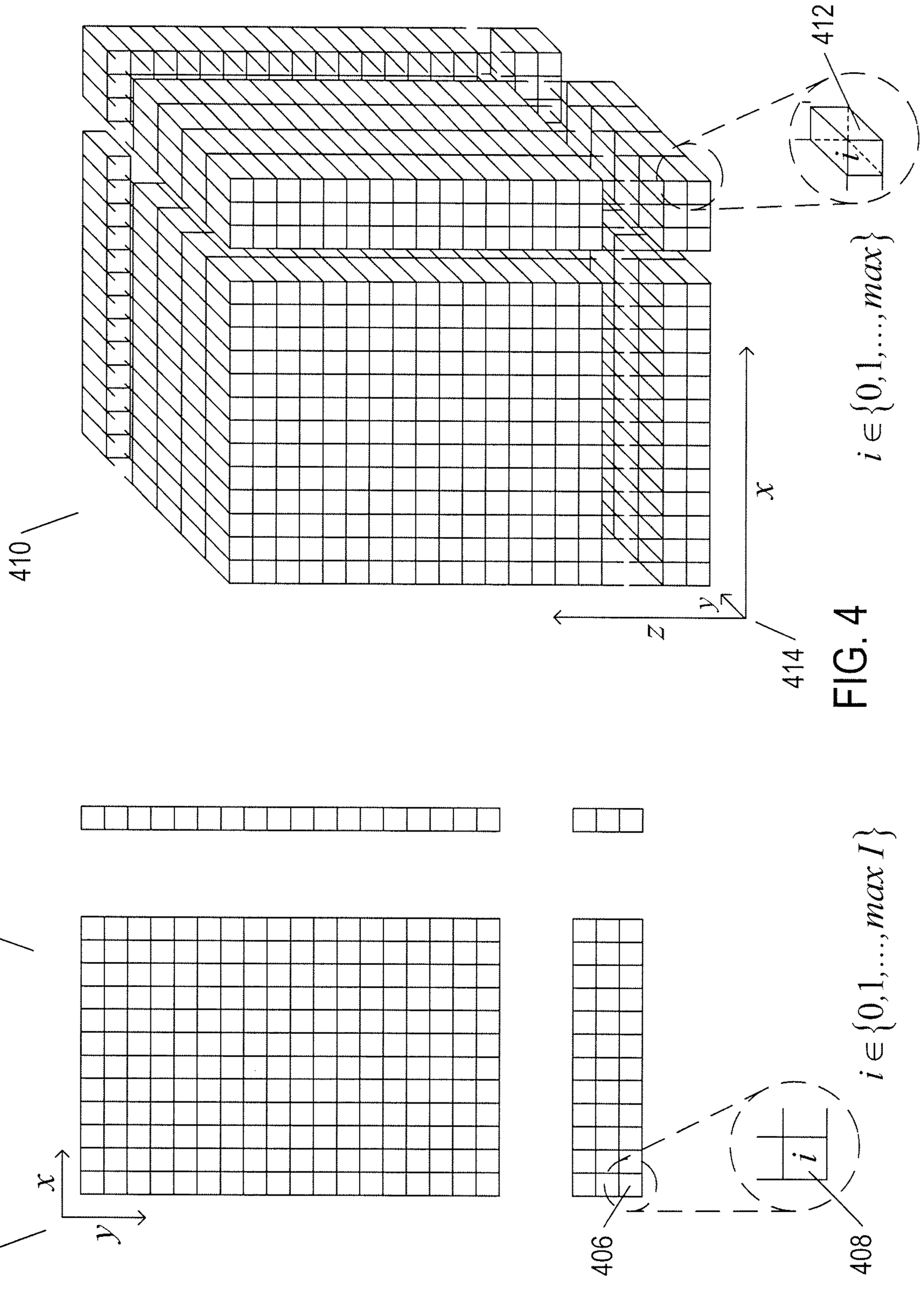

FIG. 4

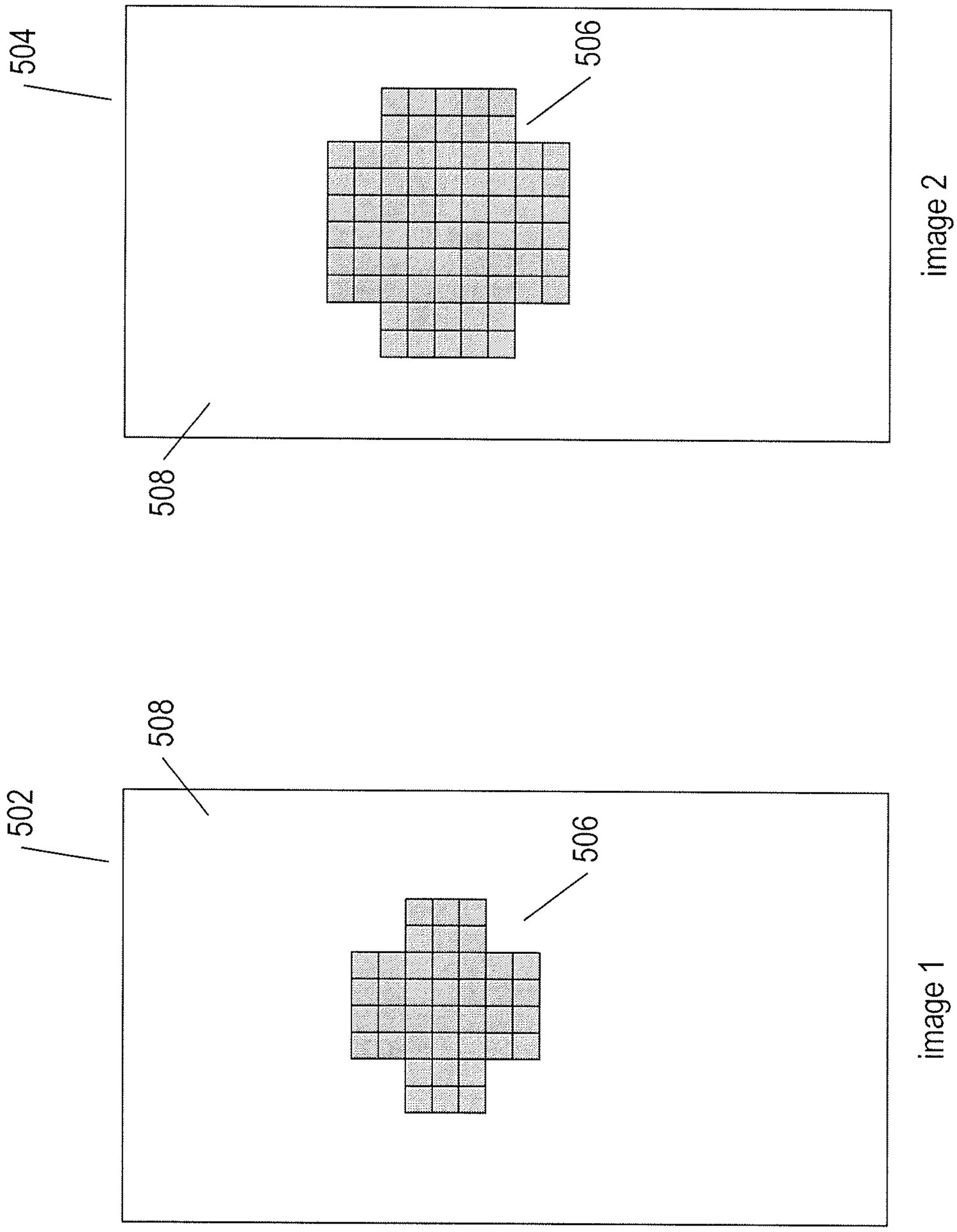

FIG. 5A

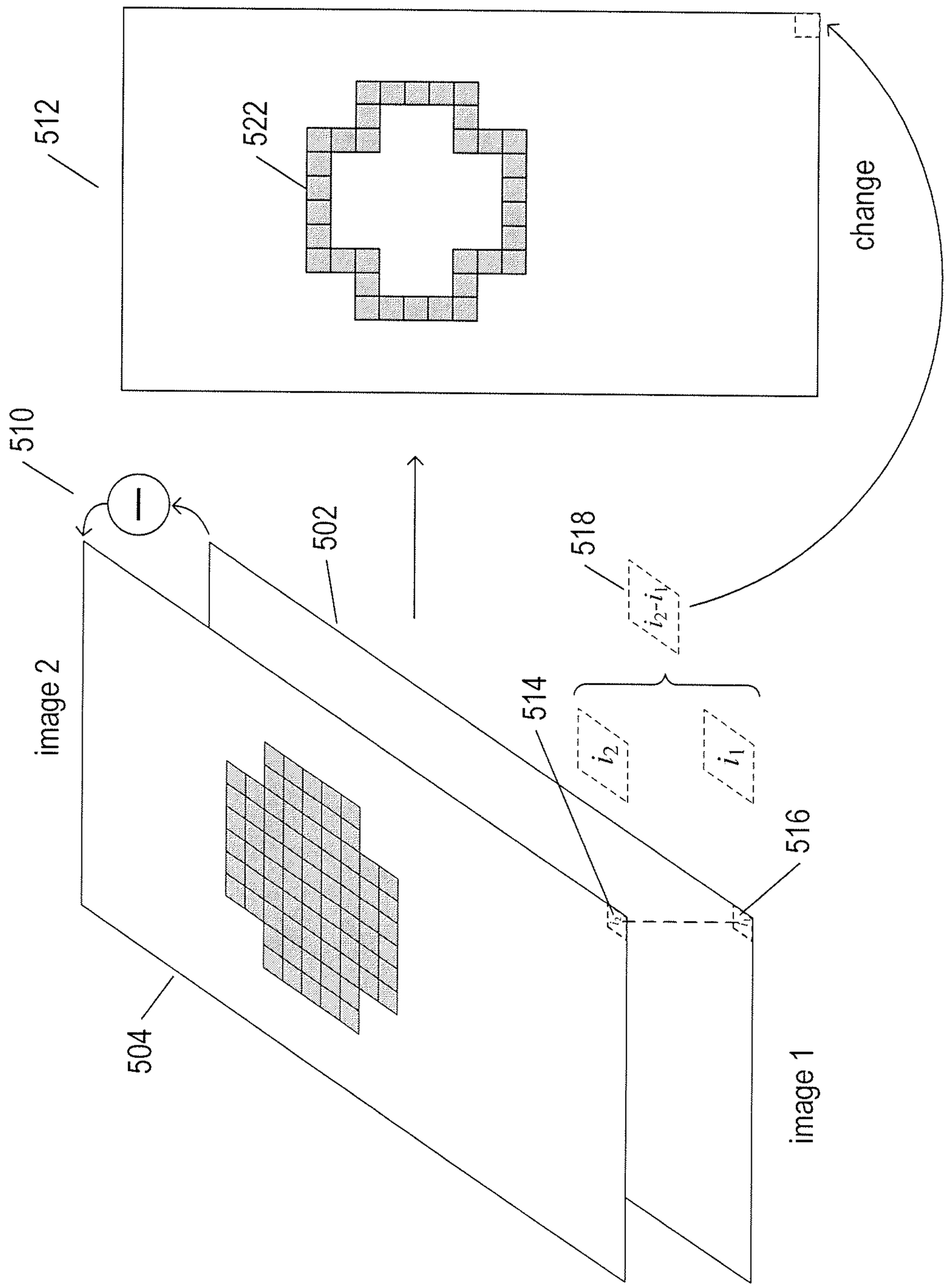
512
522
change
510
502
518
i_2-i_1
514
i_2
i_1
516
image 2
504
image 1

FIG. 5B

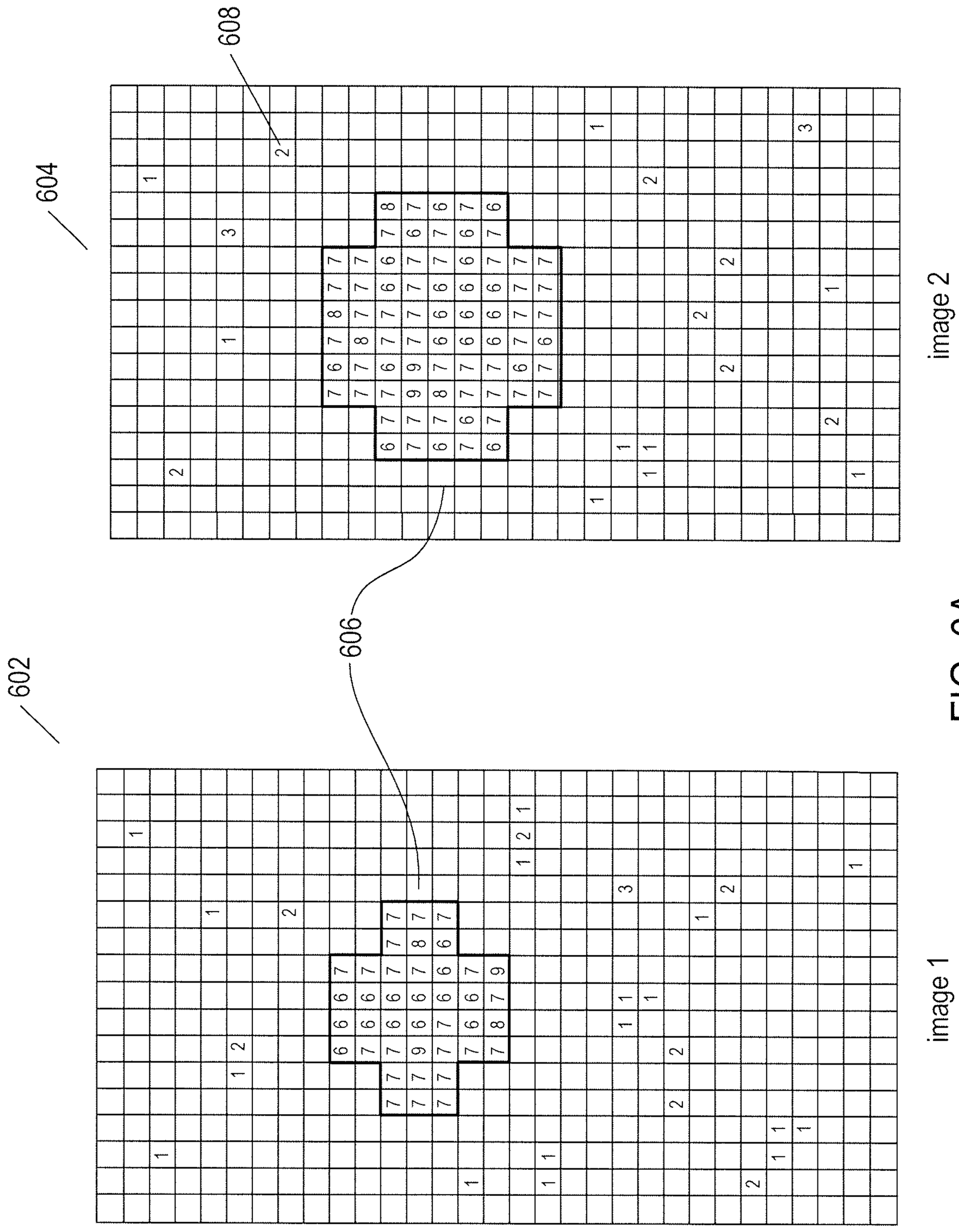

FIG 6A

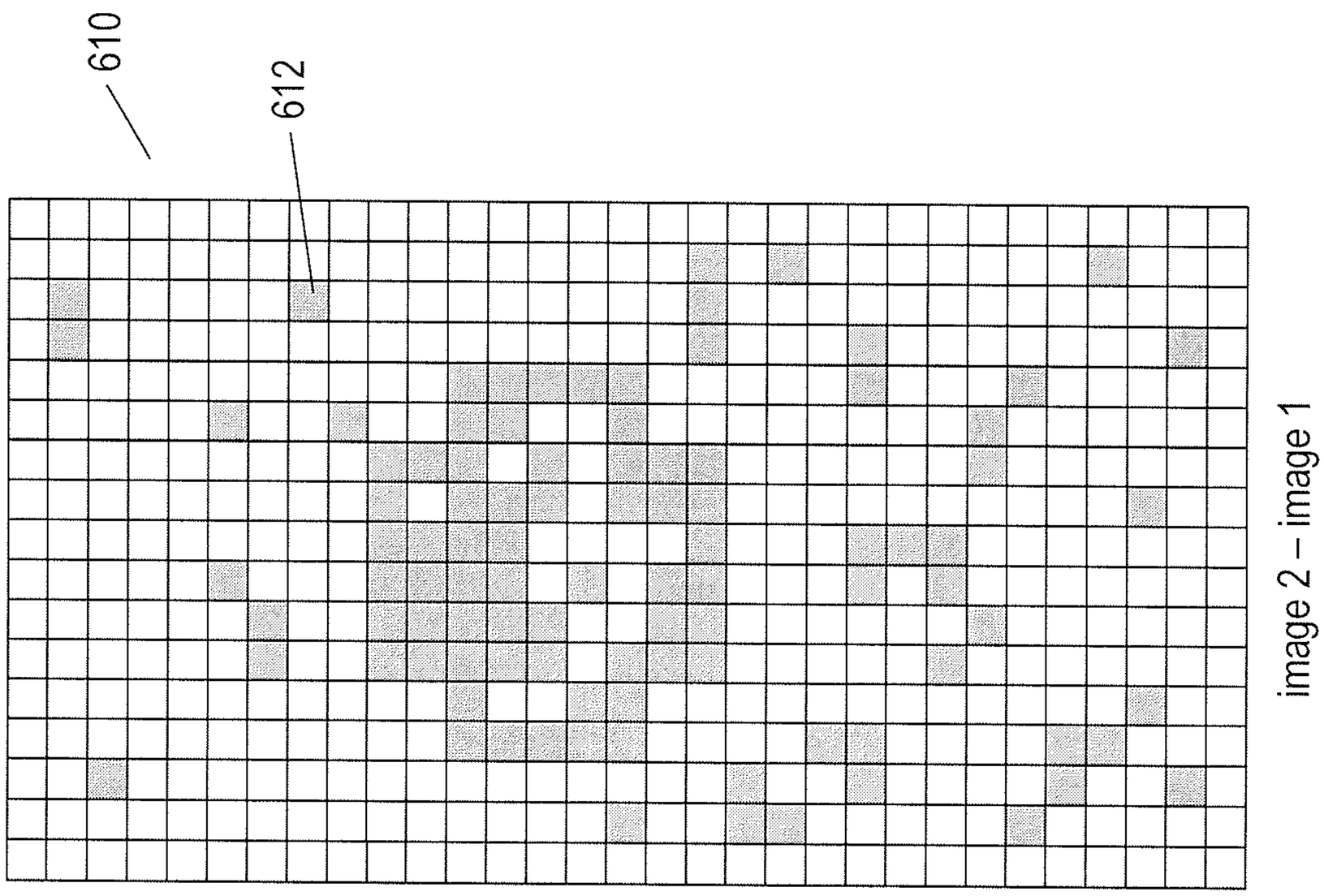

FIG 6B

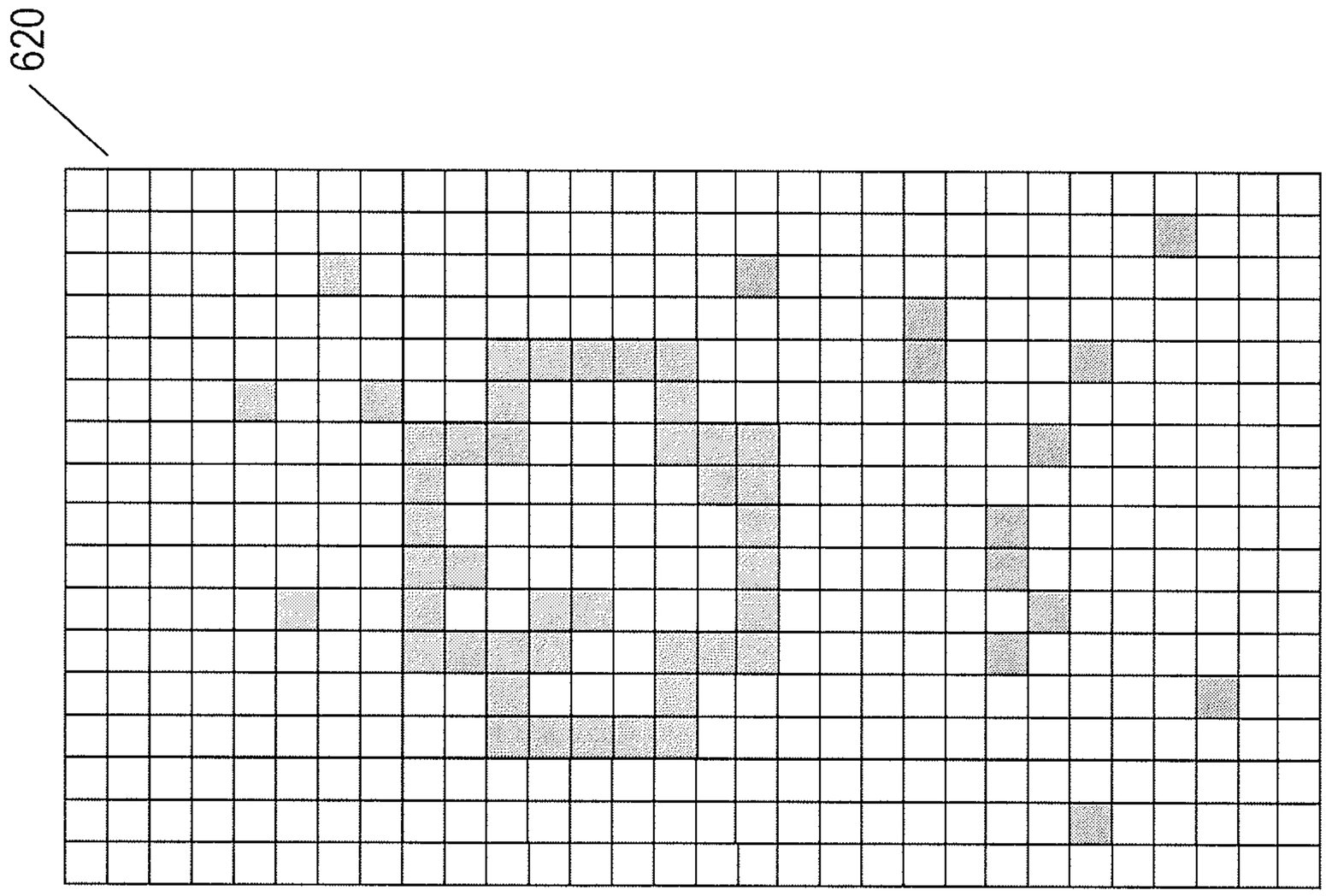

FIG. 6C

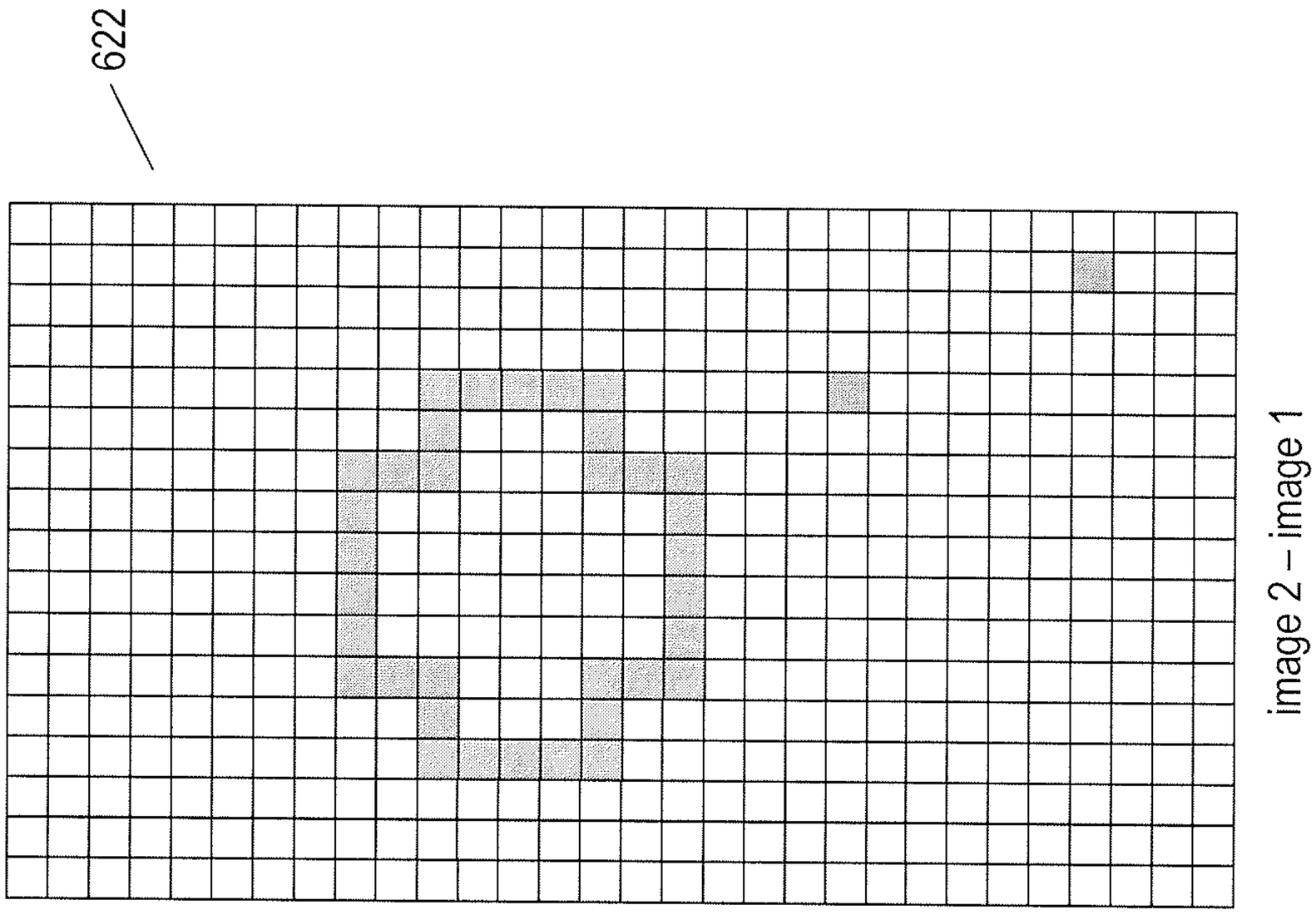

FIG. 6D

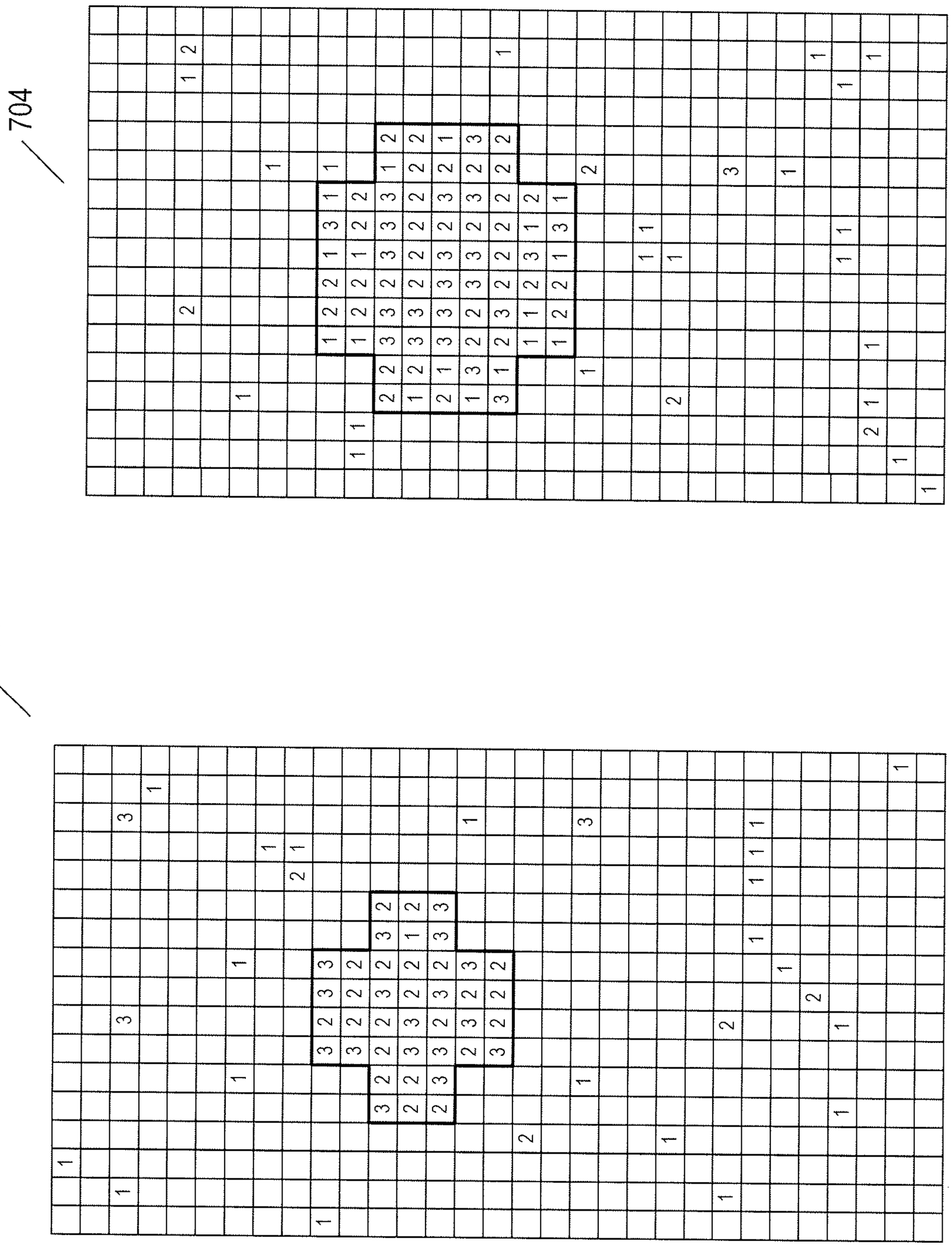

FIG. 7A

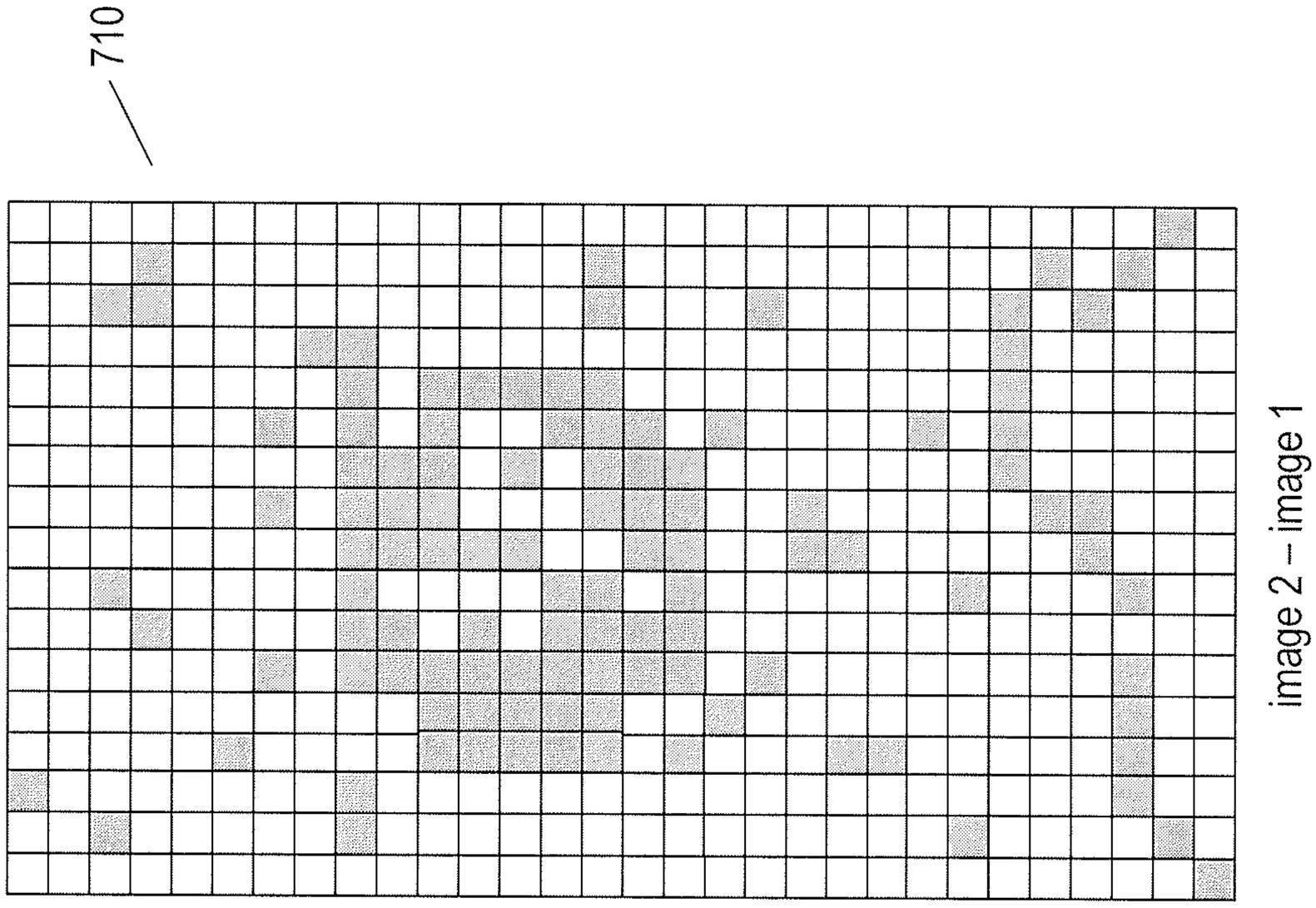

FIG. 7B

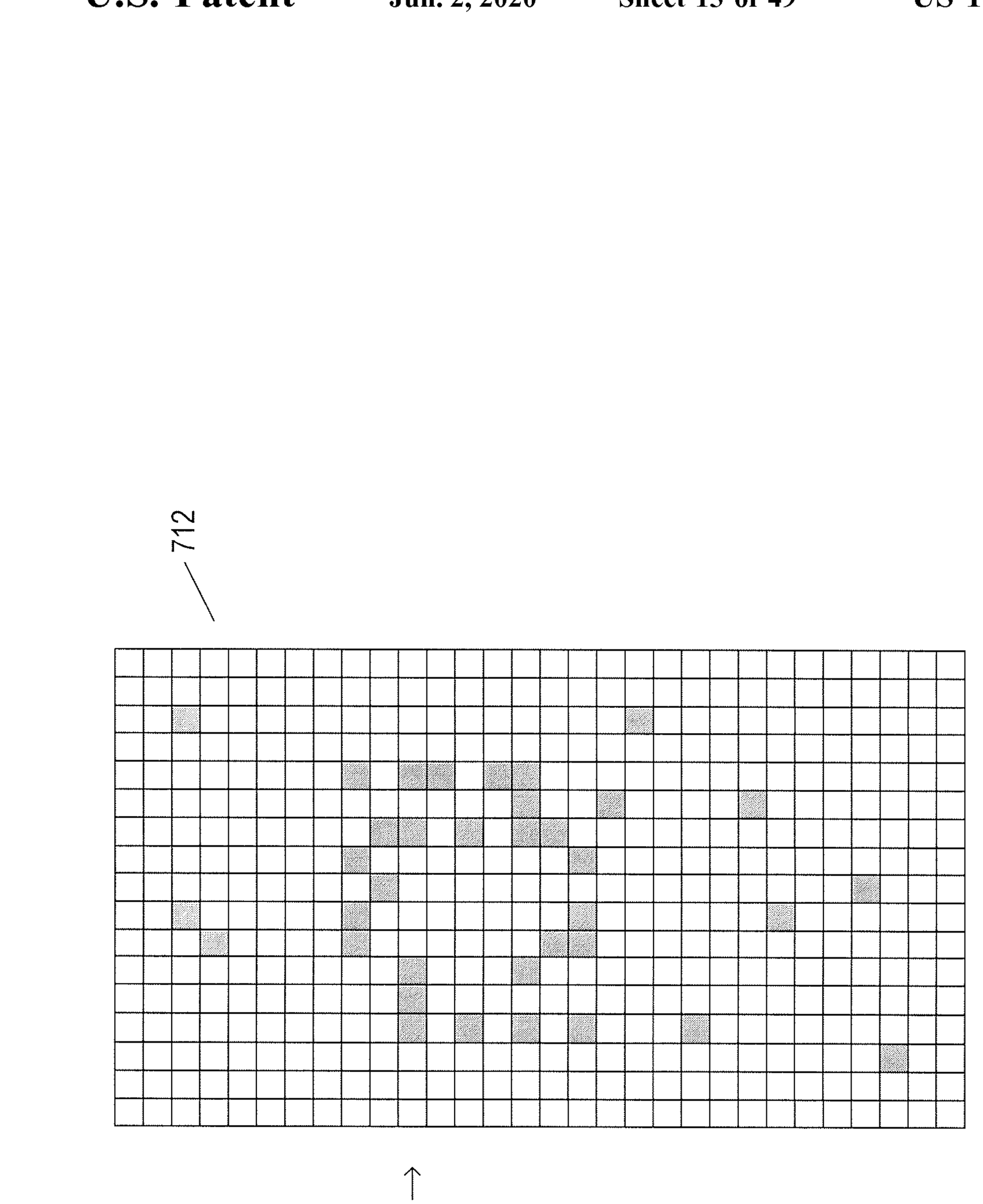

FIG. 7C

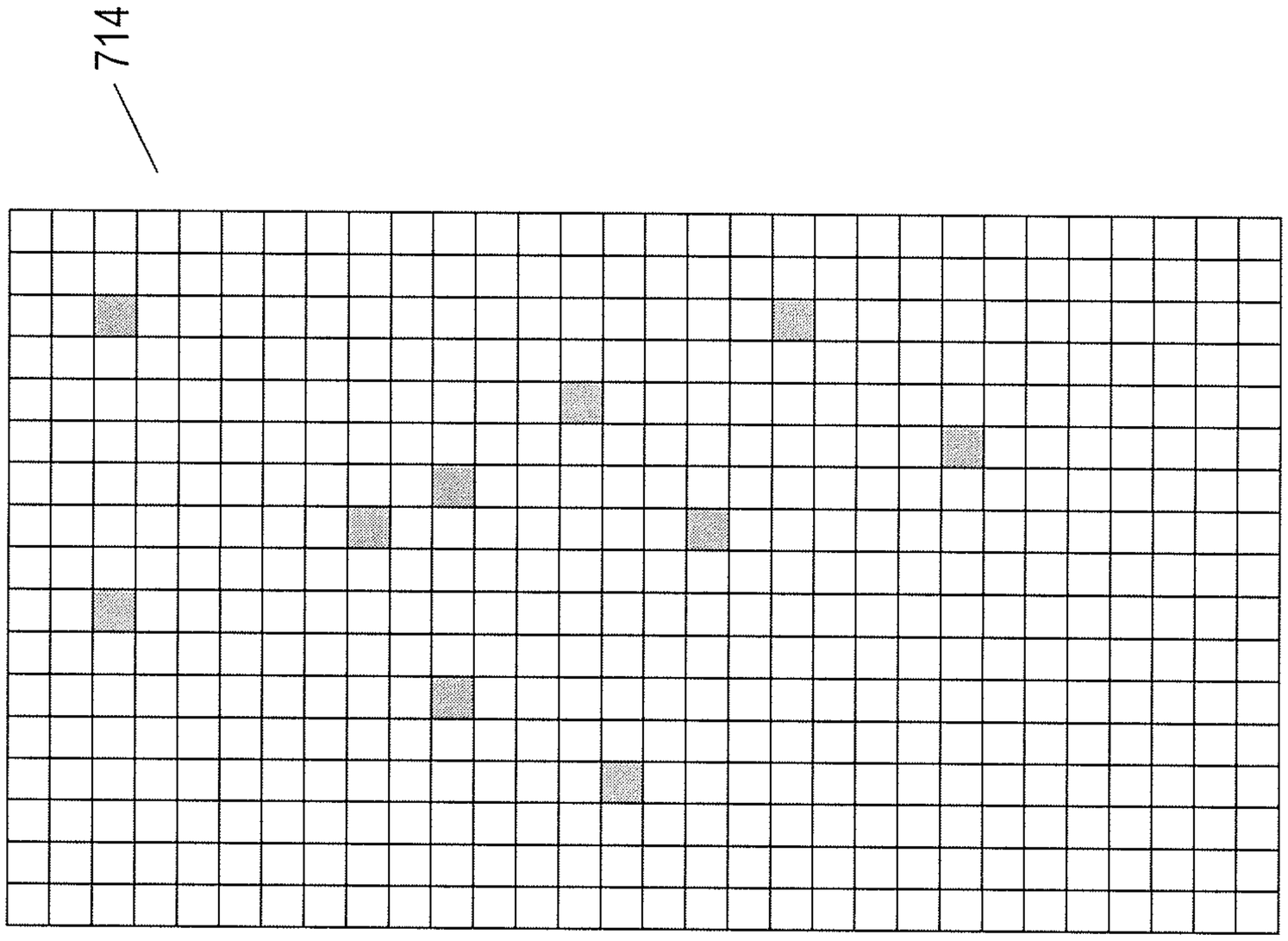

FIG. 7D

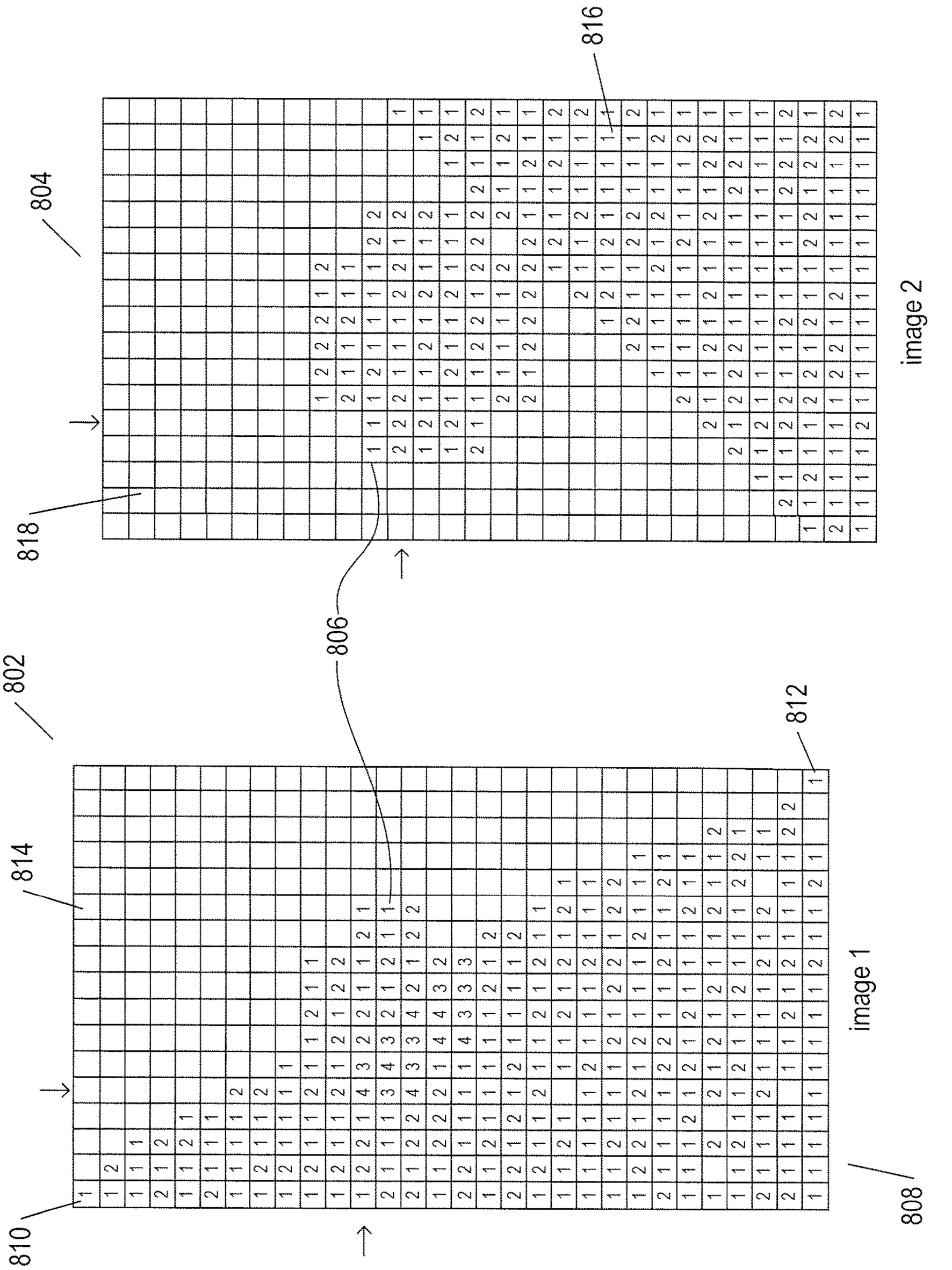

FIG. 8A

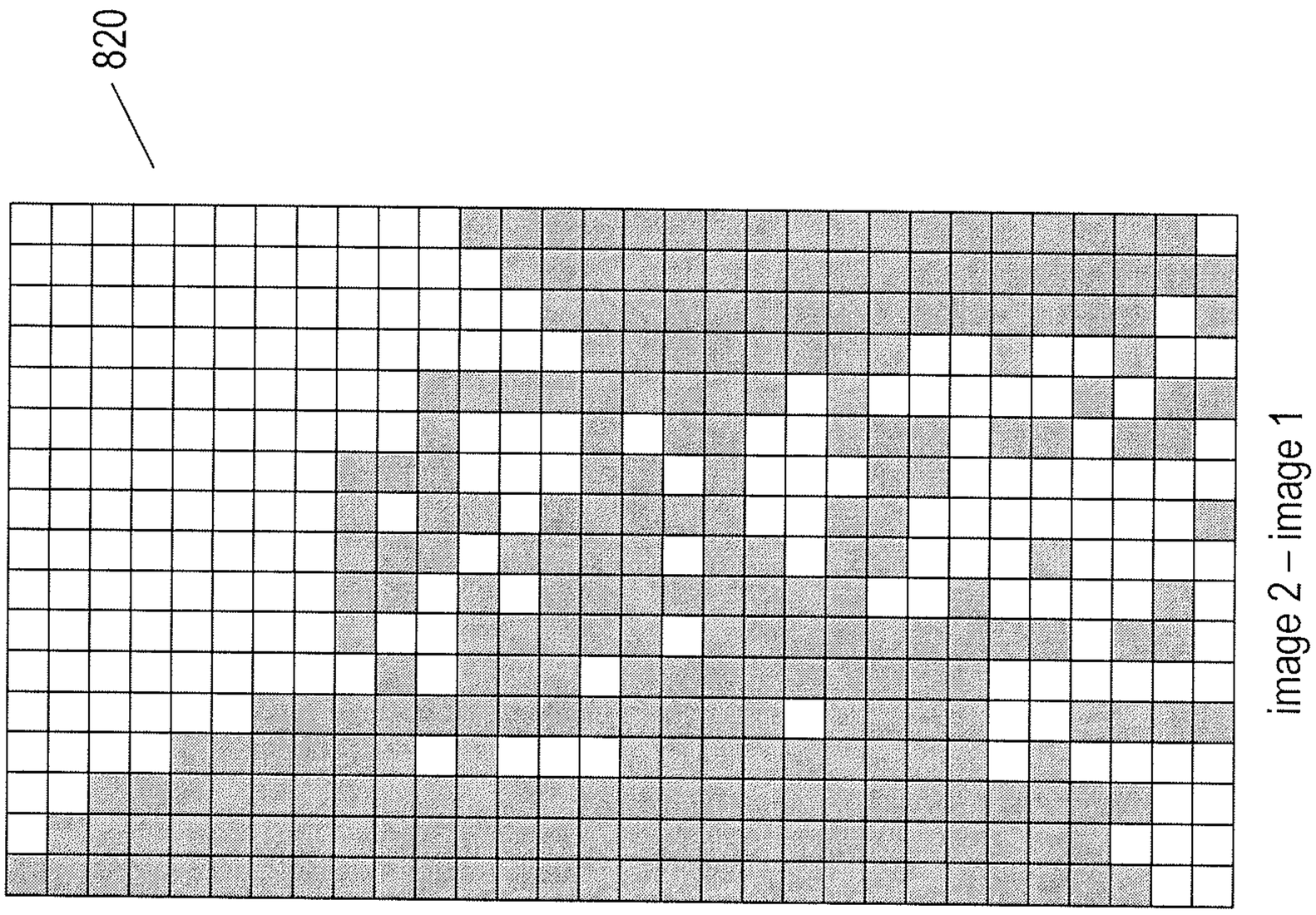

FIG. 8B

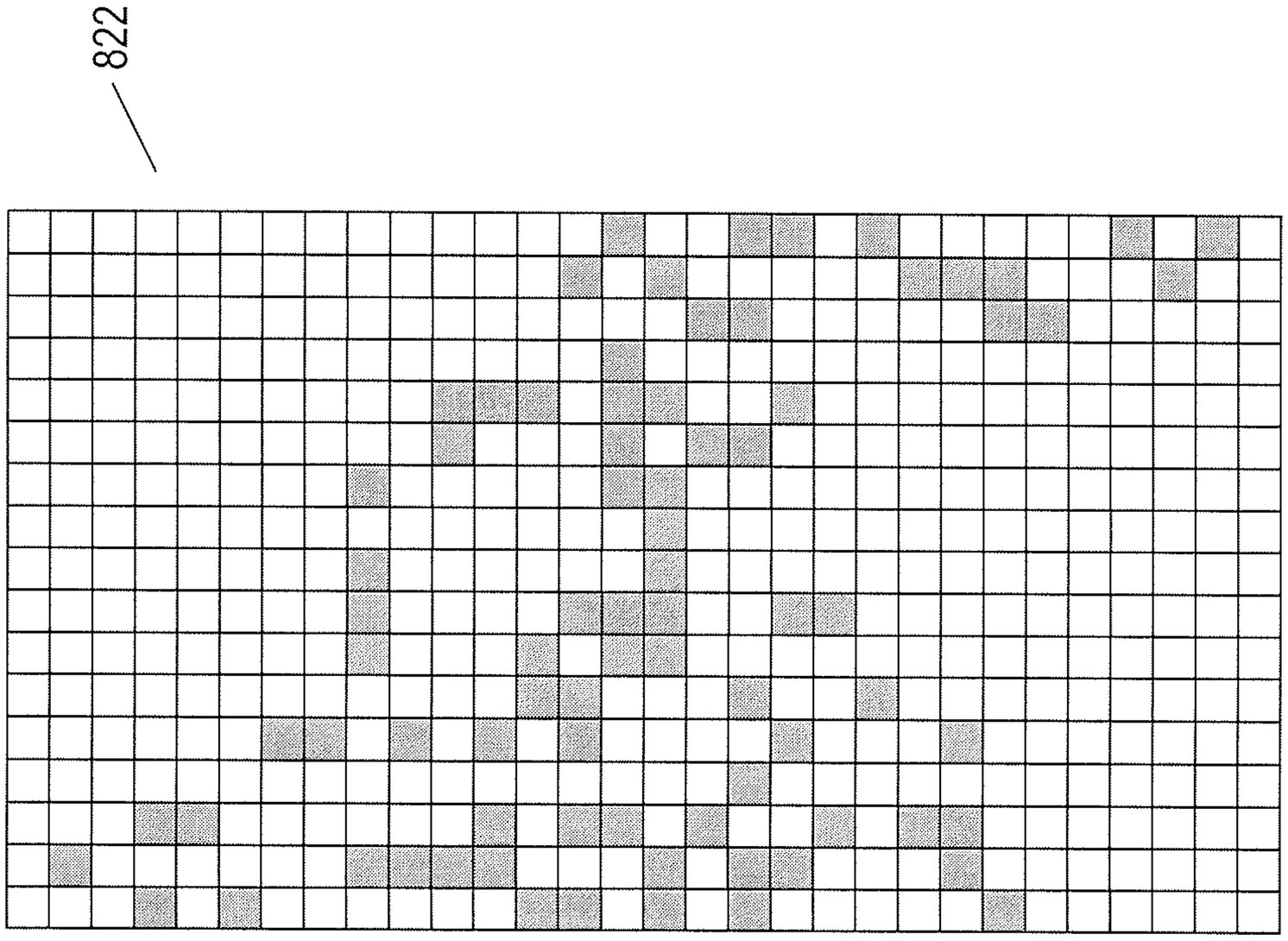

FIG. 8C

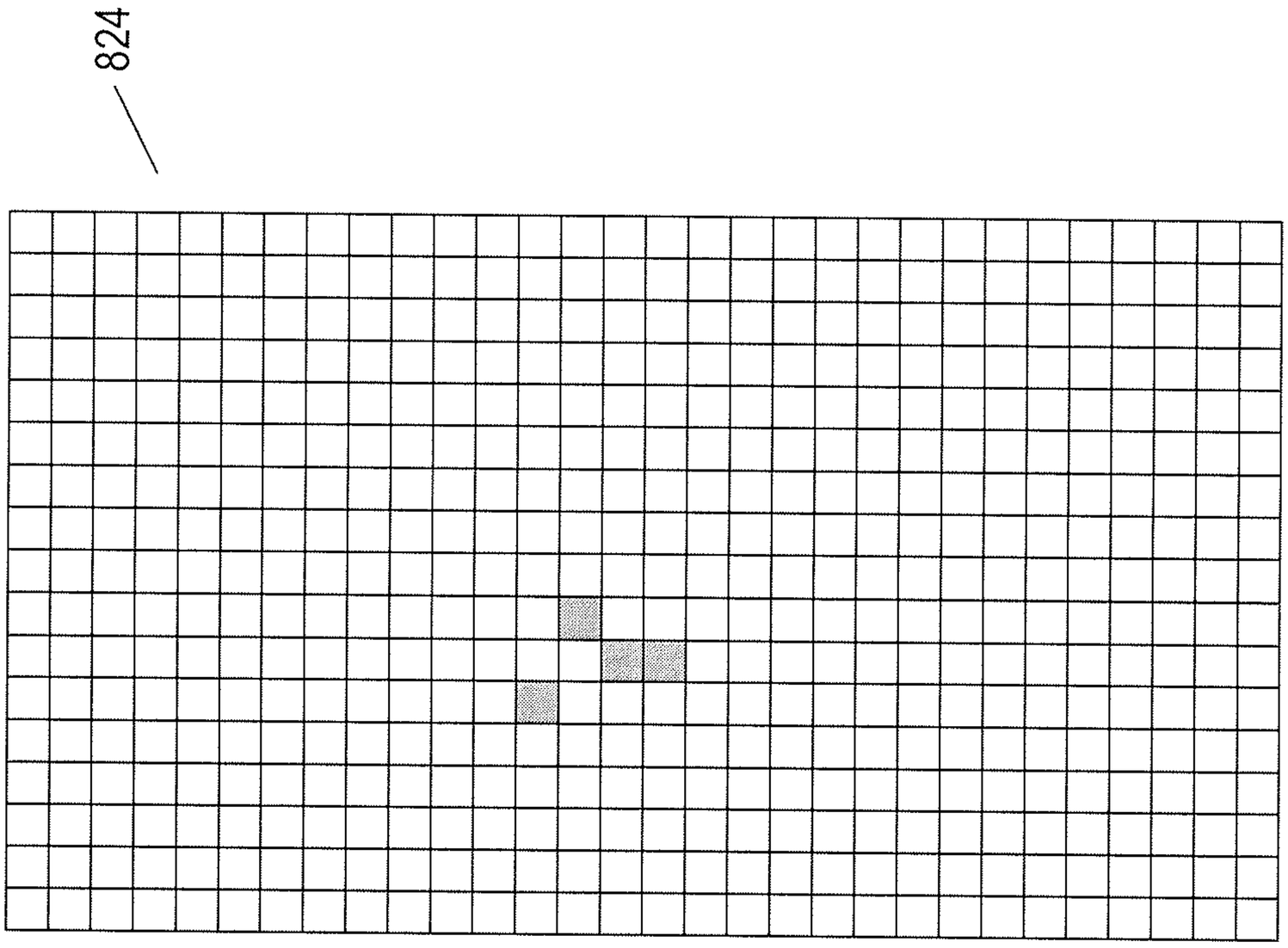

FIG 8D

904

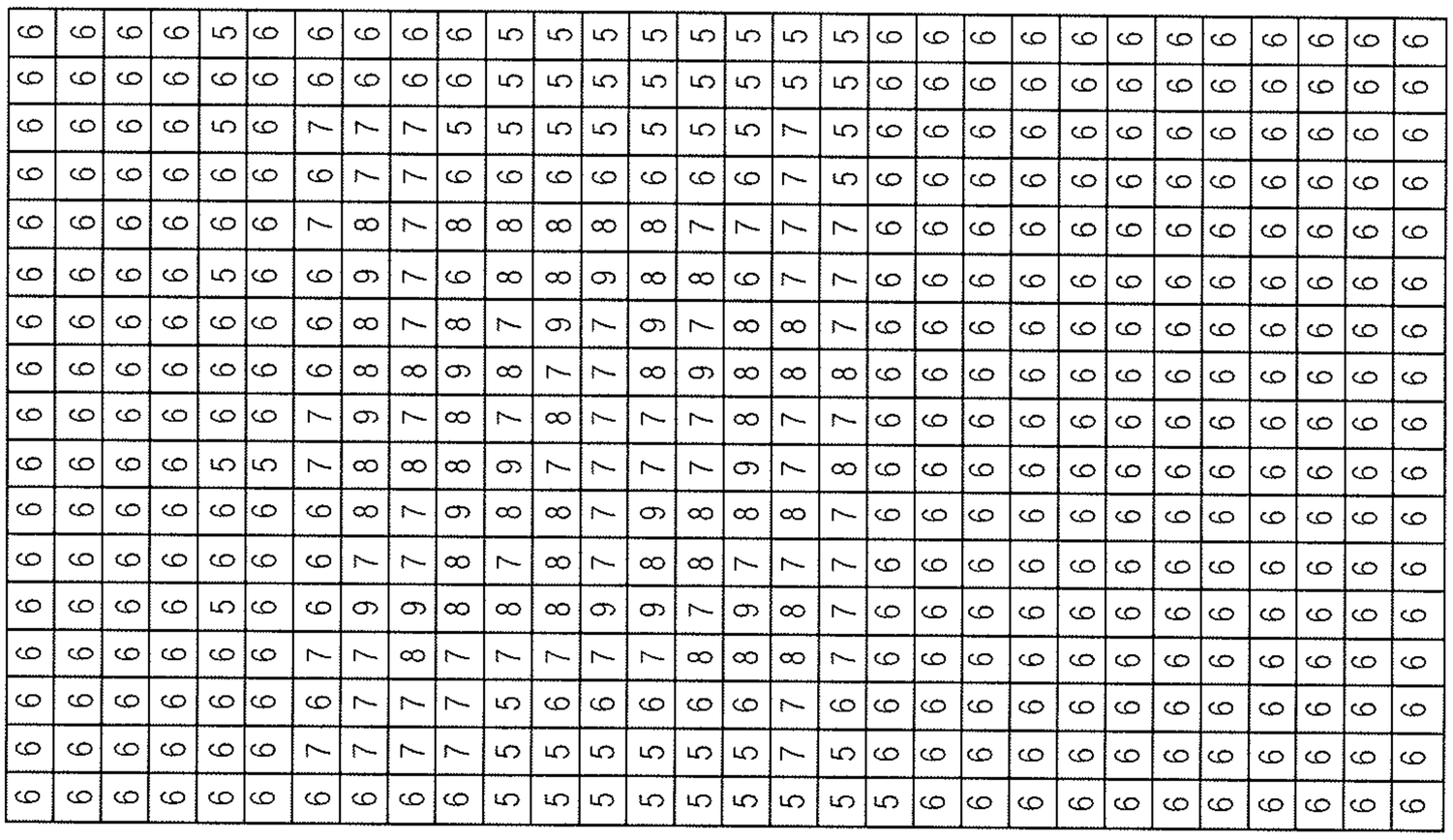

image 2

902

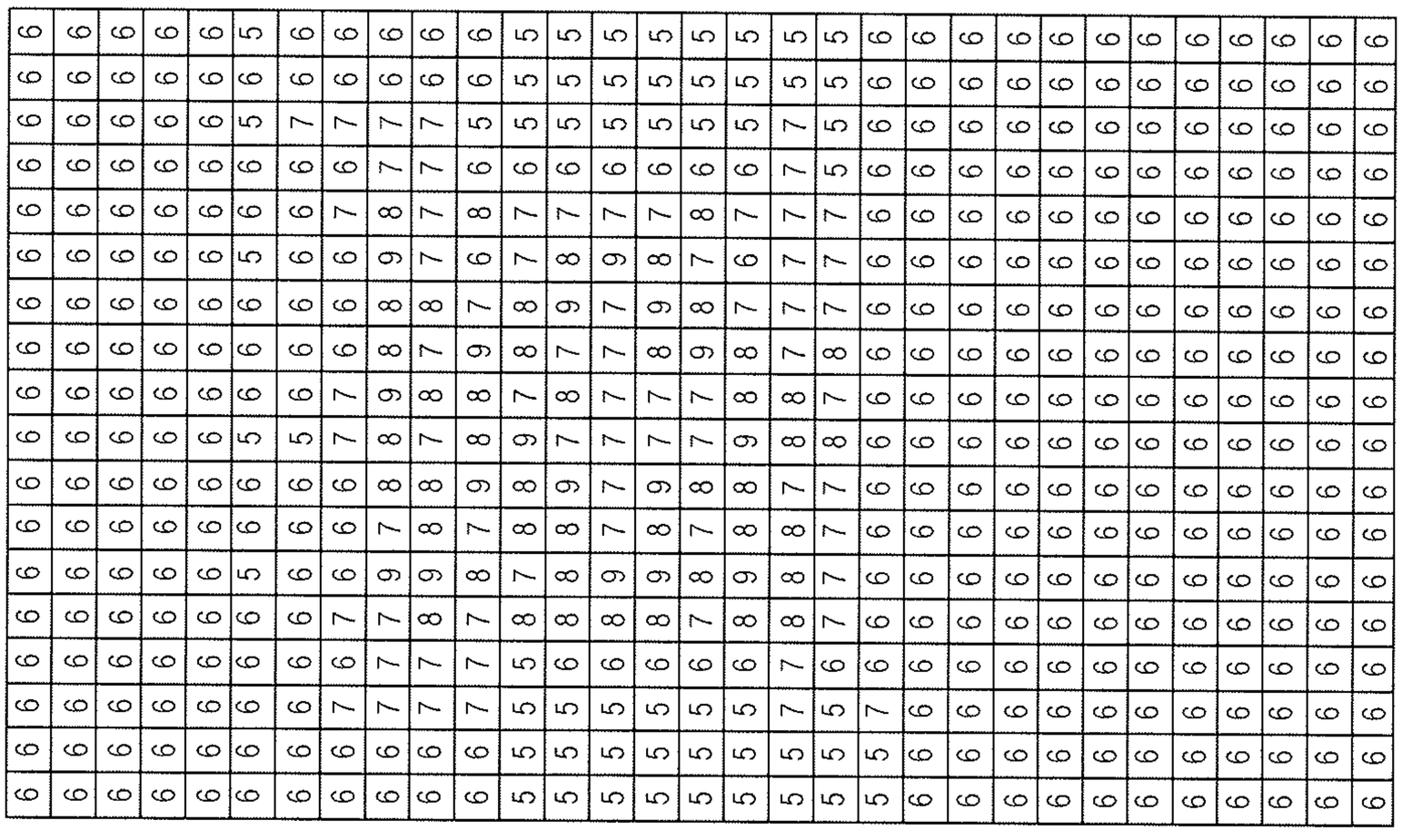

image 1

FIG. 9A

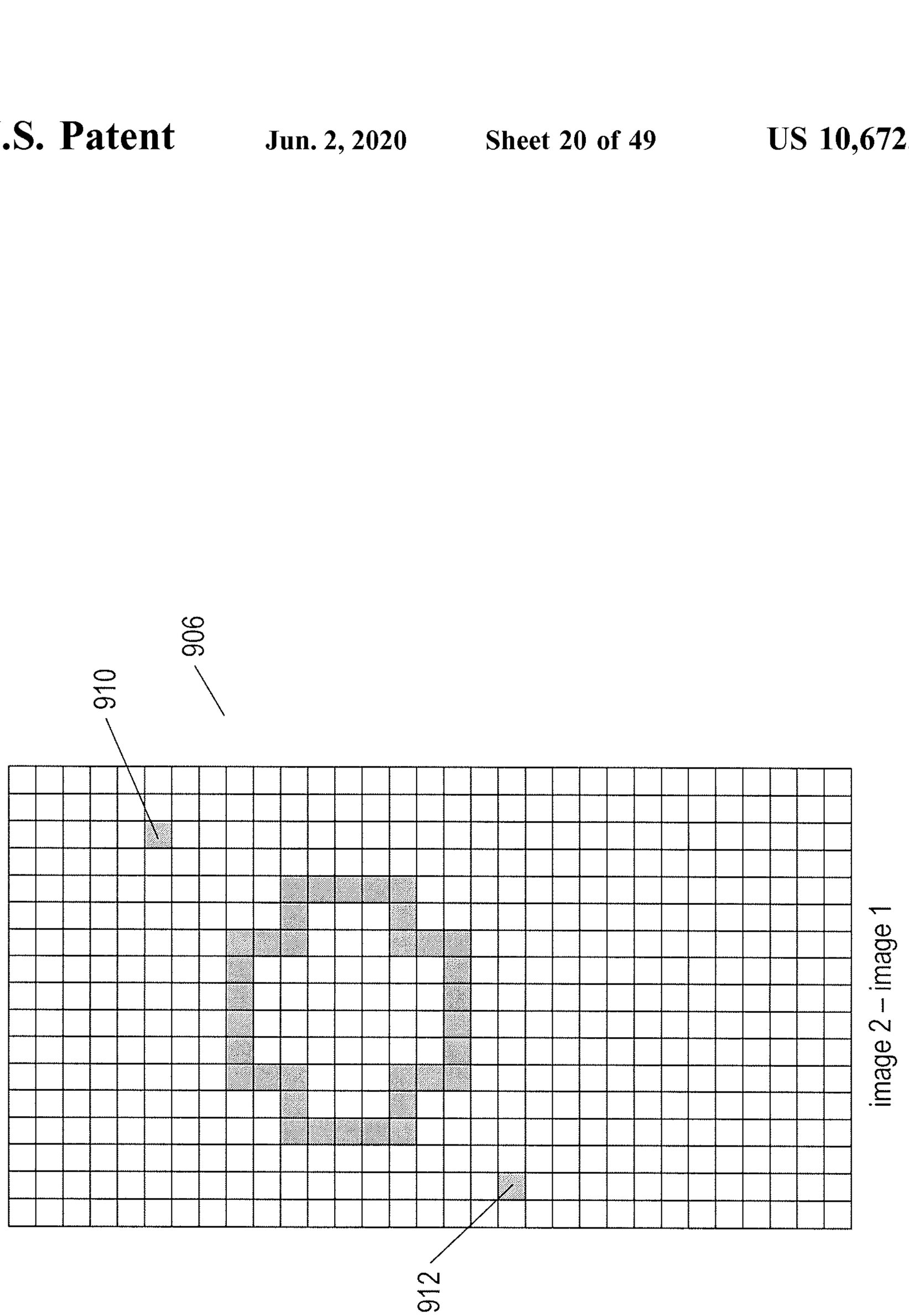

FIG. 9B

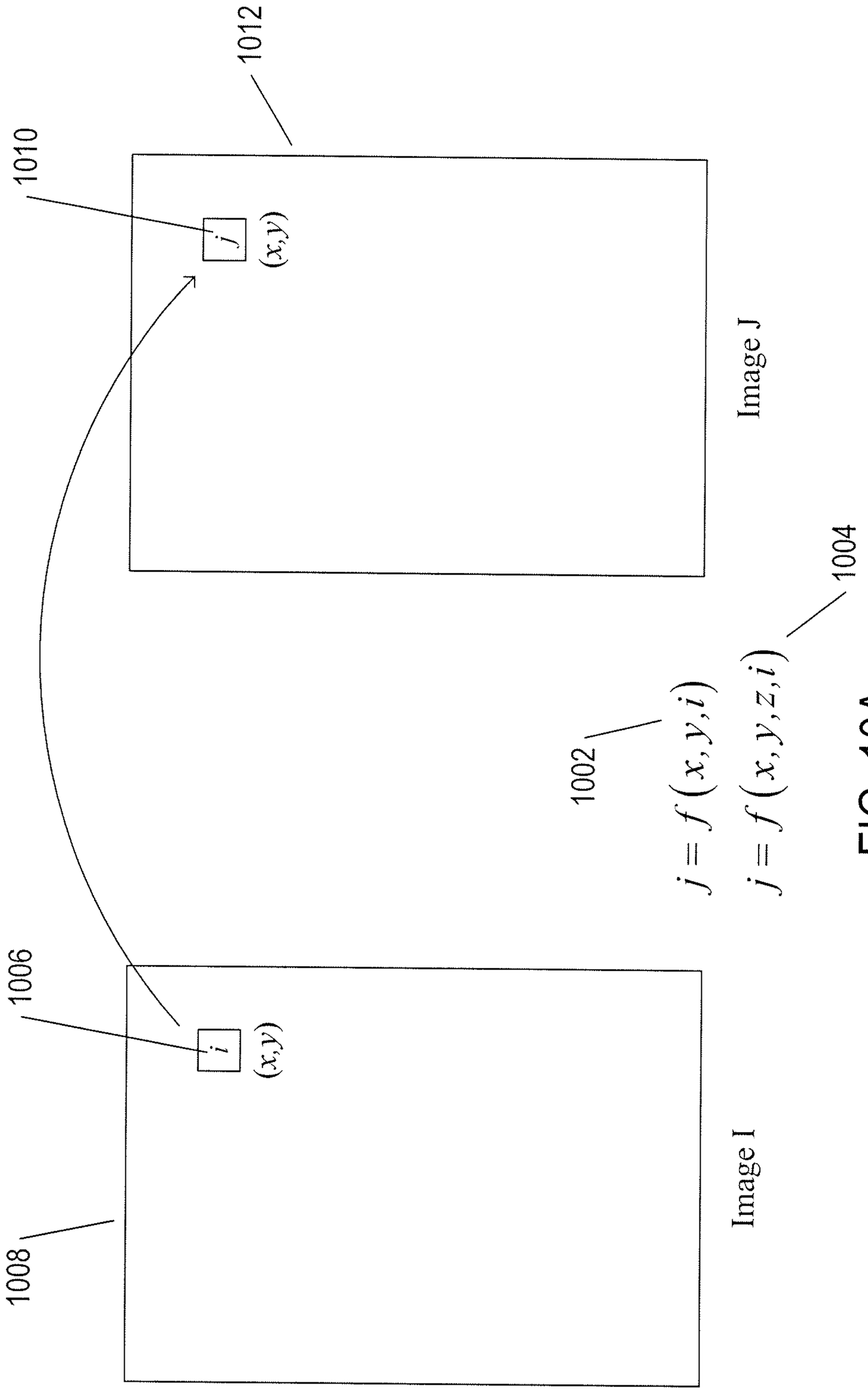
1012
1010
j
(x,y)
Image J
1002
$j = f(x, y, i)$
$j = f(x, y, z, i)$
1004
1006
i
(x,y)
1008
Image I

FIG. 10A

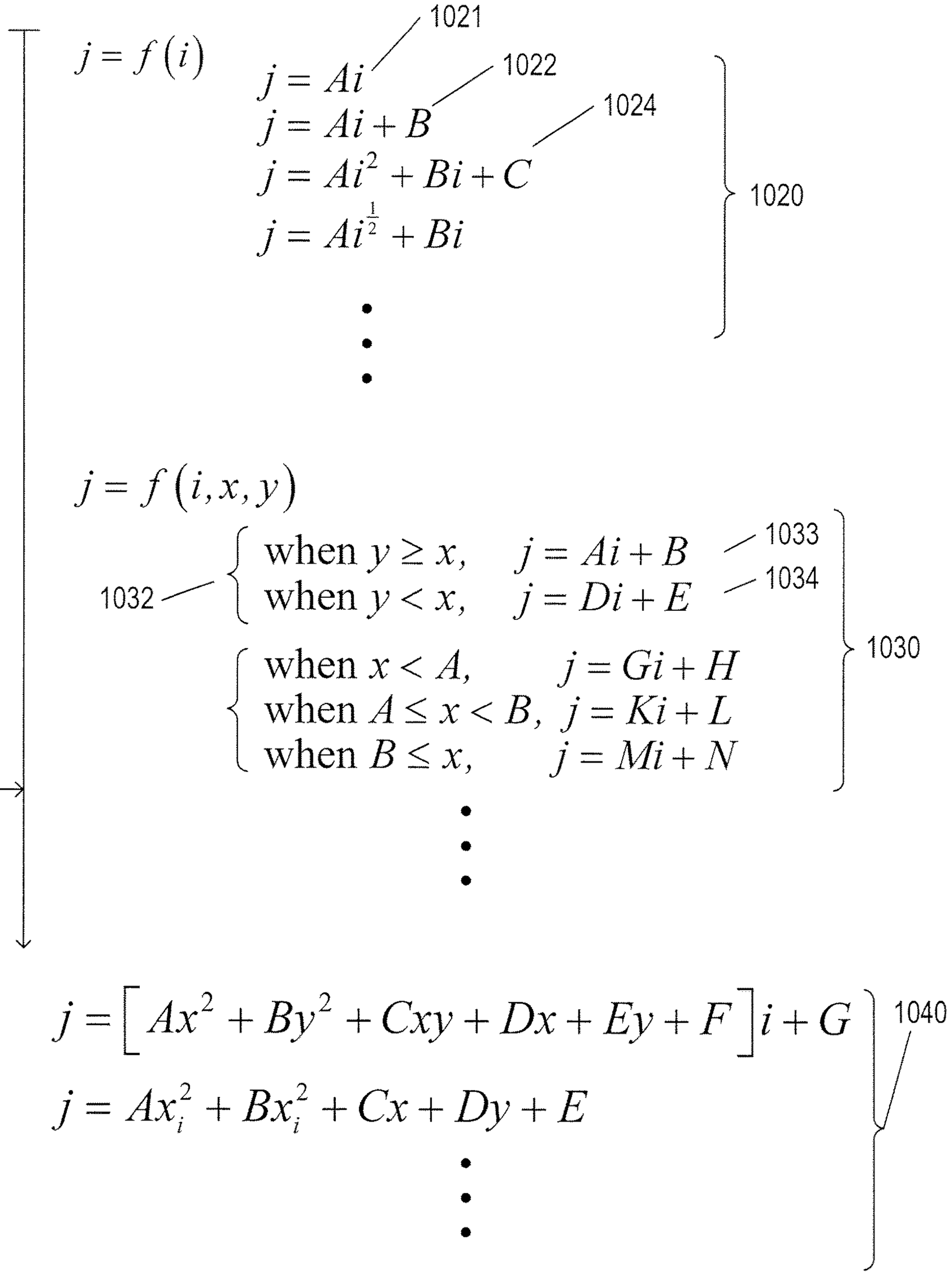
$j = f(i)$
1021
$j = Ai$
1022
$j = Ai + B$
1024
$j = Ai^2 + Bi + C$
$j = Ai^{\frac{1}{2}} + Bi$
1020
$j = f(i, x, y)$
1032
when $y \geq x$, $j = Ai + B$
1033
when $y < x$, $j = Di + E$
1034
when $x < A$, $j = Gi + H$
when $A \leq x < B$, $j = Ki + L$
when $B \leq x$, $j = Mi + N$
1030
1048
$j = \left[Ax^2 + By^2 + Cxy + Dx + Ey + F \right] i + G$
$j = Ax_i^2 + Bx_i^2 + Cx + Dy + E$
1040

FIG. 10B

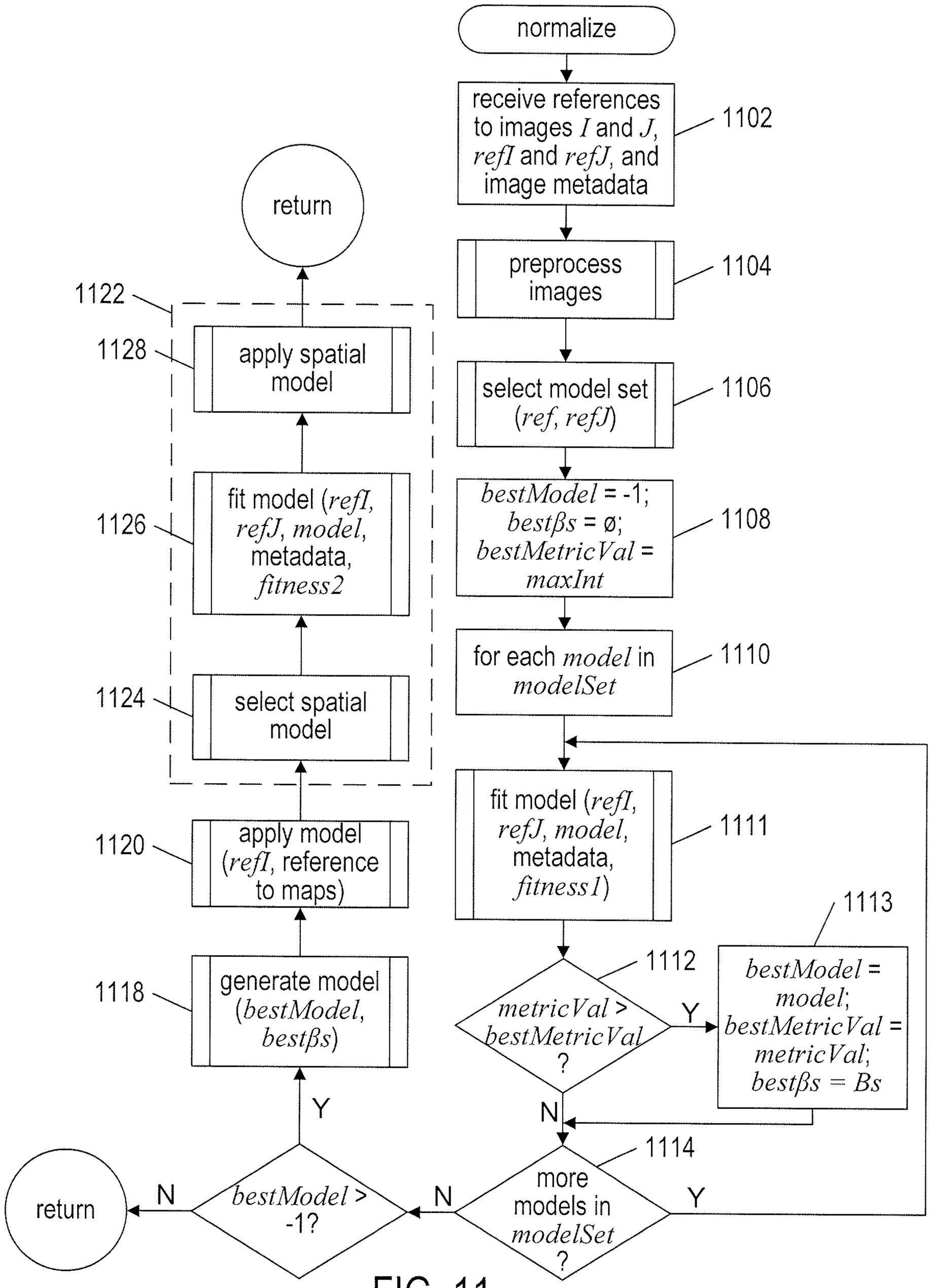
normalize
receive references to images I and J, refI and refJ, and image metadata
1102
preprocess images
1104
select model set (ref, refJ)
1106
bestModel = -1; bestβs = ø; bestMetricVal = maxInt
1108
for each model in modelSet
1110
fit model (refI, refJ, model, metadata, fitness1)
1111
1113
bestModel = model; bestMetricVal = metricVal; bestβs = Bs
metricVal > bestMetricVal ?
1112
Y
N
more models in modelSet ?
1114
Y
N
bestModel > -1?
Y
N
return
generate model (bestModel, bestβs)
1118
apply model (refI, reference to maps)
1120
select spatial model
1124
fit model (refI, refJ, model, metadata, fitness2)
1126
apply spatial model
1128
1122
return

FIG. 11

1202

			3	3	4		4	3	4			
		3	4	3	4	3	3	4	3	4		
		4	3	4	3	4	4	3	4	4		
	4	3	4	3	4	3	3	4	3	3	4	
	3	4	3	4	2	3	1	4	3	4	3	
	3	4	3	2	2	1	2	1	3	4	3	
	4	3	4	1	2	1	1	2	3	3	4	
		4	3	3	1	3	2	4	4	4		
		3	5	4	3	3	3	3	3	4		
		4	4	3	4	4	4	3	4	3		
		3	4	3	3	3	3	4	4	3		
			3	4	4		4	3	3			

1204

			9	7	9		7	9	9			
		7	7	9	7	9	9	9	7	9		
		9	9	7	9	9	7	7	11	7		
	7	7	9	7	7	7	9	7	9	9	9	
	7	9	7	9	5	7	3	7	9	7	9	
	7	9	7	3	3	5	3	5	7	9	7	
	9	7	7	5	3	5	5	3	9	7	7	
		9	9	7	5	9	3	7	7	9		
		7	7	9	7	7	7	9	7	7		
		9	9	7	9	9	7	7	9	7		
		7	7	7	9	7	7	9	9	7		
			9	7	9		9	9	7			

1206

Image A Intensity	Image B Intensity												
	0	1	2	3	4	5	6	7	8	9	10	11	12
1													
2													
3													
4													
5													

FIG. 12A

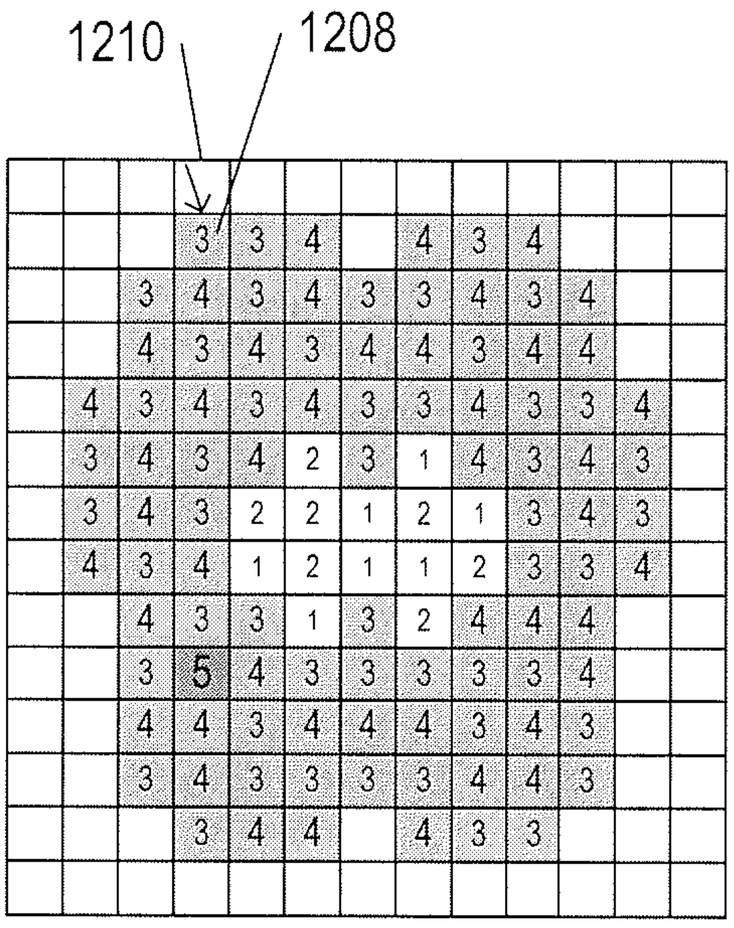

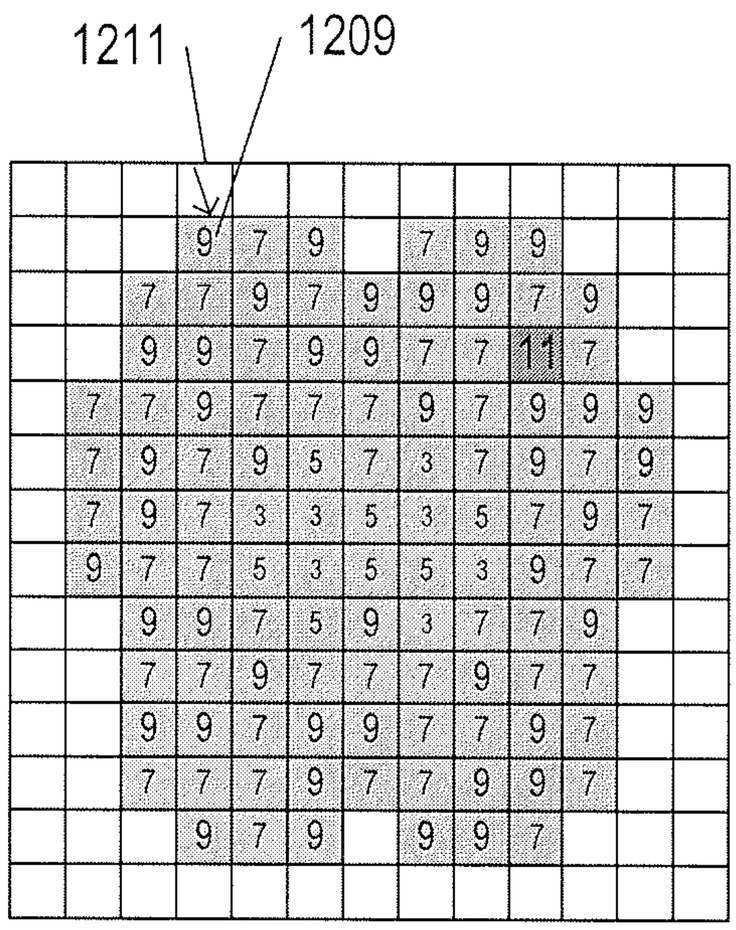

1206

Image A Intensity	Image B Intensity												
	0	1	2	3	4	5	6	7	8	9	10	11	12
1													
2													
3										1			
4													
5													

1212

FIG. 12B

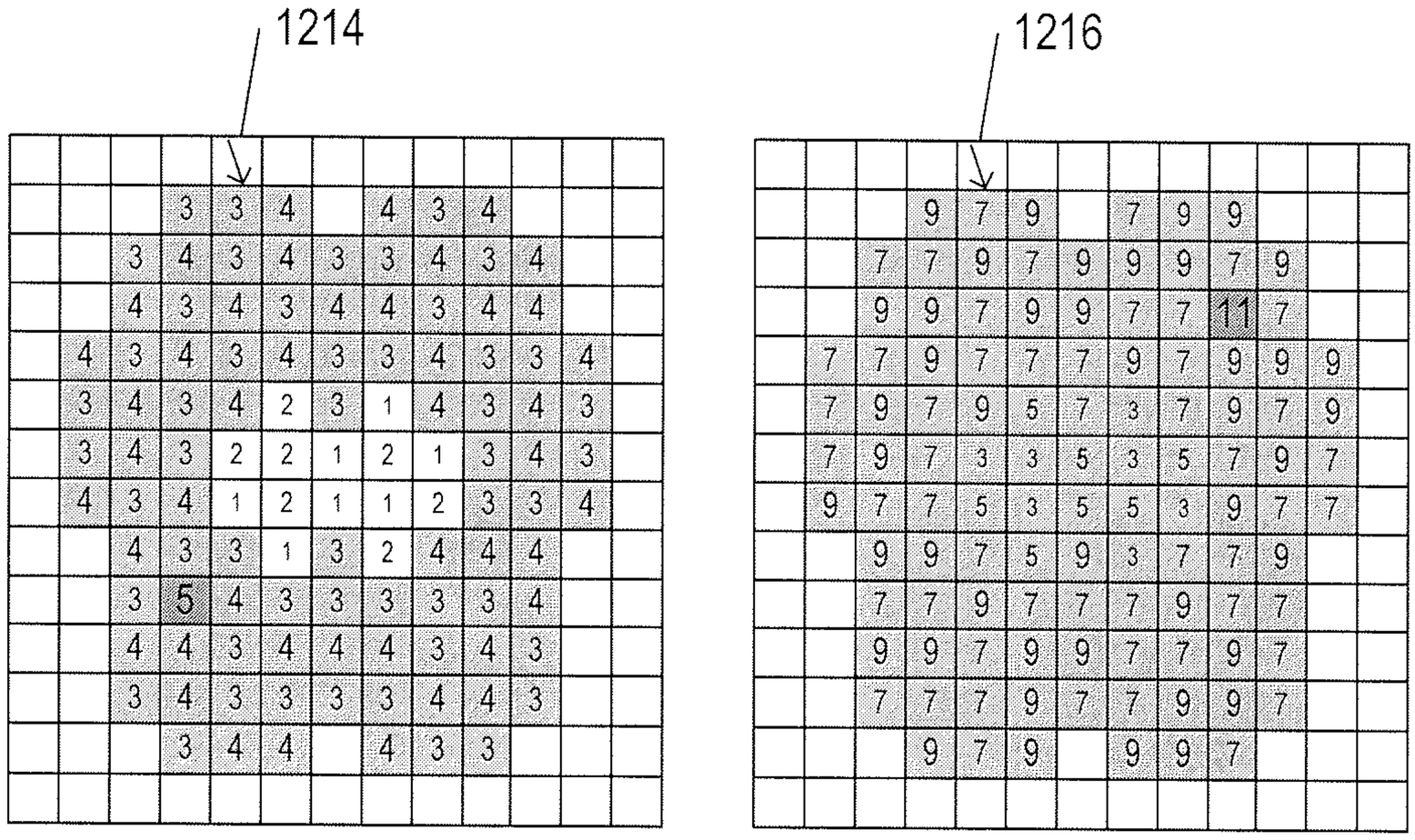

1206

Image A Intensity	Image B Intensity												
	0	1	2	3	4	5	6	7	8	9	10	11	12
1													
2													
3								1		1			
4													
5													

1218

FIG. 12C

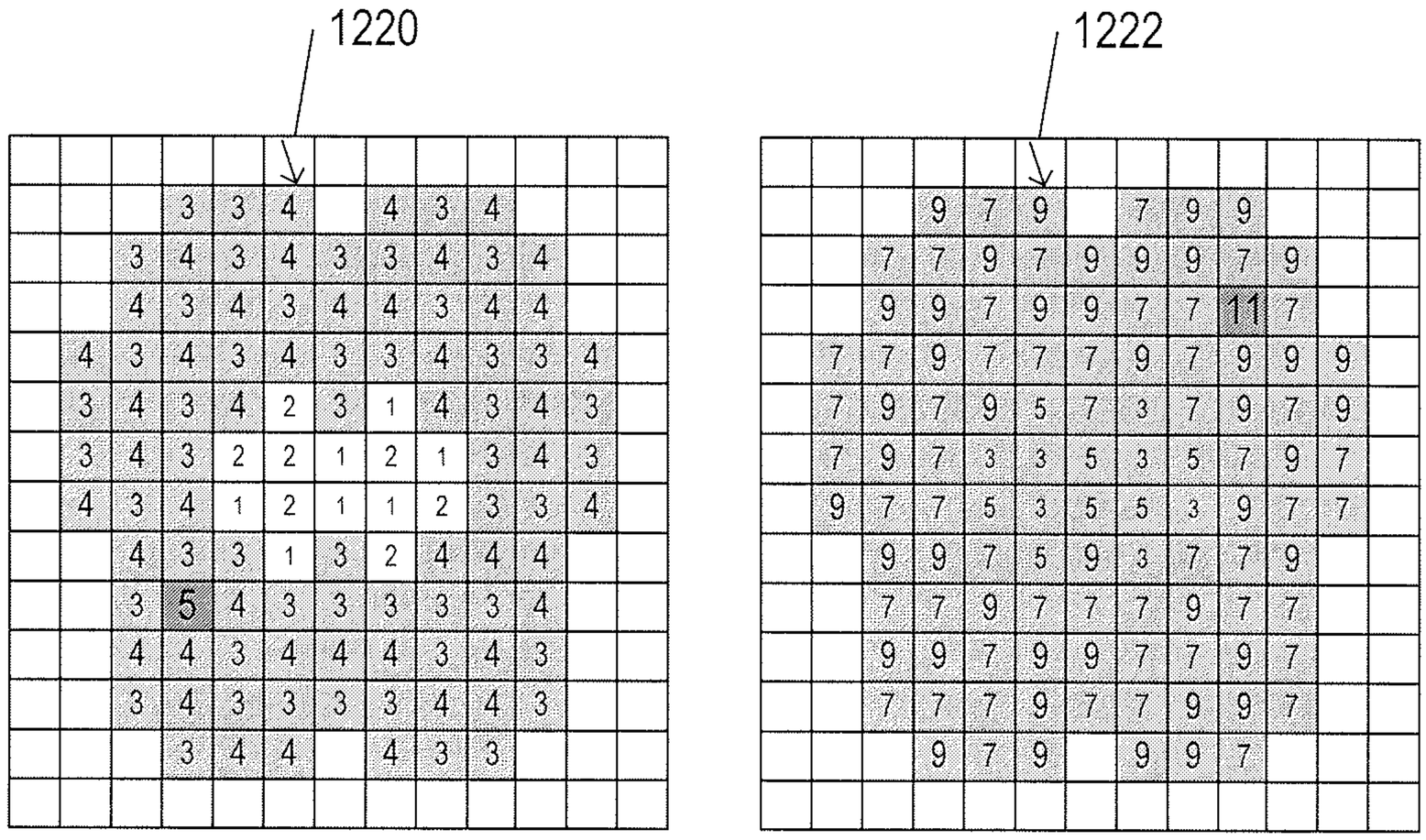

1206

Image A Intensity	Image B Intensity												
	0	1	2	3	4	5	6	7	8	9	10	11	12
1													
2													
3								1		1			
4										1			
5													

1224

FIG. 12D

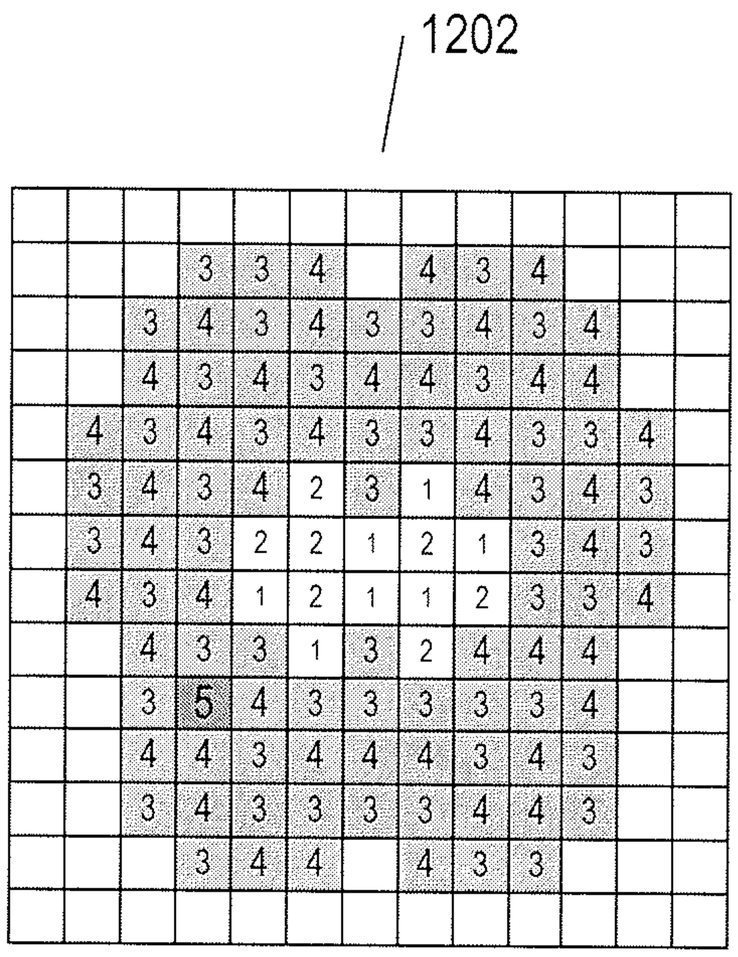

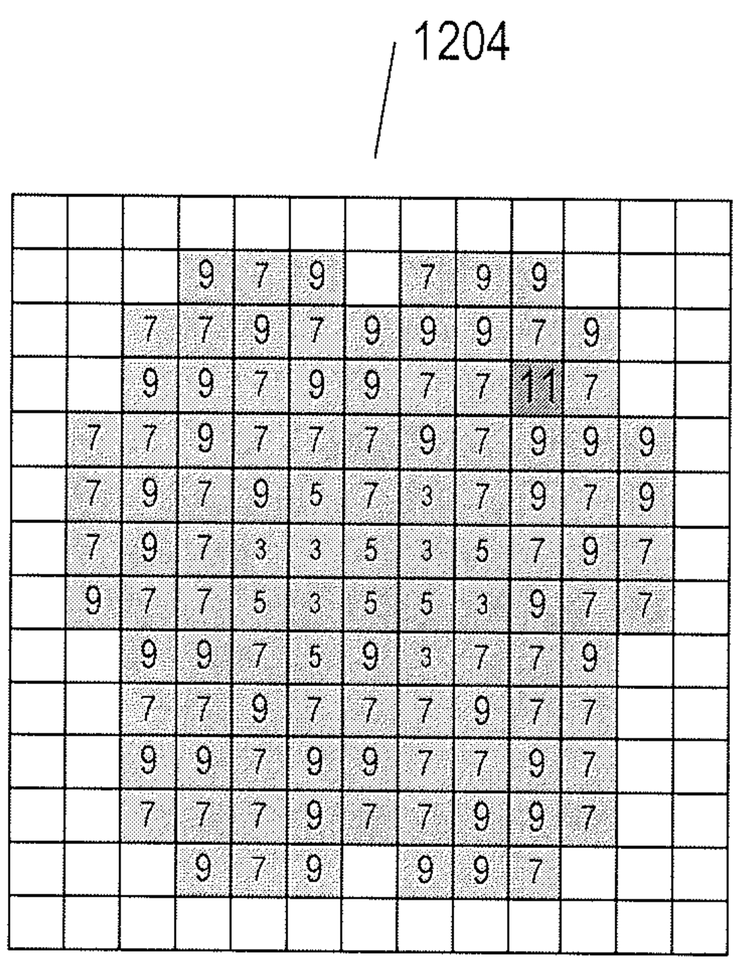

1206

Image A Intensity	Image B Intensity												
	0	1	2	3	4	5	6	7	8	9	10	11	12
1				1		6							
2				6		1							
3								31		19			
4								19		25		1	
5								1					

FIG. 12E

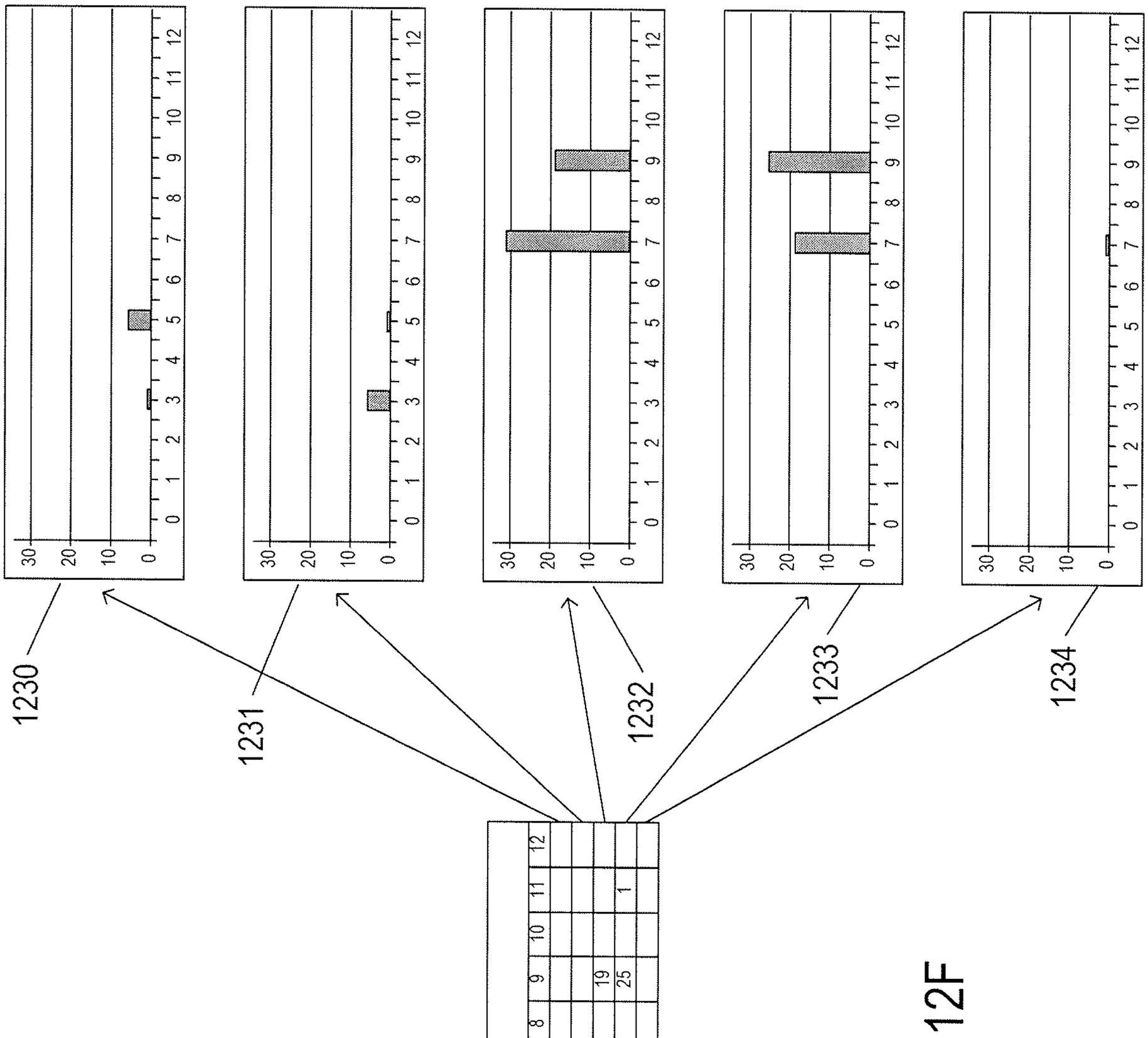
1230
1231
1232
1233
1234
1206
Image A Intensity
Image B Intensity

FIG. 12F

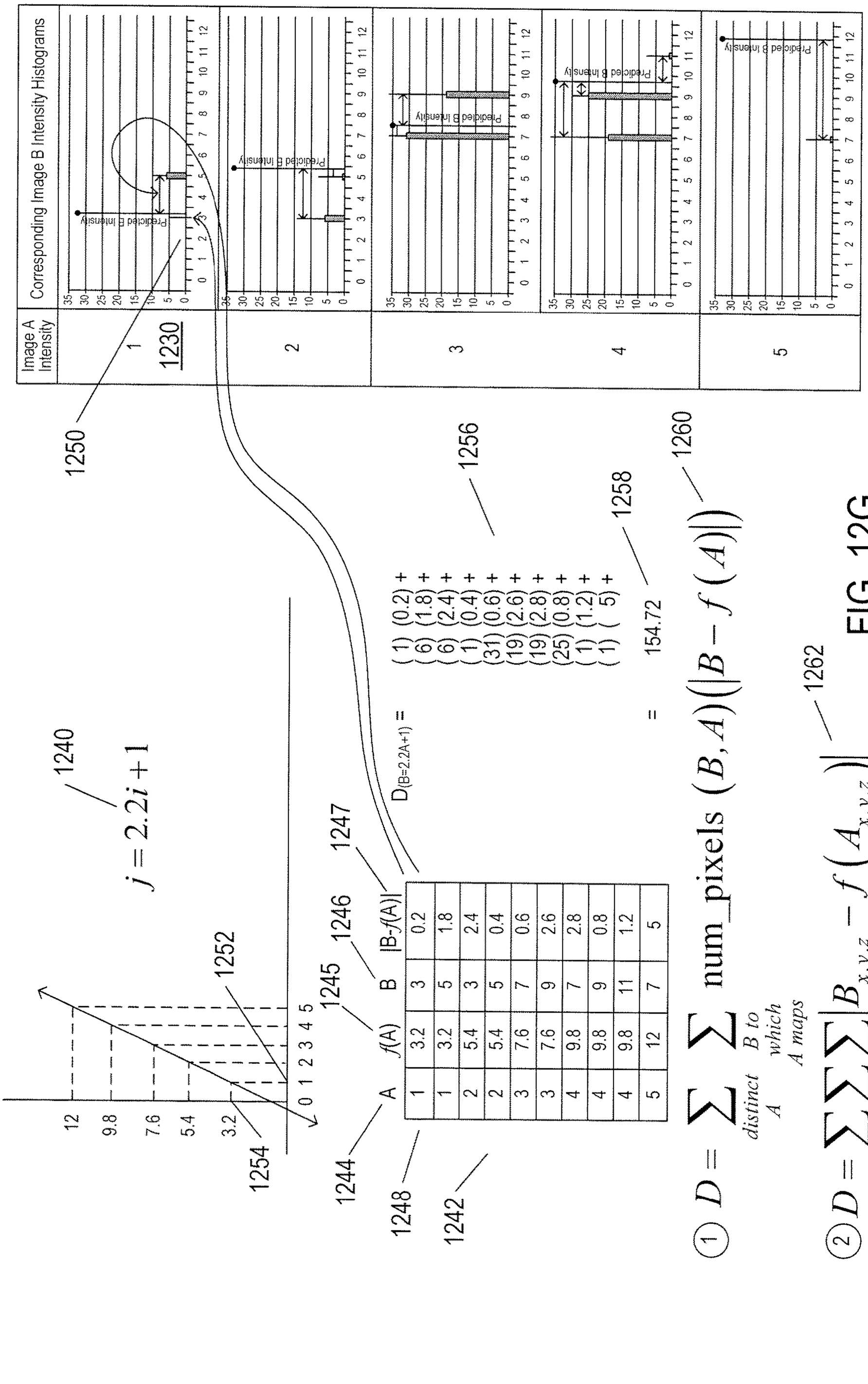
Image A Intensity
Corresponding Image B Intensity Histograms
1
2
3
4
5
1230
Predicted B Intensity
1250
1240
$j = 2.2i + 1$
1247
$D_{(B=2.2A+1)} =$
(1) (0.2) +
(6) (1.8) +
(6) (2.4) +
(1) (0.4) +
(31) (0.6) +
(19) (2.6) +
(19) (2.8) +
(25) (0.8) +
(1) (1.2) +
(1) (5) +
1256
1258
= 154.72
1260
$\left(B, A\right)\left(\left|B - f\left(A\right)\right|\right)$
1262
$f\left(A_{x,y,z}\right)\Big|$
12
9.8
7.6
5.4
3.2
0 1 2 3 4 5
1252
1254
1245
1246
1244
1248
1242
A f(A) B |B-f(A)|
1 3.2 3 0.2
1 3.2 5 1.8
2 5.4 3 2.4
2 5.4 5 0.4
3 7.6 7 0.6
3 7.6 9 2.6
4 9.8 7 2.8
4 9.8 9 0.8
4 9.8 11 1.2
5 12 7 5
① $D = \sum_{\substack{\text{distinct} \\ A}} \sum_{\substack{B \text{ to} \\ \text{which} \\ A \text{ maps}}} \text{num\_pixels}\left(B, A\right)\left(\left|B - f\left(A\right)\right|\right)$
② $D = \sum_{x} \sum_{y} \sum_{z} \left|B_{x,y,z} - f\left(A_{x,y,z}\right)\right|$

FIG. 12G

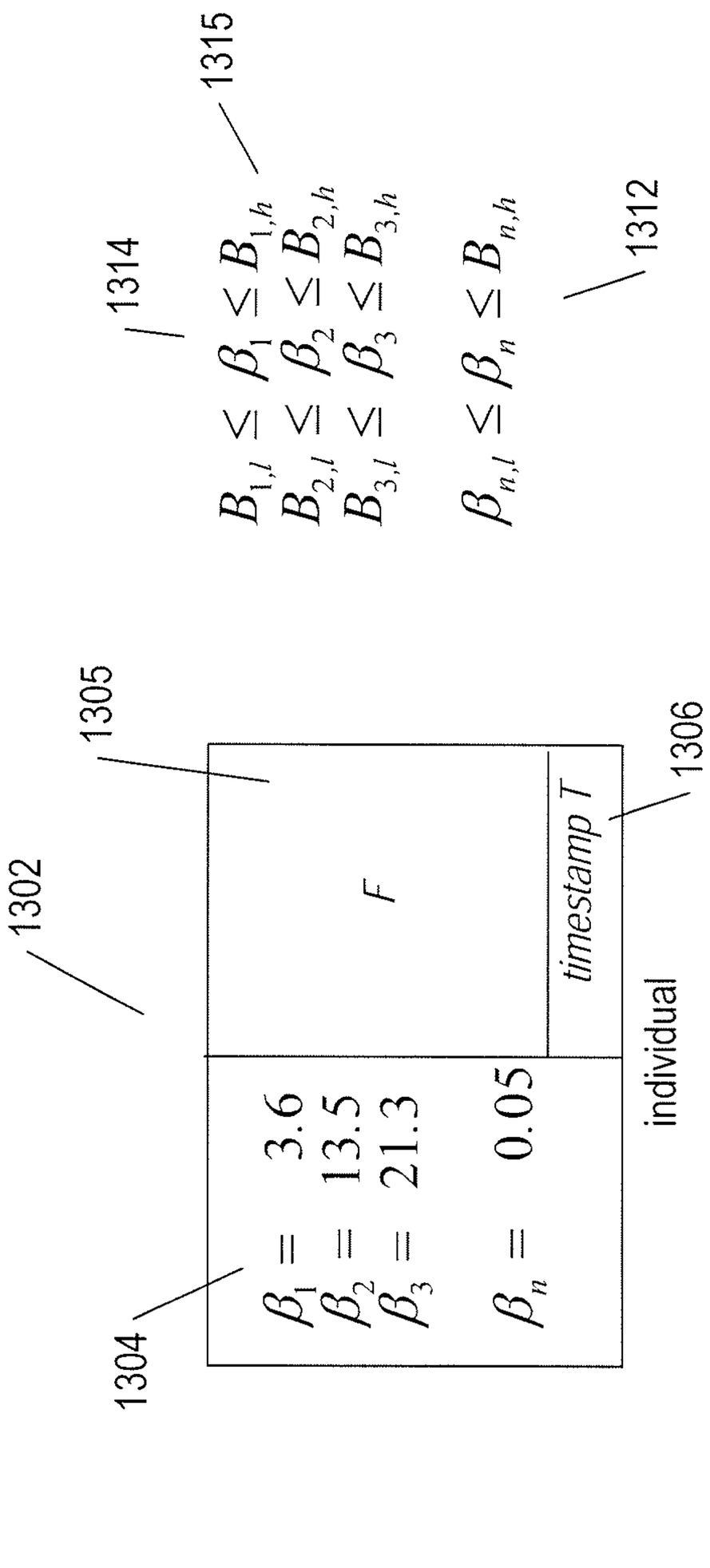
1314
1315
1312
1302
1305
1306
1304
1308
1310
individual
F
timestamp T
3.6 ≤ B1,h
13.5 ≤ B2,h
21.3 ≤ B3,h
0.05 ≤ Bn,h
B1,l ≤ β1
B2,l ≤ β2
B3,l ≤ β3
βn,l ≤ βn
β1 = 3.6
β2 = 13.5
β3 = 21.3
βn = 0.05
F = 1 − D / max D
F ∈ [0,1]

FIG. 13A

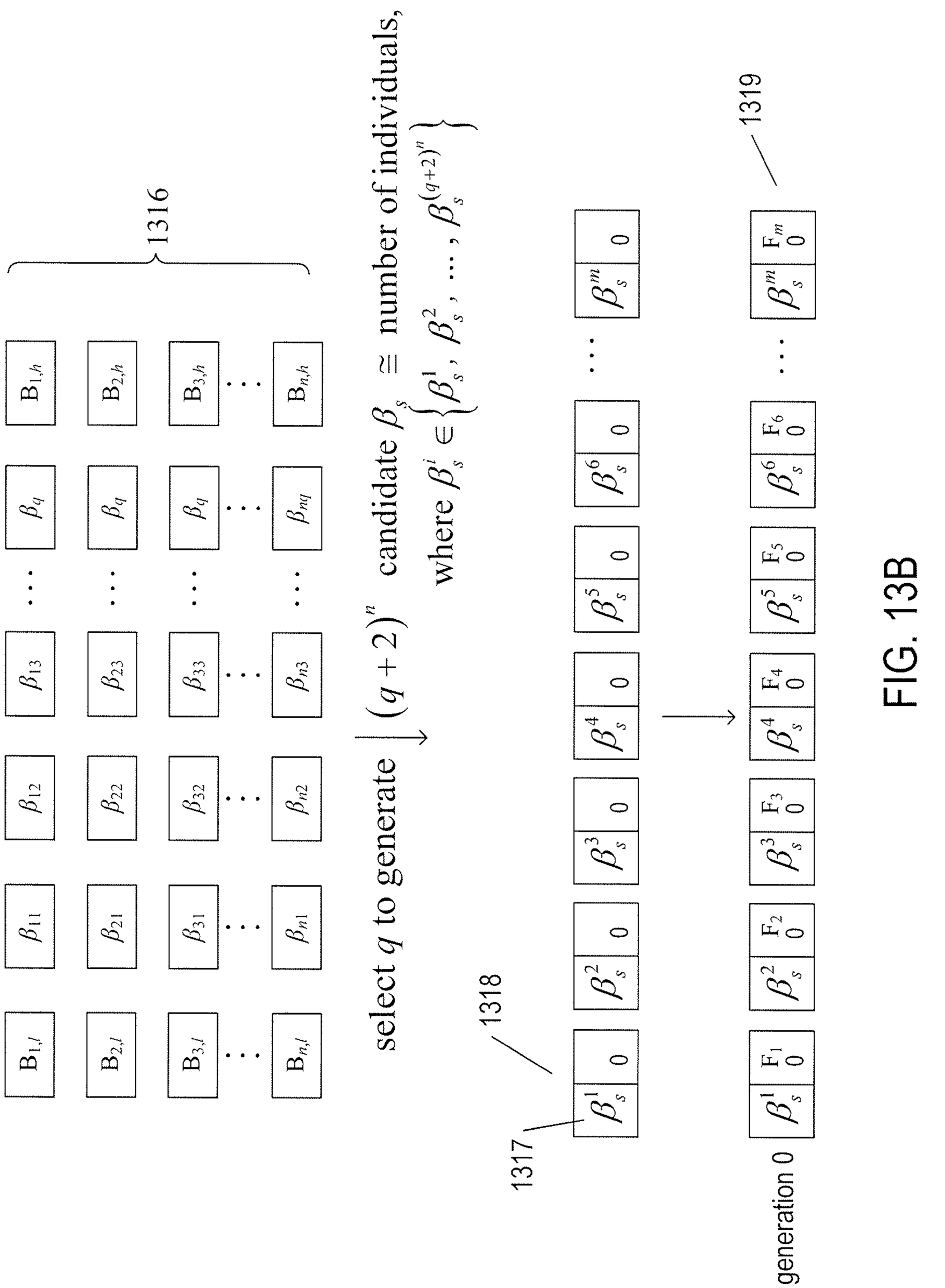
select q to generate $(q+2)^n$ candidate $\beta_s \cong$ number of individuals,
where $\beta_s^i \in \{\beta_s^1, \beta_s^2, \ldots, \beta_s^{(q+2)^n}\}$
1316
1317
1318
1319
generation 0

FIG. 13B

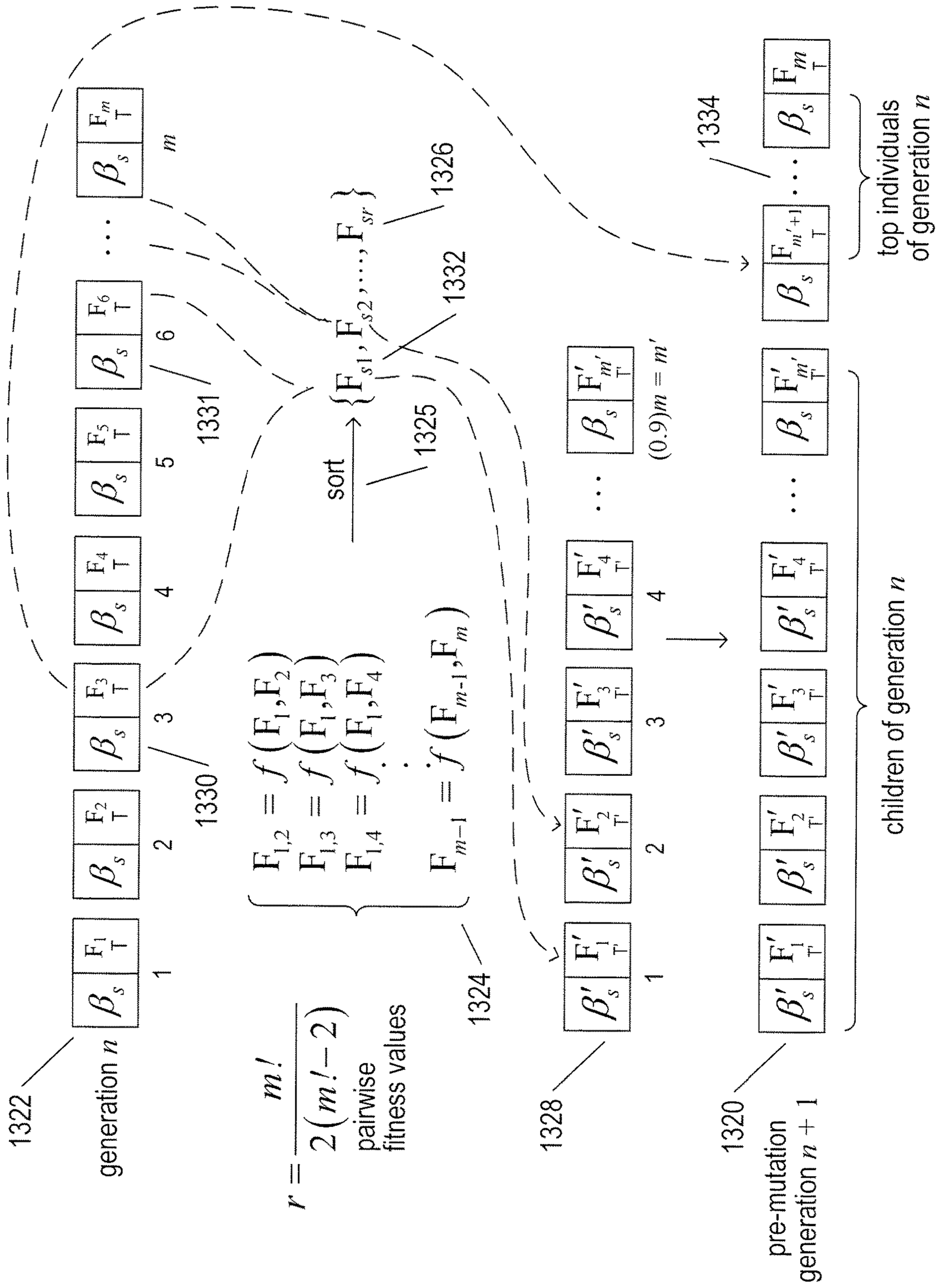
1322
generation n
1
2
3
4
5
6
m
1330
1331
1332
1334
1324
1325
1326
$r = \frac{m!}{2(m!-2)}$
pairwise fitness values
$\begin{cases} F_{1,2} = f(F_1, F_2) \\ F_{1,3} = f(F_1, F_3) \\ F_{1,4} = f(F_1, F_4) \\ \vdots \\ F_{m-1} = f(F_{m-1}, F_m) \end{cases}$
sort
$\{F_{s1}, F_{s2}, \ldots, F_{sr}\}$
top individuals of generation n
$(0.9)m = m'$
children of generation n
1328
1320
pre-mutation generation $n+1$

FIG. 13C

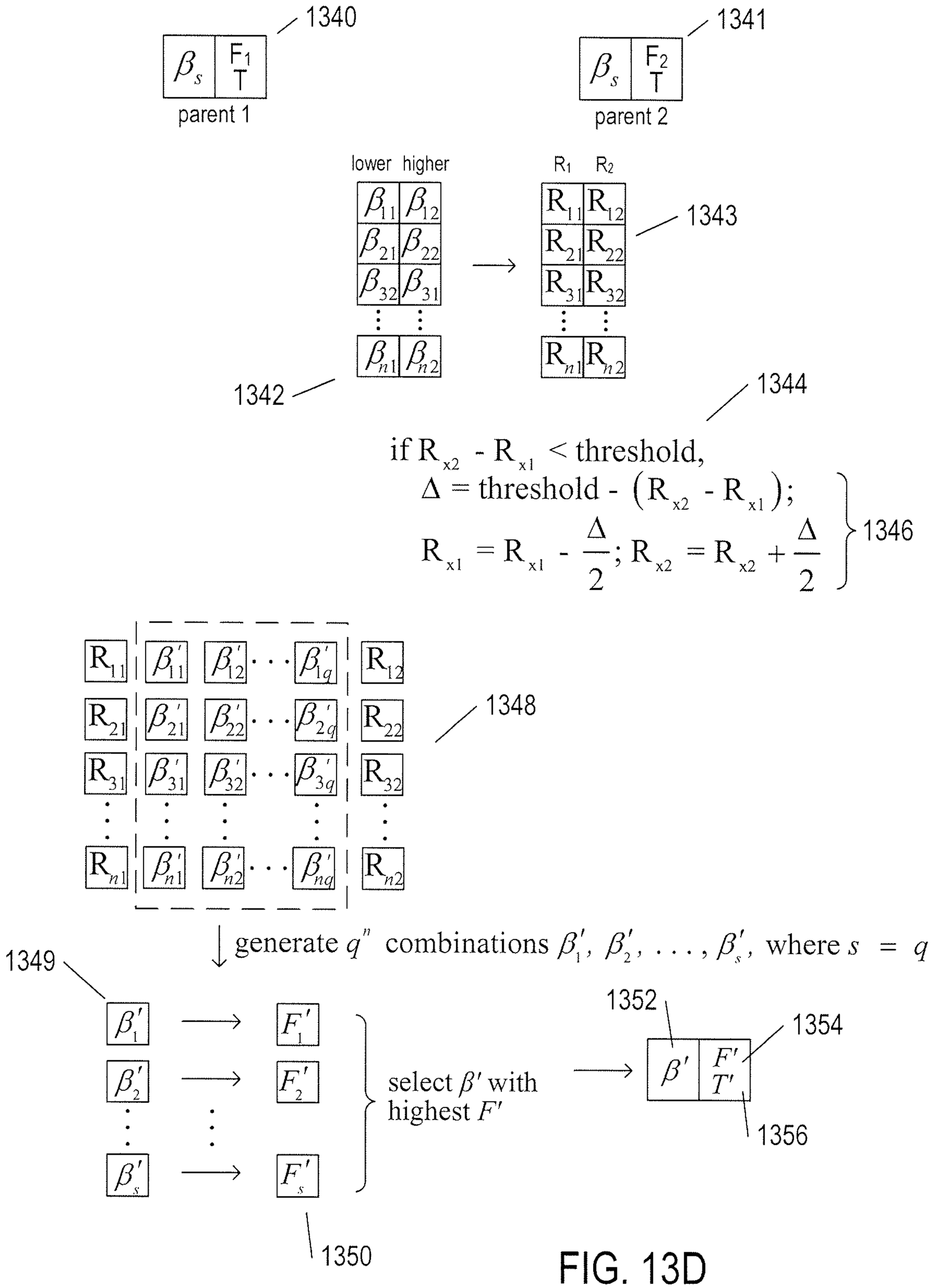
1340
β_s | F_1 T
parent 1
1341
β_s | F_2 T
parent 2
lower higher
β_{11} β_{12}
β_{21} β_{22}
β_{32} β_{31}
β_{n1} β_{n2}
1342
R_1 R_2
R_{11} R_{12}
R_{21} R_{22}
R_{31} R_{32}
R_{n1} R_{n2}
1343
1344
if $R_{x2} - R_{x1} < \text{threshold}$,
$\Delta = \text{threshold} - (R_{x2} - R_{x1})$;
$R_{x1} = R_{x1} - \frac{\Delta}{2}$; $R_{x2} = R_{x2} + \frac{\Delta}{2}$
1346
R_{11} β'_{11} $\beta'_{12} \cdots \beta'_{1q}$ R_{12}
R_{21} β'_{21} $\beta'_{22} \cdots \beta'_{2q}$ R_{22}
R_{31} β'_{31} $\beta'_{32} \cdots \beta'_{3q}$ R_{32}
R_{n1} β'_{n1} $\beta'_{n2} \cdots \beta'_{nq}$ R_{n2}
1348
generate q^n combinations $\beta'_1, \beta'_2, \ldots, \beta'_s$, where $s = q^n$
1349
β'_1 F'_1
β'_2 F'_2
β'_s F'_s
select β' with highest F'
1350
1352
β' F' T'
1354
1356

FIG. 13D

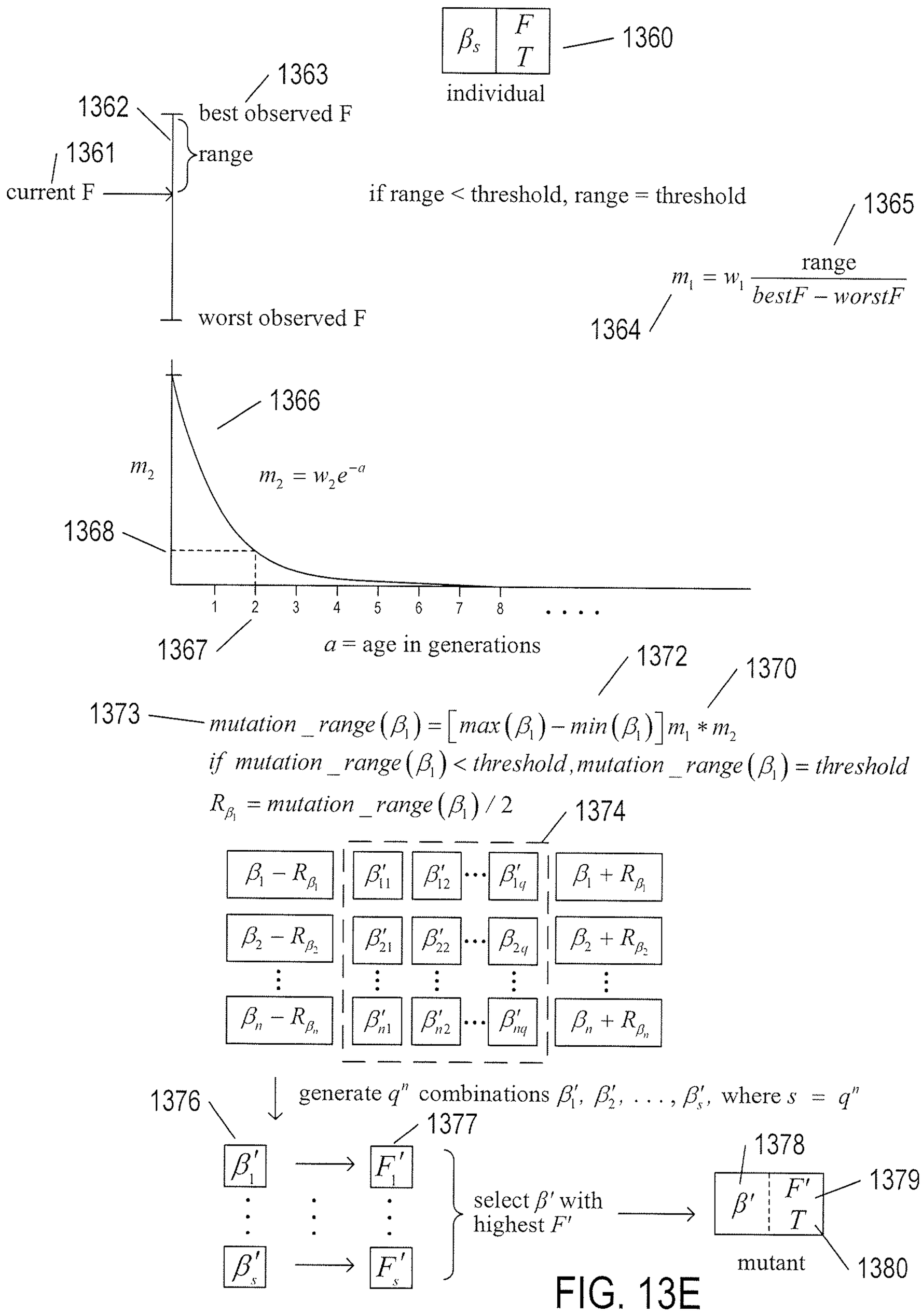
β_s F T
1360
individual
1363
1362
best observed F
1361
range
current F
worst observed F
if range < threshold, range = threshold
1365
$m_1 = w_1 \frac{\text{range}}{bestF - worstF}$
1364
1366
m_2
$m_2 = w_2 e^{-a}$
1368
1 2 3 4 5 6 7 8 . . . .
1367
a = age in generations
1372
1370
1373
$mutation\_range(\beta_1) = [max(\beta_1) - min(\beta_1)] m_1 * m_2$
$if\ mutation\_range(\beta_1) < threshold, mutation\_range(\beta_1) = threshold$
$R_{\beta_1} = mutation\_range(\beta_1) / 2$
1374
$\beta_1 - R_{\beta_1}$ β'_{11} β'_{12} ... β'_{1q} $\beta_1 + R_{\beta_1}$
$\beta_2 - R_{\beta_2}$ β'_{21} β'_{22} ... β_{2q} $\beta_2 + R_{\beta_2}$
$\beta_n - R_{\beta_n}$ β'_{n1} β'_{n2} ... β'_{nq} $\beta_n + R_{\beta_n}$
generate q^n combinations $\beta'_1, \beta'_2, \ldots, \beta'_s$, where $s = q^n$
1376
1377
β'_1 F'_1
β'_s F'_s
select β' with highest F'
1378
1379
β' F' T
mutant
1380

FIG. 13E

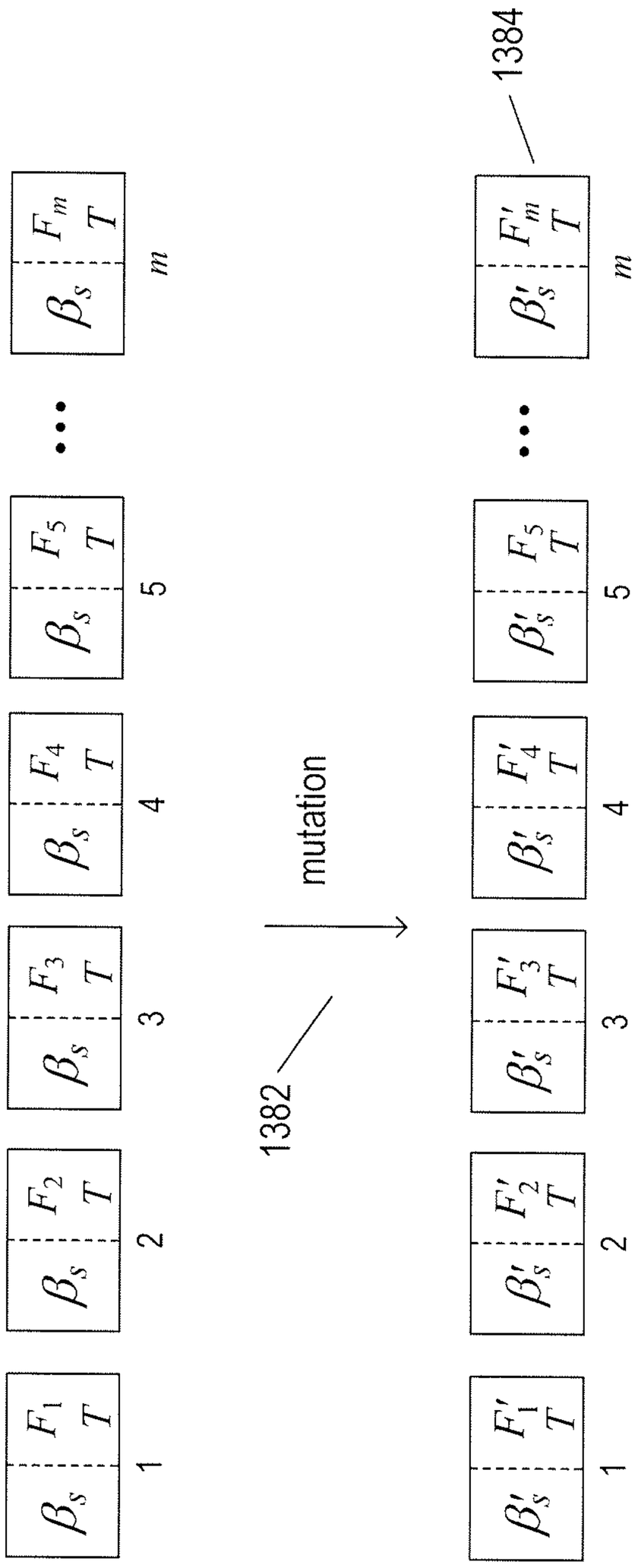
pre-mutation
generation $n+1$
generation $n+1$
mutation
1382
1384
β_s
F_1
T
1
F_2
2
F_3
3
F_4
4
F_5
5
β'_s
F'_1
F'_2
F'_3
F'_4
F'_5
m

FIG. 13F

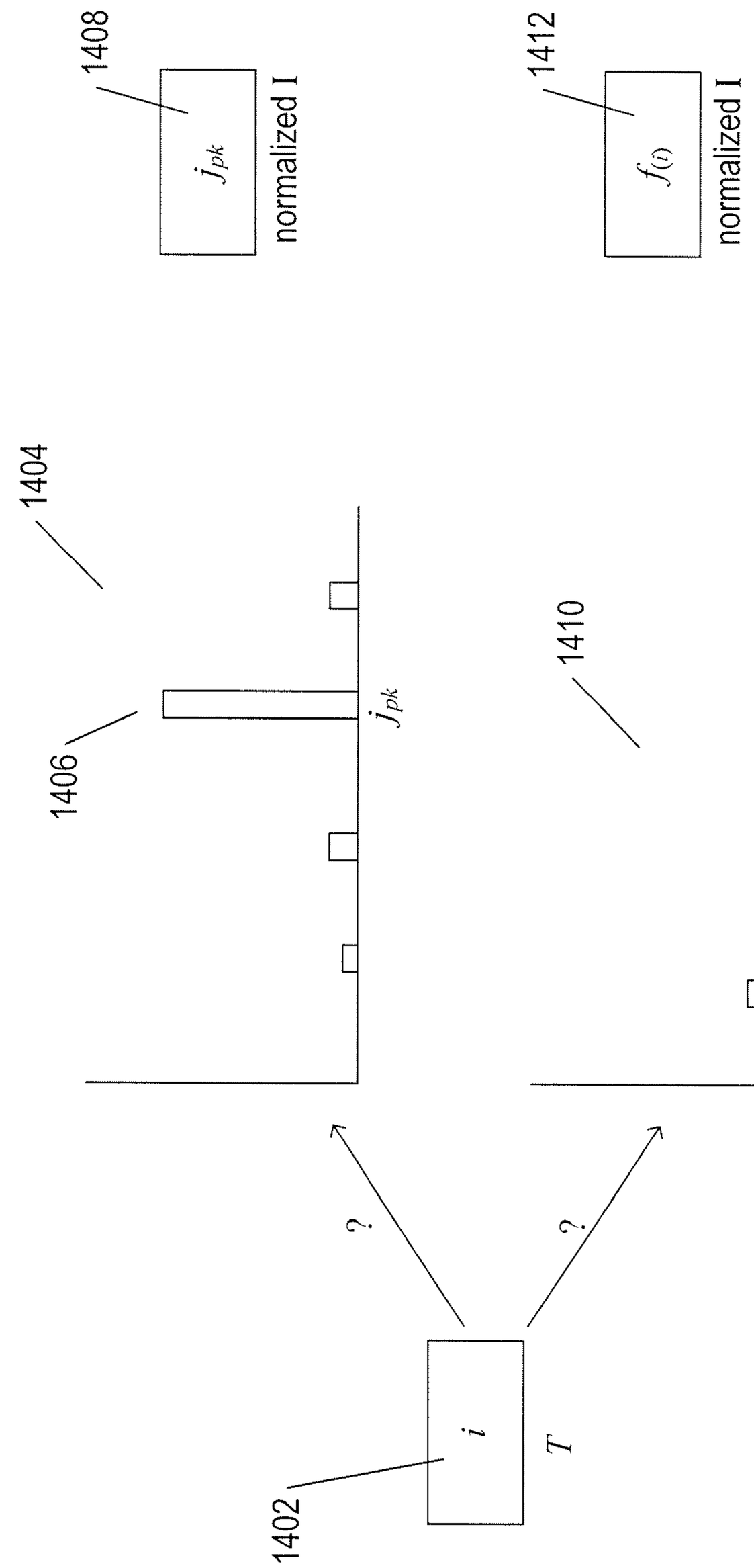
1408
j_{pk}
normalized I
1412
$f_{(i)}$
normalized I
1404
1406
j_{pk}
1410
?
?
1402
i
T

FIG. 14A

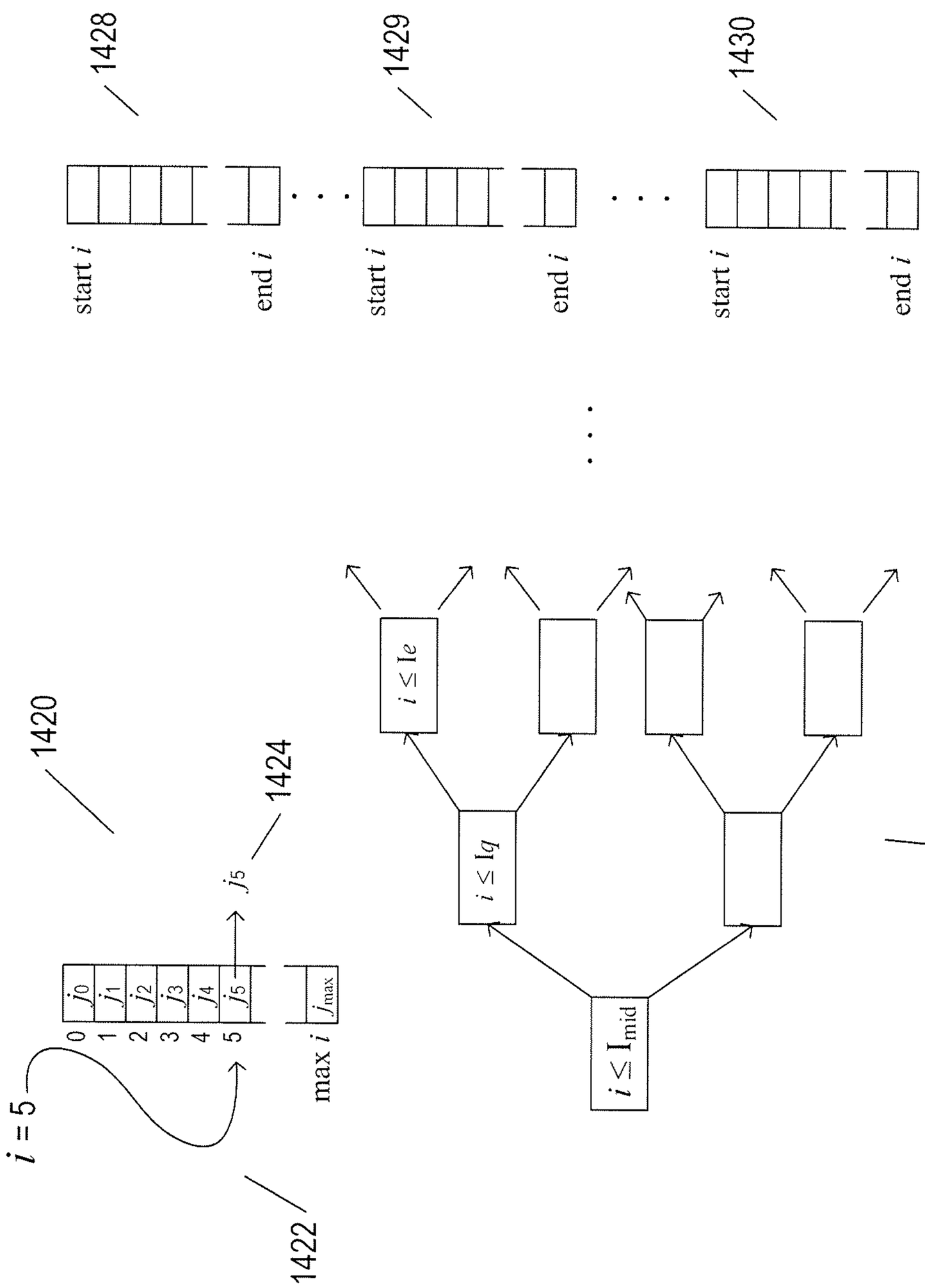
1428
1429
1430
start i
end i
start i
end i
start i
end i
1420
1424
j_5
$i = 5$
0 1 2 3 4 5
j_0 j_1 j_2 j_3 j_4 j_5
max i
j_{max}
1422
$i \leq Ie$
$i \leq Iq$
$i \leq I_{mid}$
1426

FIG. 14B

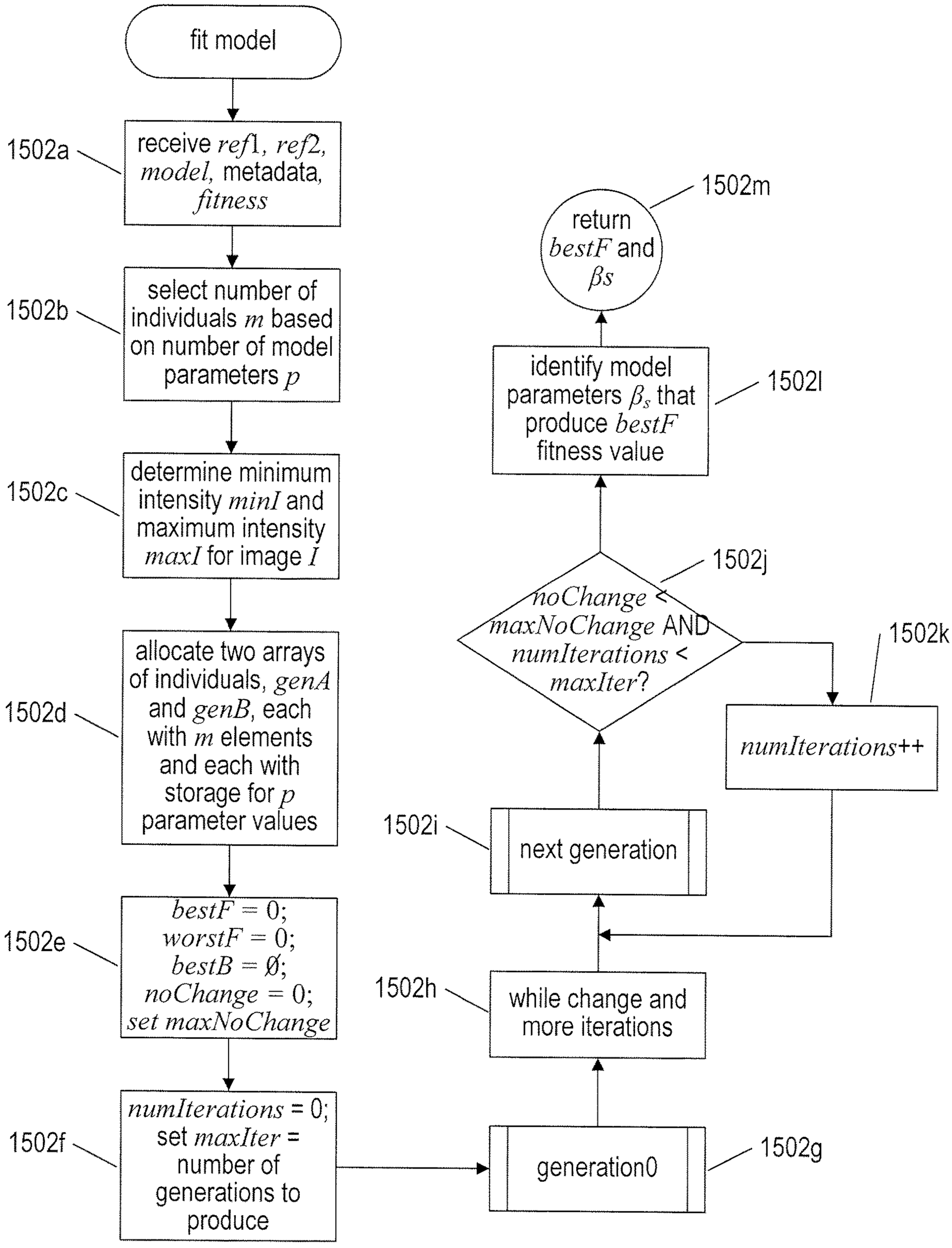
fit model
1502a
receive ref1, ref2, model, metadata, fitness
1502b
select number of individuals m based on number of model parameters p
1502c
determine minimum intensity minI and maximum intensity maxI for image I
1502d
allocate two arrays of individuals, genA and genB, each with m elements and each with storage for p parameter values
1502e
bestF = 0; worstF = 0; bestB = ∅; noChange = 0; set maxNoChange
1502f
numIterations = 0; set maxIter = number of generations to produce
1502g
generation0
1502h
while change and more iterations
1502i
next generation
1502j
noChange < maxNoChange AND numIterations < maxIter?
1502k
numIterations++
1502l
identify model parameters βs that produce bestF fitness value
1502m
return bestF and βs

FIG. 15A

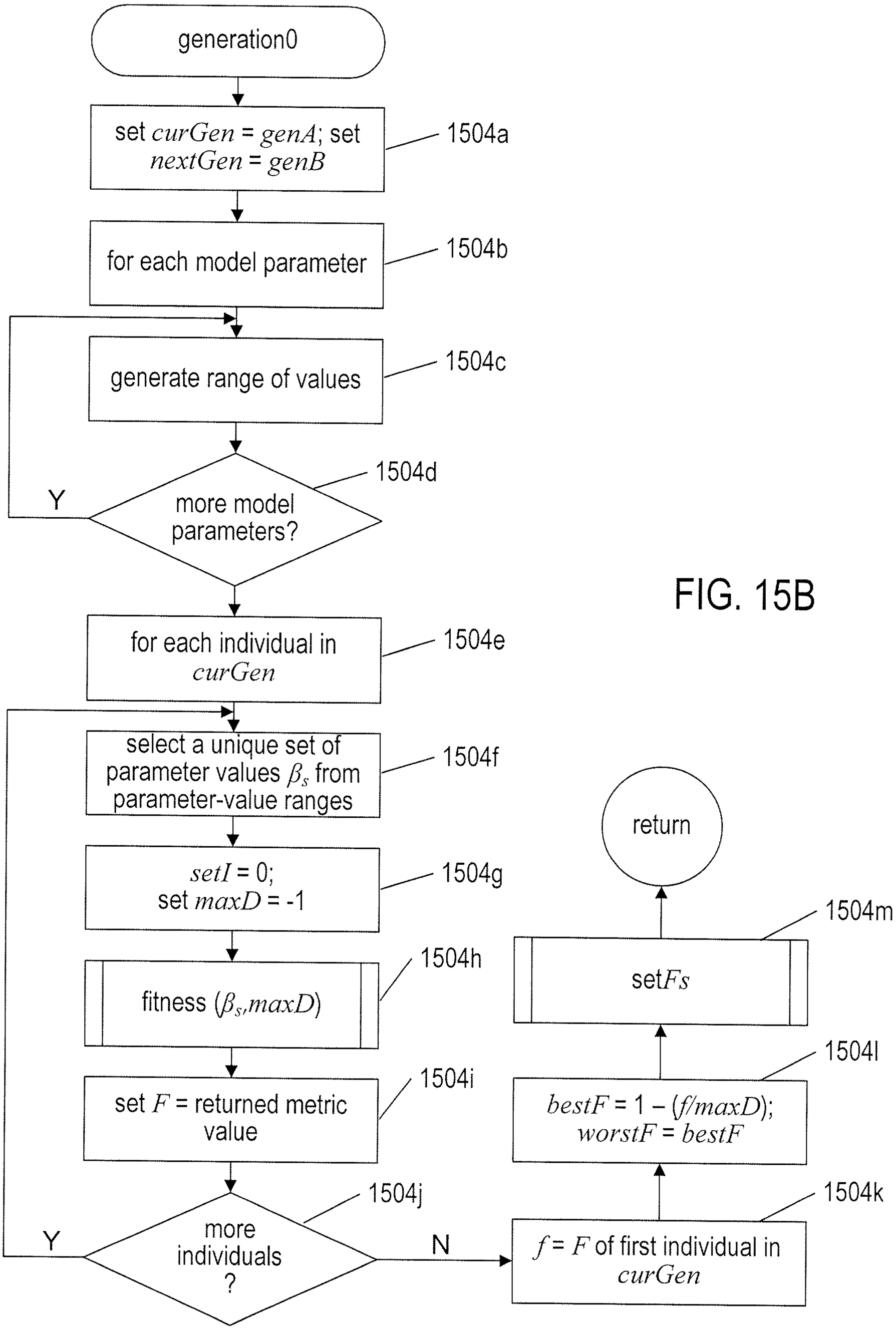
generation0
set curGen = genA; set nextGen = genB
1504a
for each model parameter
1504b
generate range of values
1504c
more model parameters?
1504d
Y
for each individual in curGen
1504e
select a unique set of parameter values β_s from parameter-value ranges
1504f
setI = 0; set maxD = -1
1504g
fitness (β_s,maxD)
1504h
set F = returned metric value
1504i
more individuals ?
1504j
Y
N
f = F of first individual in curGen
1504k
bestF = 1 – (f/maxD); worstF = bestF
1504l
setFs
1504m
return

FIG. 15B

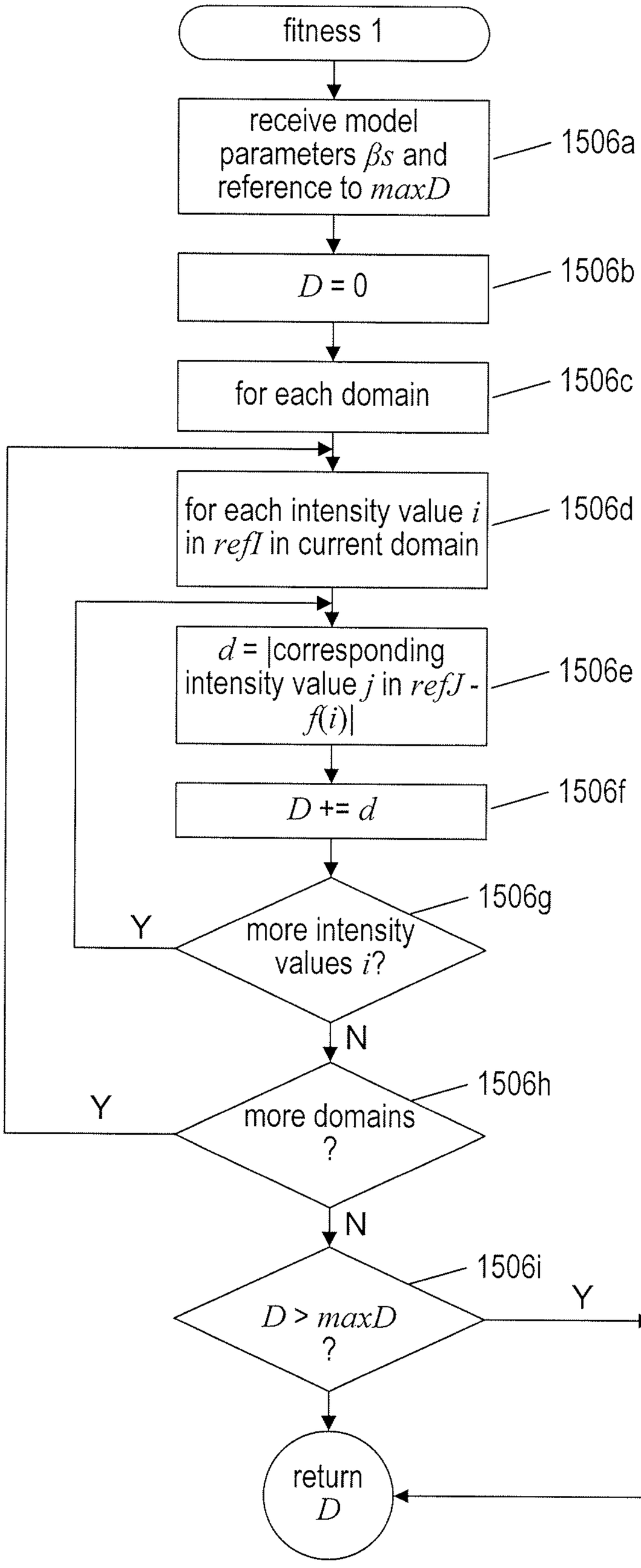
fitness 1
receive model parameters βs and reference to maxD
1506a
D = 0
1506b
for each domain
1506c
for each intensity value i in refI in current domain
1506d
d = |corresponding intensity value j in refJ - f(i)|
1506e
D += d
1506f
more intensity values i?
1506g
Y
N
more domains ?
1506h
Y
N
D > maxD ?
1506i
Y
maxD = D
1506j
return D

FIG. 15C

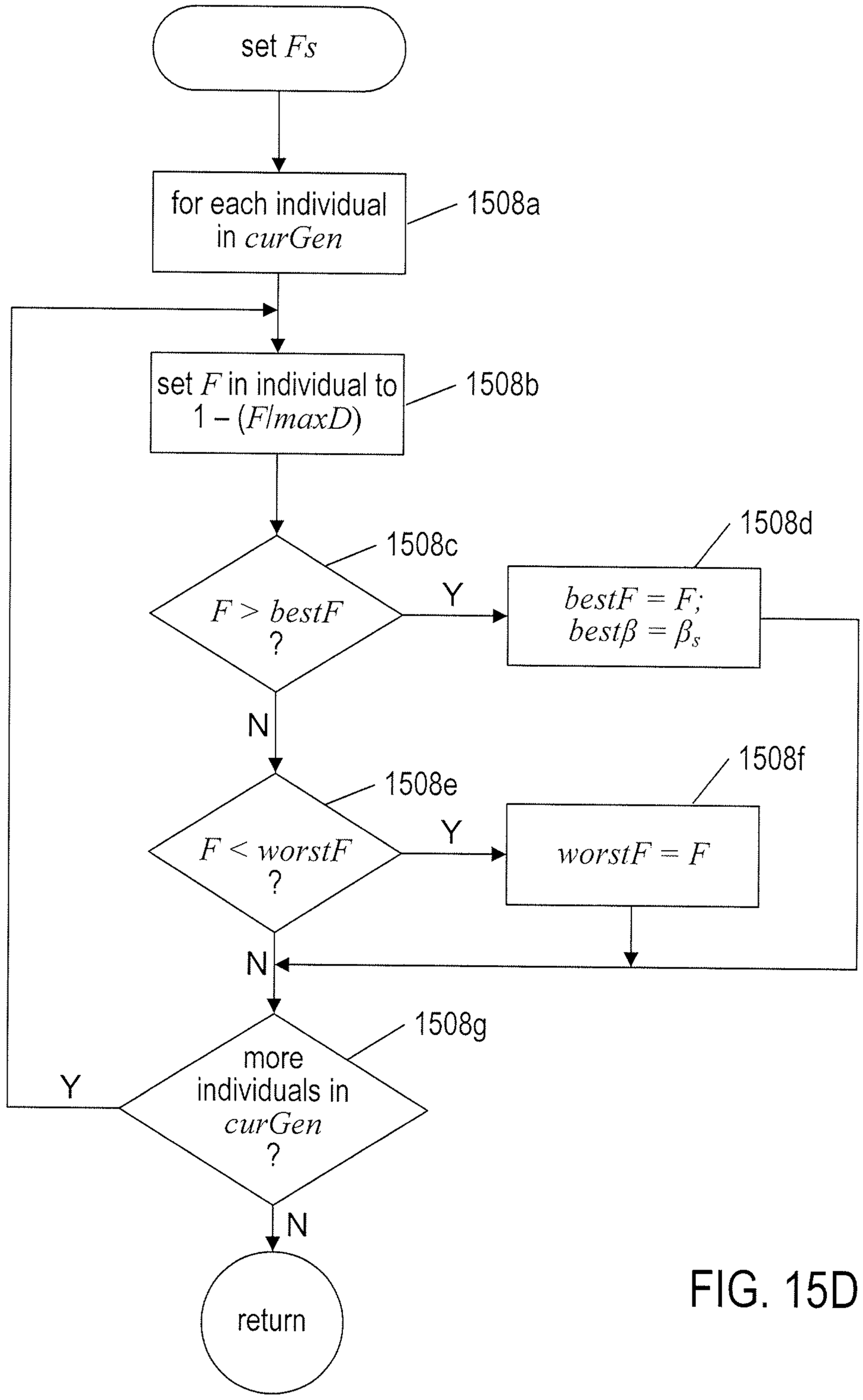
set Fs
for each individual in curGen
1508a
set F in individual to 1 – (F/maxD)
1508b
F > bestF ?
1508c
Y
bestF = F; bestβ = βs
1508d
N
F < worstF ?
1508e
Y
worstF = F
1508f
N
more individuals in curGen ?
1508g
Y
N
return

FIG. 15D

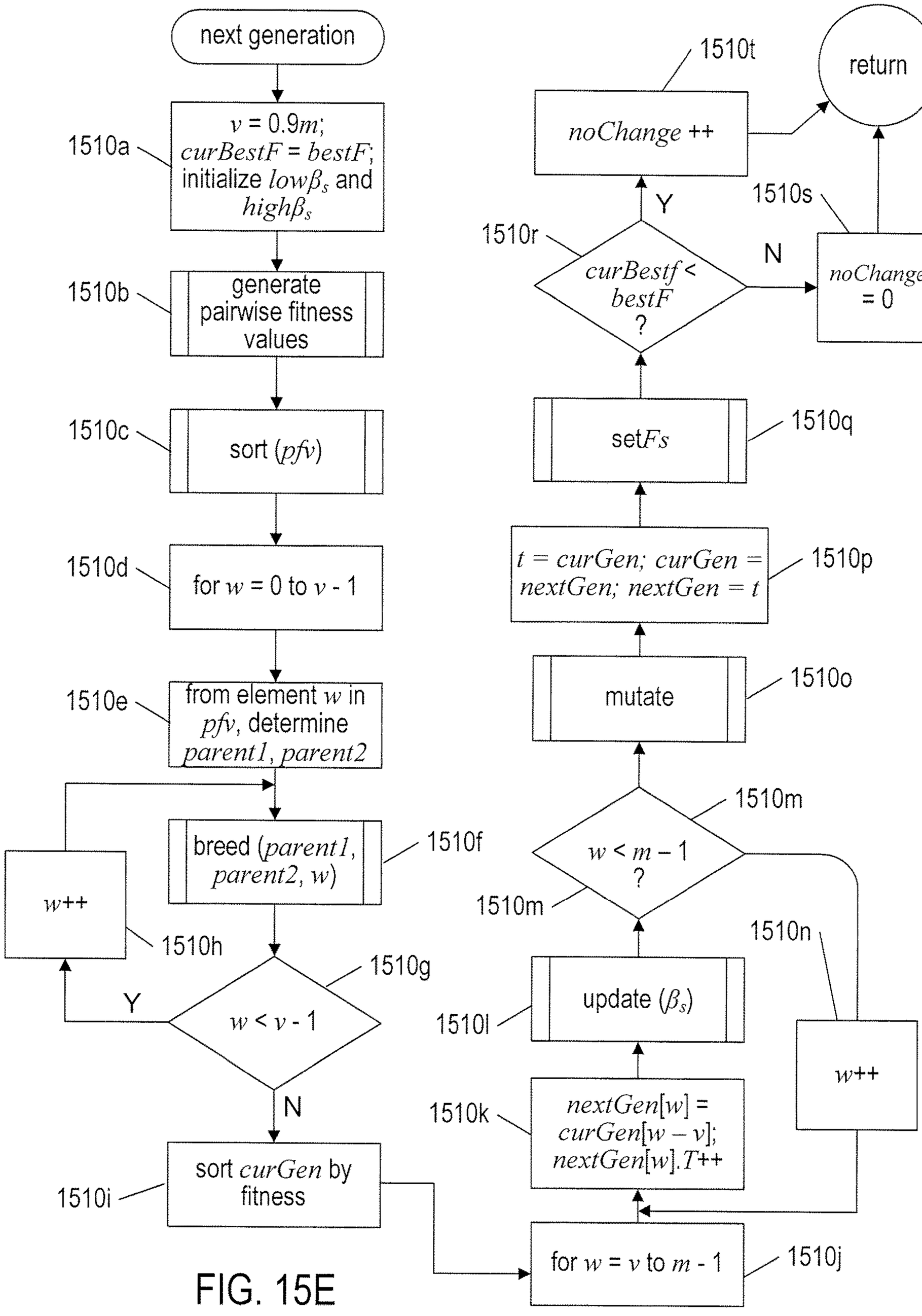
next generation
1510a
$v = 0.9m$; $curBestF = bestF$; initialize $low\beta_s$ and $high\beta_s$
1510b
generate pairwise fitness values
1510c
sort (pfv)
1510d
for w = 0 to v - 1
1510e
from element w in pfv, determine $parent1$, $parent2$
1510f
breed ($parent1$, $parent2$, w)
w++
1510h
1510g
Y
$w < v - 1$
N
1510i
sort $curGen$ by fitness
1510j
for $w = v$ to $m - 1$
1510k
$nextGen[w] = curGen[w - v]$; $nextGen[w].T$++
1510l
update (β_s)
1510m
$w < m - 1$?
1510m
1510n
w++
1510o
mutate
1510p
$t = curGen$; $curGen = nextGen$; $nextGen = t$
1510q
setFs
1510r
$curBestf < bestF$?
Y
N
1510s
$noChange$ = 0
1510t
$noChange$ ++
return

FIG. 15E

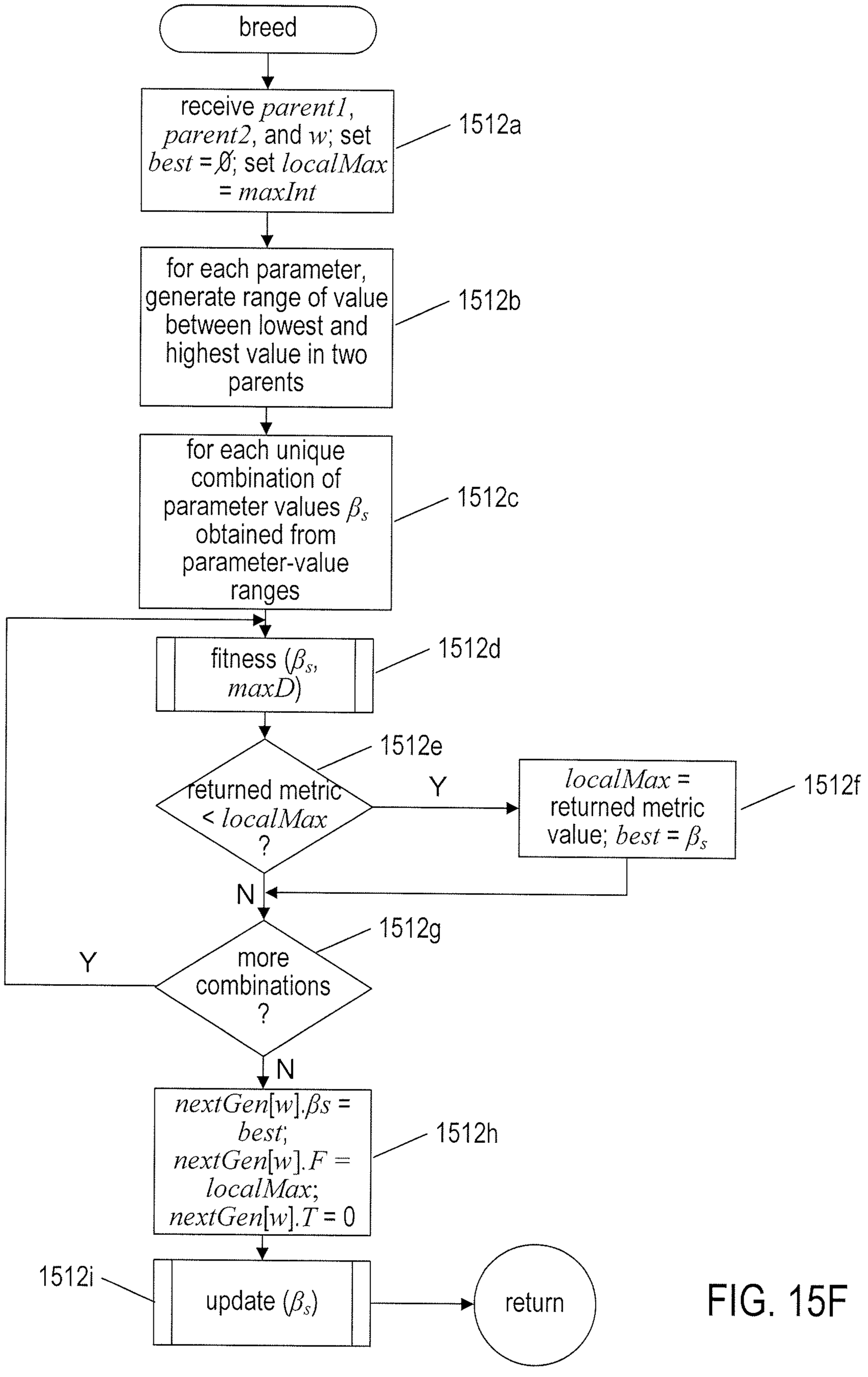
breed
receive parent1, parent2, and w; set best = Ø; set localMax = maxInt
1512a
for each parameter, generate range of value between lowest and highest value in two parents
1512b
for each unique combination of parameter values β_s obtained from parameter-value ranges
1512c
fitness (β_s, maxD)
1512d
1512e
returned metric < localMax ?
Y
localMax = returned metric value; best = β_s
1512f
N
1512g
more combinations ?
Y
N
nextGen[w].βs = best; nextGen[w].F = localMax; nextGen[w].T = 0
1512h
1512i
update (β_s)
return

FIG. 15F

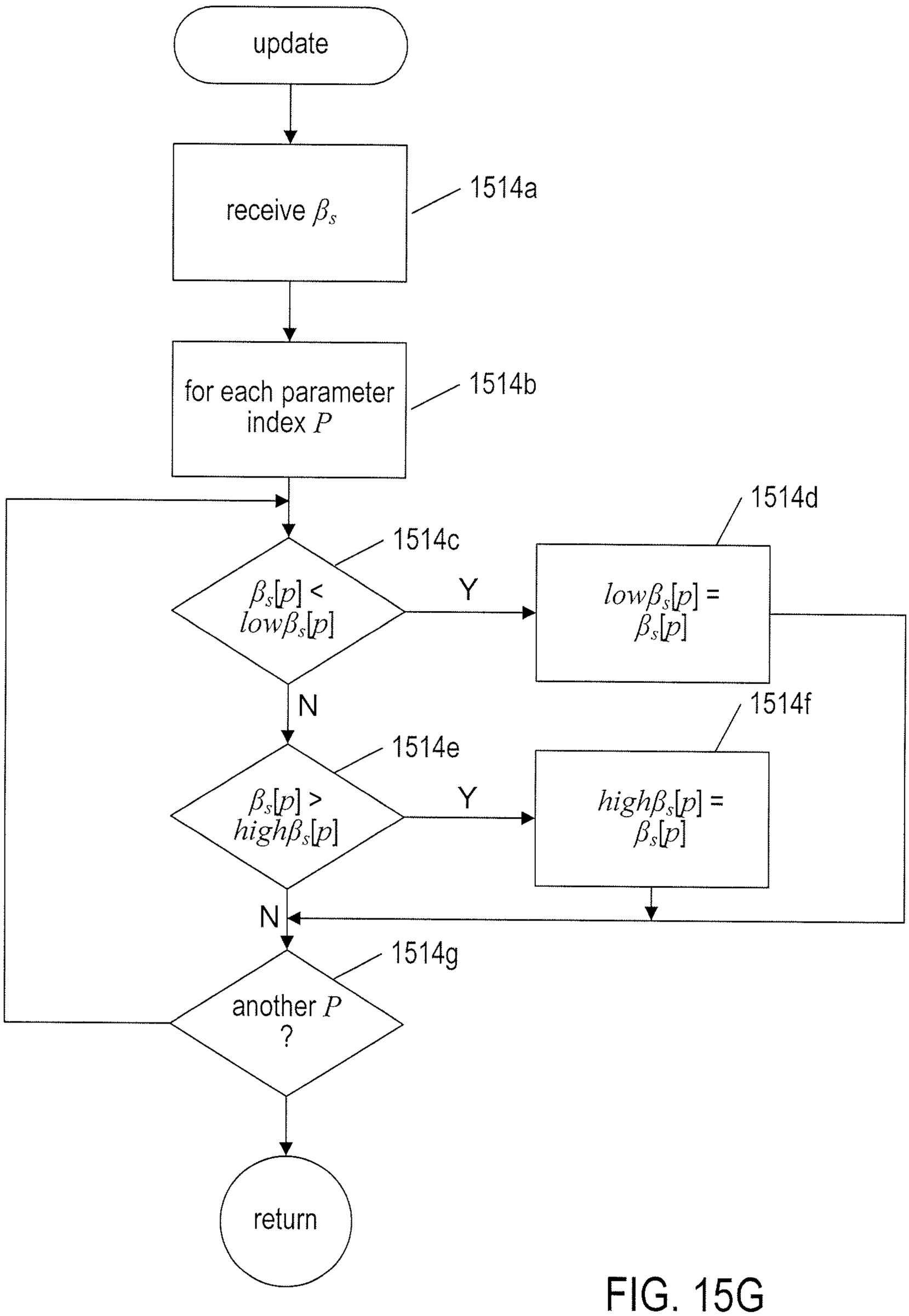
update
receive β_s
1514a
for each parameter index P
1514b
1514c
$\beta_s[p] < low\beta_s[p]$
Y
1514d
$low\beta_s[p] = \beta_s[p]$
N
1514e
$\beta_s[p] > high\beta_s[p]$
Y
1514f
$high\beta_s[p] = \beta_s[p]$
N
1514g
another P ?
return

FIG. 15G

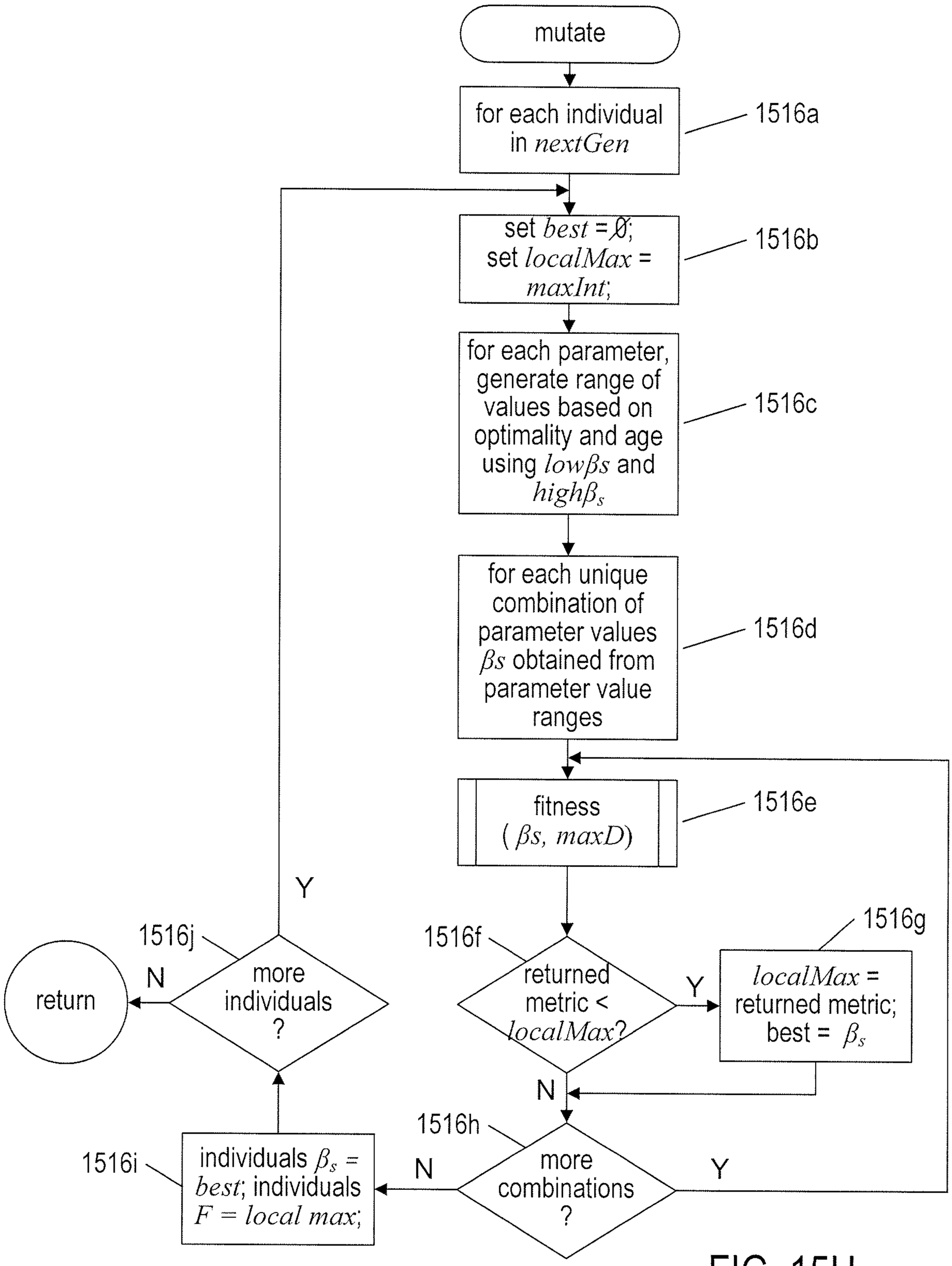
mutate
for each individual in nextGen
1516a
set best = Ø; set localMax = maxInt;
1516b
for each parameter, generate range of values based on optimality and age using lowβs and highβs
1516c
for each unique combination of parameter values βs obtained from parameter value ranges
1516d
fitness (βs, maxD)
1516e
Y
1516f
returned metric < localMax?
Y
1516g
localMax = returned metric; best = βs
N
1516h
more combinations ?
N
Y
1516i
individuals βs = best; individuals F = local max;
1516j
more individuals ?
N
return
Y

FIG. 15H

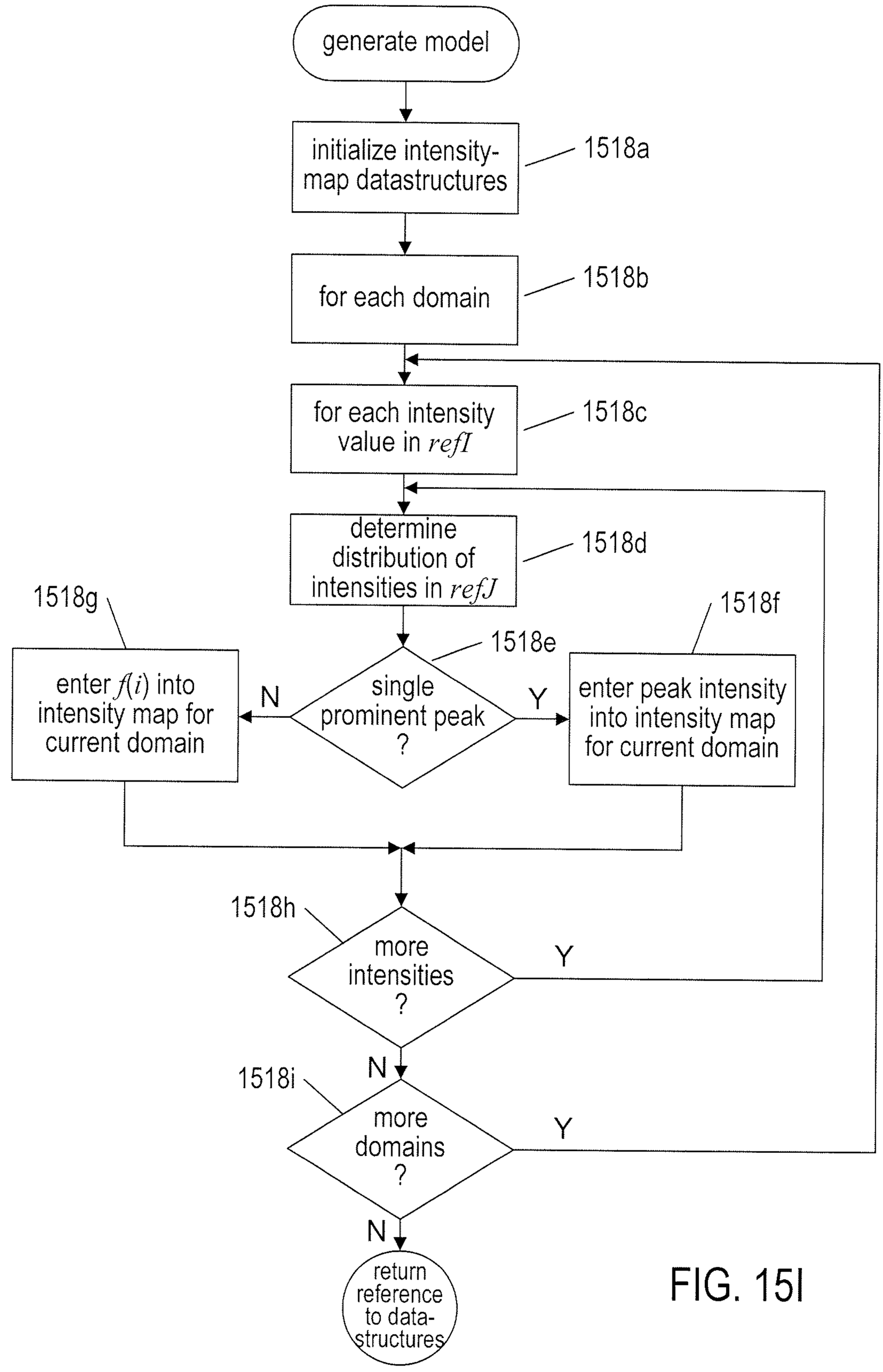
generate model
initialize intensity-map datastructures
1518a
for each domain
1518b
for each intensity value in refI
1518c
determine distribution of intensities in refJ
1518d
1518g
enter f(i) into intensity map for current domain
N
1518e
single prominent peak ?
Y
1518f
enter peak intensity into intensity map for current domain
1518h
more intensities ?
Y
N
1518i
more domains ?
Y
N
return reference to data-structures

FIG. 15I

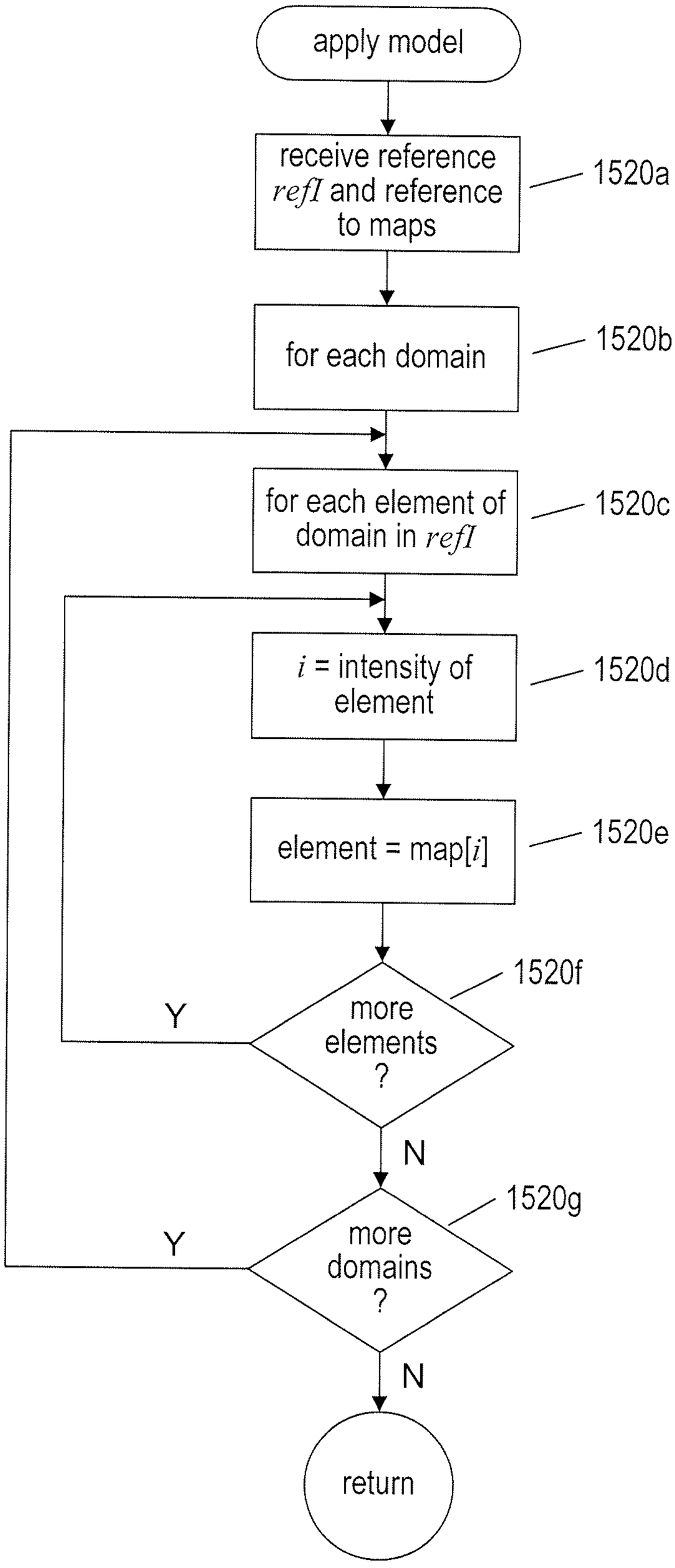
apply model
receive reference *refI* and reference to maps
1520a
for each domain
1520b
for each element of domain in *refI*
1520c
i = intensity of element
1520d
element = map[*i*]
1520e
more elements ?
1520f
Y
N
more domains ?
1520g
Y
N
return

FIG. 15J

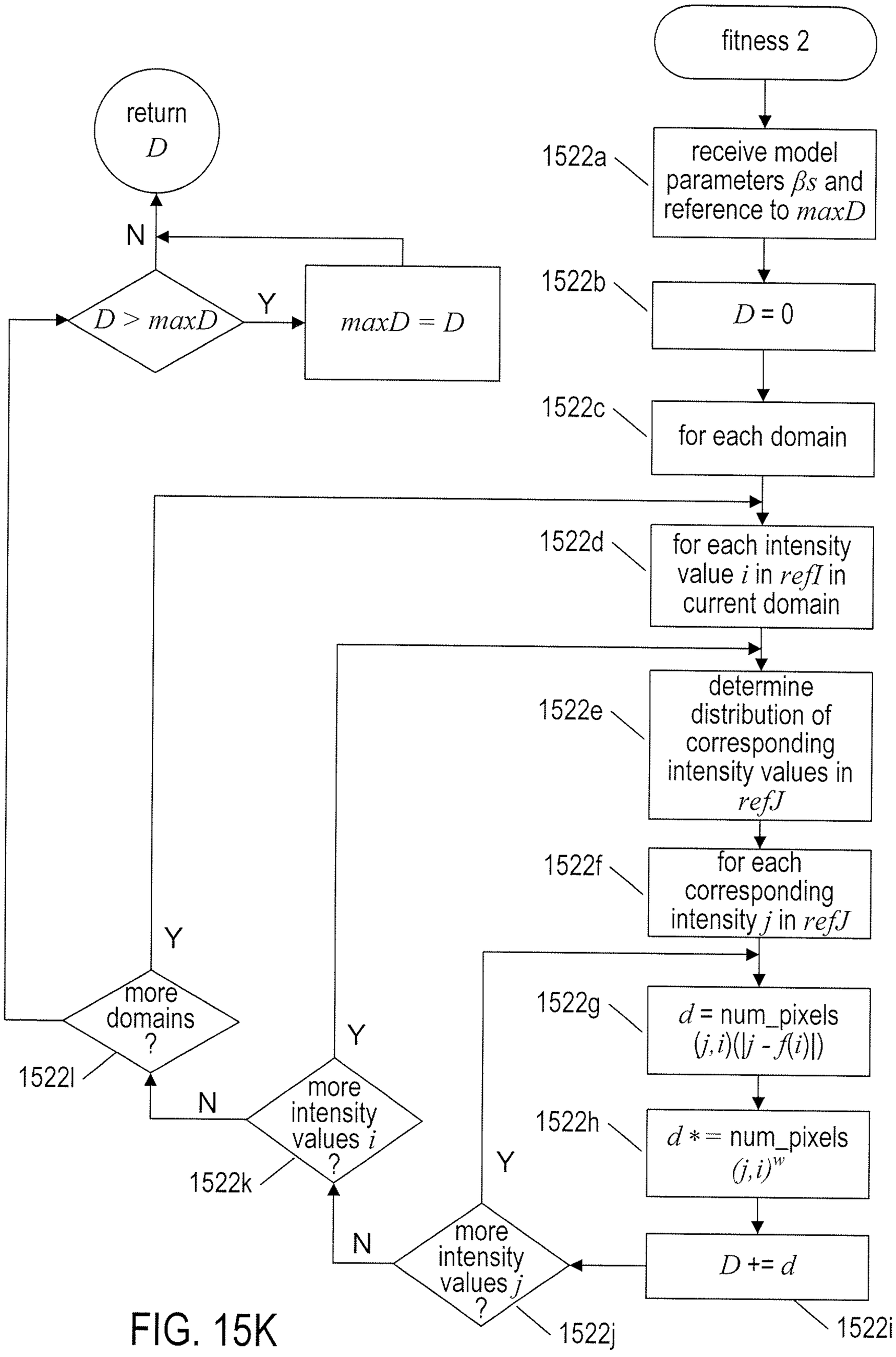
fitness 2
1522a
receive model parameters βs and reference to maxD
1522b
D = 0
1522c
for each domain
1522d
for each intensity value i in refI in current domain
1522e
determine distribution of corresponding intensity values in refJ
1522f
for each corresponding intensity j in refJ
1522g
d = num_pixels (j,i)(|j - f(i)|)
1522h
d *= num_pixels (j,i)^w
1522i
D += d
1522j
more intensity values j ?
Y
N
1522k
more intensity values i ?
Y
N
1522l
more domains ?
Y
N
return D

FIG. 15K

METHODS AND SYSTEMS FOR NORMALIZING IMAGES

CROSS-REFERENCE TO RELATED APPLICATION

This application is a divisional of application Ser. No. 15/347,681, filed Nov. 9, 2016.

TECHNICAL FIELD

The current application is directed to digital-image processing and, in particular, to methods and systems that normalize intensities within images in preparation for digital-image comparison.

BACKGROUND

Digital-image processing is a broad and a important field that provides foundation technologies for many types of diagnosis, monitoring, surveillance, data collection, and data analysis. Digital-image-processing methods are used in medical imaging, optical-character-recognition systems, processing and analysis of image data collected by surveillance, monitoring, and remote-sensing systems, production of informational and entertainment videos, and digital photography. A variety of sophisticated mathematical techniques have been developed to address many problem domains in digital-image processing, including reduction of noise in digital images, sharpening of imaged features in digital images, extraction of information from digital images, and many other such problem domains.

In many areas of digital-image processing and analysis, two or more different images are compared in order to extract differential information from the two or more images corresponding to various types of changes. As one example, frames of surveillance videos may be compared to one another by automated techniques in order to extract information related to temporal changes in the environment being monitored. Surveillance videos are often collected continuously from various types of environments, such as building entrances and the interiors of train stations and airports, and automated, analytical methodologies based on automated comparison of frames from such videos are applied to hours of days of recorded surveillance video in order to pinpoint particular anomalous events that occurred at particular points of time during surveillance. In other cases, frame-comparison-based methods are employed in real time to detect anomalous events and trigger alerts. As another example, a time sequence of digital medical images of a tumor or other pathology may be compared in order to detect changes in the tumor or other pathology over time. Often, digital images are compared by subtracting the intensity values in one image from the intensity values of another, in order to detect intensity differences between the two images. However, many intensity differences between images may arise from phenomena unrelated to the types of changes and events of interest. For example, the intensities in two different medical images may differ systematically due to differences in the imaging devices used to acquire the images, differences in image-device settings and parameters, random and systematic noise in the digital images, and many other types of intensity-altering phenomena. Normalization of images is therefore a major problem domain in image processing. Normalization seeks to reduce or eliminate systematic intensity variation between images, in preparation for image comparison, without losing or obscuring the meaningful, but often subtle, intensity differences that are sought to be extracted by digital-image-comparison techniques.

SUMMARY

The current document is directed to digital-image-normalization methods and systems that generate accurate intensity mappings between the intensities in two digital images. The intensity mapping generated from two digital images is used to normalize or adjust the intensities in one image in order to produce a pair of normalized digital images to which various types of change-detection methodologies can be applied in order to extract differential data. In one approach, a mapping model is selected to provide a basis for statistically meaningful intensity normalization. In this implementation, a genetic optimization approach is used to determine and refine model parameters. The implementation produces a hybrid intensity mapping that includes both intensity mappings calculated by application of the mapping model and intensity mappings obtained directly from comparison of the images.

BRIEF DESCRIPTION OF THE DRAWINGS

FIG. **1** provides a general architectural diagram for various types of computers.

FIG. **2** illustrates generalized hardware and software components of a general-purpose computer system, such as a general-purpose computer system having an architecture similar to that shown in FIG. **1**.

FIG. **3** illustrates a virtual machine and virtual-machine execution environment.

FIG. **4** illustrates two different types of digital images.

FIGS. **5**A-B illustrate digital-image comparison.

FIGS. **6**A-D illustrate the effect of noise on the digital-image-comparison process discussed above with reference to FIGS. **5**A-B.

FIGS. **7**A-D show similar examples to those shown in FIG. **6**A-D, but with the pixels corresponding to the imaged cruciform object having relatively low intensity values compared to the intensities of the pixels corresponding to the imaged cruciform object in FIG. **6**A.

FIGS. **8**A-D show a different example of image comparison using the same illustration conventions used in FIGS. **6**A-D and FIGS. **7**A-D.

FIGS. **9**A-B illustrate a typical result obtained by digital-image comparison.

FIGS. **10**A-B illustrate underlying concepts of the currently disclosed normalization methods and systems.

FIG. **11** provides a control-flow diagram for one implementation of the currently disclosed methods and systems.

FIGS. **12**A-G illustrate tabulation of pixel-intensity mappings and generation of a difference metric value for a particular mapping model.

FIGS. **13**A-F illustrate aspects of a genetic mapping-function-parameter-fitting method that is used to optimize parameter values for a mapping function that maps intensities from a first image to a second image within at least a pair of image domains.

FIGS. **14**A-B illustrate the final intensity-mapping model produced by the currently disclosed methods and system.

FIGS. **15**A-K provide control-flow diagrams that illustrate one implementation of the routine "fit model," called in step **1111** of FIG. **11**.

DETAILED DESCRIPTION OF EMBODIMENTS

The current document is directed to digital-image-normalization methods and systems. In a first subsection, below,

an overview of computer systems is provided, with reference to FIGS. **1-3**. In a second subsection, provided below, a description of digital images and digital-image-comparison operations is provided with reference to FIGS. **4-9**B. In a third subsection, implementations of the currently disclosed methods and systems are provided with reference to FIGS. **10**A-**15**K.

Overview of Computer Systems and Computer Architecture

FIG. **1** provides a general architectural diagram for various types of computers. The computer system contains one or multiple central processing units ("CPUs") **102-105**, one or more electronic memories **108** interconnected with the CPUs by a CPU/memory-subsystem bus **110** or multiple busses, a first bridge **112** that interconnects the CPU/memory-subsystem bus **110** with additional busses **114** and **116**, or other types of high-speed interconnection media, including multiple, high-speed serial interconnects. These busses or serial interconnections, in turn, connect the CPUs and memory with specialized processors, such as a graphics processor **118**, and with one or more additional bridges **120**, which are interconnected with high-speed serial links or with multiple controllers **122-127**, such as controller **127**, that provide access to various different types of mass-storage devices **128**, electronic displays, input devices, and other such components, subcomponents, and computational resources. It should be noted that computer-readable data-storage devices include optical and electromagnetic disks, electronic memories, and other physical data-storage devices. Those familiar with modern science and technology appreciate that electromagnetic radiation and propagating signals do not store data for subsequent retrieval, and can transiently "store" only a byte or less of information per mile, far less information than needed to encode even the simplest of routines.

FIG. **2** illustrates generalized hardware and software components of a general-purpose computer system, such as a general-purpose computer system having an architecture similar to that shown in FIG. **1**. The computer system **200** is often considered to include three fundamental layers: (1) a hardware layer or level **202**; (2) an operating-system layer or level **204**; and (3) an application-program layer or level **206**. The hardware layer **202** includes one or more processors **208**, system memory **210**, various different types of input-output ("I/O") devices **210** and **212**, and mass-storage devices **214**. Of course, the hardware level also includes many other components, including power supplies, internal communications links and busses, specialized integrated circuits, many different types of processor-controlled or microprocessor-controlled peripheral devices and controllers, and many other components. The operating system **204** interfaces to the hardware level **202** through a low-level operating system and hardware interface **216** generally comprising a set of non-privileged computer instructions **218**, a set of privileged computer instructions **220**, a set of non-privileged registers and memory addresses **222**, and a set of privileged registers and memory addresses **224**. In general, the operating system exposes non-privileged instructions, non-privileged registers, and non-privileged memory addresses **226** and a system-call interface **228** as an operating-system interface **230** to application programs **232-236** that execute within an execution environment provided to the application programs by the operating system. The operating system, alone, accesses the privileged instructions, privileged registers, and privileged memory addresses. By reserving access to privileged instructions, privileged registers, and privileged memory addresses, the operating system can ensure that application programs and other higher-level computational entities cannot interfere with one another's execution and cannot change the overall state of the computer system in ways that could deleteriously impact system operation. The operating system includes many internal components and modules, including a scheduler **242**, memory management **244**, a file system **246**, device drivers **248**, and many other components and modules. To a certain degree, modern operating systems provide numerous levels of abstraction above the hardware level, including virtual memory, which provides to each application program and other computational entities a separate, large, linear memory-address space that is mapped by the operating system to various electronic memories and mass-storage devices. The scheduler orchestrates interleaved execution of various different application programs and higher-level computational entities, providing to each application program a virtual, stand-alone system devoted entirely to the application program. From the application program's standpoint, the application program executes continuously without concern for the need to share processor resources and other system resources with other application programs and higher-level computational entities. The device drivers abstract details of hardware-component operation, allowing application programs to employ the system-call interface for transmitting and receiving data to and from communications networks, mass-storage devices, and other I/O devices and subsystems. The file system **246** facilitates abstraction of mass-storage-device and memory resources as a high-level, easy-to-access, file-system interface.

FIG. **3** illustrates a type of virtual machine and virtual-machine execution environment, using the same illustration conventions as used in FIG. **2**. FIG. **3** shows a first type of virtualization. The computer system **300** in FIG. **3** includes the same hardware layer **302** as the hardware layer **202** shown in FIG. **2**. However, rather than providing an operating system layer directly above the hardware layer, as in FIG. **2**, the virtualized computing environment illustrated in FIG. **3** features a virtualization layer **304** that interfaces through a virtualization-layer/hardware-layer interface **306**, equivalent to interface **216** in FIG. **2**, to the hardware. The virtualization layer provides a hardware-like interface **308** to a number of virtual machines, such as virtual machine **310**, executing above the virtualization layer in a virtual-machine layer **212**. Each virtual machine includes one or more application programs or other higher-level computational entities packaged together with an operating system, referred to as a "guest operating system," such as application **314** and guest operating system **316** packaged together within virtual machine **310**. Each virtual machine is thus equivalent to the operating-system layer **204** and application-program layer **206** in the general-purpose computer system shown in FIG. **2**. Each guest operating system within a virtual machine interfaces to the virtualization-layer interface **308** rather than to the actual hardware interface **306**. The virtualization layer partitions hardware resources into abstract virtual-hardware layers to which each guest operating system within a virtual machine interfaces. The guest operating systems within the virtual machines, in general, are unaware of the virtualization layer and operate as if they were directly accessing a true hardware interface. The virtualization layer ensures that each of the virtual machines currently executing within the virtual environment receive a fair allocation of underlying hardware resources and that all virtual machines receive sufficient resources to progress in

execution. The virtualization-layer interface **308** may differ for different guest operating systems. For example, the virtualization layer is generally able to provide virtual hardware interfaces for a variety of different types of computer hardware. This allows, as one example, a virtual machine that includes a guest operating system designed for a particular computer architecture to run on hardware of a different architecture. The number of virtual machines need not be equal to the number of physical processors or even a multiple of the number of processors.

The virtualization layer includes a virtual-machine-monitor module **318** ("VMM") that virtualizes physical processors in the hardware layer to create virtual processors on which each of the virtual machines executes. For execution efficiency, the virtualization layer attempts to allow virtual machines to directly execute non-privileged instructions and to directly access non-privileged registers and memory. However, when the guest operating system within a virtual machine accesses virtual privileged instructions, virtual privileged registers, and virtual privileged memory through the virtualization-layer interface **308**, the accesses result in execution of virtualization-layer code to simulate or emulate the privileged resources. The virtualization layer additionally includes a kernel module **320** that manages memory, communications, and data-storage machine resources on behalf of executing virtual machines ("VM kernel"). The VM kernel, for example, maintains shadow page tables on each virtual machine so that hardware-level virtual-memory facilities can be used to process memory accesses. The VM kernel additionally includes routines that implement virtual communications and data-storage devices as well as device drivers that directly control the operation of underlying hardware communications and data-storage devices. Similarly, the VM kernel virtualizes various other types of I/O devices, including keyboards, optical-disk drives, and other such devices. The virtualization layer essentially schedules execution of virtual machines much like an operating system schedules execution of application programs, so that the virtual machines each execute within a complete and fully functional virtual hardware layer.

Digital Images and Digital-Image-Comparison Operations

FIG. **4** illustrates two different types of digital images. A two-dimensional digital image **402** is a rectilinear grid of pixels, with each pixel identified by the grid-cell coordinates of the pixel according to a two-dimensional Cartesian coordinate system **404**. Each pixel, such as pixel **406**, includes an intensity value i **408**. In the current discussion, digital images are considered to have grayscale intensities, where i is one of a number of successive integer intensity values ranging from 0 to maxI. For example, maxI may equal 255, in which case each pixel intensity is encoded as a byte. Alternatively, each pixel intensity may be encoded as a two-byte word, in which case maxI is 65,535. Each pixel of an RGB-encoded color image may include three different intensity values for the three color channels red, green, and blue or may include another type of encoding according to another of various other color models. A three-dimensional digital image **410** is a volume of voxels, such as voxel **412**, the positions of which are generally described by a three-dimensional Cartesian coordinate system **414**. The currently disclosed methods and systems for image normalization are applicable both to two-dimensional and to three-dimensional digital images.

FIGS. **5**A-B illustrate digital-image comparison. In FIG. **5**A, a first digital image **502** and a second digital image **504** are acquired by digital-image-capture devices at two different points in time. In this example, as in all the remaining examples provided below, pixels are shown with exaggerated dimensions relative to the image size, for clarity of illustration. In a typical digital image, there may be several hundred or more pixels per centimeter in the x and y directions of a two-dimensional digital image or tens to a hundreds of voxels per centimeter in the x, y, and z directions of a three-dimensional digital image. Pixel sizes often depend on the medium in which pixels are displayed and may differ dramatically among printed images and images rendered for display on LCD display devices.

Both the first image **502** and the second image **504** in FIG. **5**A show a cruciform imaged object **506** with relatively low-intensity pixels on a high-intensity background **508**. In one convention, small-magnitude intensity values correspond to dark or black pixels while high-magnitude intensity values correspond to light or white pixels. In the example shown in FIG. **5**A, it is obvious that the cruciform object is larger in the second image **504** than in the first image **502**. However, in many real-world imaging examples, the differences between the contents of two images are not apparent to a human viewer by visual inspection. Instead, many of the most interesting differences may be quite subtle.

In order to automatically process the pair of images shown in FIG. **5**A to determine the differences between the two images, the pixel intensities of the corresponding pixels in the two images may be subtracted, as shown by the digital-image-subtraction operation **510** in FIG. **5**B, to produce a difference image **512**. The subtraction operation involves, for a given pair of corresponding pixels **514** and **516**, generating a single difference pixel **518** containing the difference of the intensities in the original pixel pair **514** and **516** that is placed into the same position in the difference image **512** as the positions of the pixel pair in the original images **502** and **504**. The computed differences are often resealed to fall within the intensity range [0, maxI]. In this example case, the difference image **512** displays those pixels **522** that have different intensity values in the original digital images **502** and **504** and those differences accurately reflect a cruciform border region that represents growth of the cruciform object.

While straight subtraction of digital images is one method for creating a difference image that highlights differences between two original images, there are many other techniques for generating difference images that use different or additional operations on the intensity values of the two original images. Nonetheless, all of the various different types of comparison operations between digital images seek to highlight meaningful differences between the two images. Meaningful differences are generally differences in image intensities that reflect physical differences in the imaged objects and environments, such as change of tissue type in medical images or the sudden appearance of an object in the imaged environment in a surveillance-video frame. Automated comparison operations are used to detect and display subtle differences in images that would not be apparent to human viewers and to automate the process of identifying even differences in image sequences that would be apparent during visual inspection, were there time for visual inspection, such as in surveillance videos, or both.

FIGS. **6**A-D illustrate the effect of noise on the digital-image-comparison process discussed above with reference to FIGS. **5**A-B. FIGS. **6**A-D use common illustration conventions subsequently used for FIGS. **7**A-**9**B. Each digital

image is shown as a rectilinear grid of pixels with single-digit intensity values. Blank pixels are assumed to have the intensity value 0. FIG. **6**A shows a pair of images **602** and **604** similar to images **502** and **504** in FIG. **5**A. In this example, the imaged cruciform object **606** has relatively high intensity values while the background pixels have relatively low intensity values. Rendered as positive images, the cruciform object would appear lightly colored or white on a dark background, but, for clarity of illustration, negative or inverse renderings of the images are shown in FIG. **6**A. In addition to relatively high-intensity pixels that comprise the cruciform object **606**, each image contains low-intensity values corresponding to noise. For example, pixel **608** in the second image **604** has an intensity value of 2 while the pixel at the same location in the first image **602** has an intensity value 0. In many cases, noise is a stochastic phenomena and produces different patterns of anomalous pixels in each different image. Furthermore, the intensities of the pixels within the imaged cruciform object **606** in each image are non-uniform, the non-uniformity a product of both noise and perhaps image-acquisition-device-characteristic differences. As a result, when a difference image **610**, shown in FIG. **6**B, is produced by the comparison method **510** discussed above with reference to FIG. **5**B, the difference image is visually cluttered. In FIG. **6**B, the non-0 valued pixels are shown darkened while the 0-valued pixels are shown unshaded, an inverted or negative image of the positive difference image produced by the difference operation. This cluttered difference image does include the same difference pixels **522** produced in the example shown in FIG. **5**B, but also includes non-0 valued pixels, such as pixel **612** at the position of pixel **608** in the second image shown in FIG. **6**A, resulting from noise. Noise can therefore clutter and mask the differences of interest or meaning in a difference image produced by a comparison operation. A thresholding operation may be used to attempt to eliminate noise pixels from a difference image. As shown in FIG. **6**C, only difference pixels with unrescaled absolute-value intensities greater than 1 are shaded in the thresholded difference image **620**. By removing difference pixels with intensities 1 and −1, much of the clutter in the difference image **610** shown in FIG. **6**B has been removed. An even better difference image **622** is shown in FIG. **6**D, produced by showing only those difference pixels with at least absolute-value difference intensity 2. When the intensity differences of the pairs of pixels in the original image of interest are large compared to the intensity differences of noise pixels and background pixels, thresholding can remove much of the unwanted noise signal to produce a clear, meaningful difference image.

However, when the intensity-valued differences of the pixel pairs of interest in the original images have magnitudes on the order of the magnitudes of noise differences, thresholding may not be effective. FIGS. **7**A-D show similar examples to those shown in FIG. **6**A-D, but with the pixels corresponding to the imaged cruciform object having relatively low intensity values compared to the intensities of the pixels corresponding to the imaged cruciform object in FIG. **6**A. The unthresholded difference image **710** in FIG. **7**B produced by the comparison operation **510** discussed above with reference to FIG. **5**B applied to original images **702** and **704** shown in FIG. **7**A is more visually cluttered than difference image **610** in FIG. **6**B. A thresholded version of the difference image **712** in FIG. **7**C, with difference pixels having unrescaled absolute-value intensities less than 2 not displayed, has less clutter but does not reveal the cruciform-outline pattern of the difference pixels of interest, originally shown in the difference image **512** in FIG. **5**B. A second thresholded difference image **714** in which only difference pixels with unrescaled absolute-value intensities of 2 or greater are displayed, provides relatively little information. Thus, as shown in the example of FIGS. **7**A-D, when the intensity differences between two images are subtle, the differences may be entirely masked by the presence of noise in the two images.

FIGS. **8**A-D show a different example of image comparison using the same illustration conventions used in FIGS. **6**A-D and FIGS. **7**A-D. The original images **802** and **804** shown in FIG. **8**A both contain the imaged cruciform object **806**. However, original image **802** additionally includes a systematic variation in image intensity, with the portion of the image **808** below a diagonal line from the top left-hand pixel **810** to the bottom right-hand pixel **812** having higher intensities than the portion of the image **814** above the diagonal line. Similarly, the second original image **804** has a lower, roughly triangular region **816** with generally higher intensities than the upper portion **818** of the image. Such systematic intensity differences and patterns may be caused by shading or illumination differences in the environment being imaged or by systematic variations in recorded pixel intensities during image capture within the image-capture device. FIG. **8**B shows the unthresholded difference image **820** in similar fashion to the unthresholded difference images shown in FIGS. **6**B and **7**B. Because of the systematic pixel-intensity differences within each of the original images, the unthresholded difference **820** appears to have more difference pixels than non-difference pixels and is dominated by differences generated from the systematic intensity variation within the two original images rather than from the increase in size of the cruciform object **806**. When the difference image is thresholded to remove difference pixels with unrescaled absolute-value intensities less than 2, the thresholded difference image **822**, shown in FIG. **8**C, is much less cluttered, but also fails to clearly show the differences of interest that represent an increase in size of the cruciform object. When the difference image is thresholded to remove difference pixels with unrescaled absolute-value intensities of 1 and 2, to produce the difference image **824** shown in FIG. **8**D, there is almost no difference information of interest remaining in the thresholded difference image. Thus, systematic intensity variation within the original images may completely frustrate an attempt to extract meaningful difference information from the two images.

FIGS. **9**A-B illustrate a typical result obtained by digital-image comparison. In the examples of FIGS. **5**A-**8**D, the difference pixels of interest were readily apparently from visual inspection of the example original images shown in FIGS. **5**A, **6**A, **7**A, and **8**A. By contrast, in many real-world image-analysis problems, the differences may not be readily apparent during visual inspection of the original images. For example, FIG. **9**A shows original images **902** and **904** in which all of the pixels have intermediate or high intensities. Neither the imaged cruciform object nor the increase in size of the imaged cruciform object is readily apparent from these displayed intensities. However, when the two images are differenced to produce difference image **906** shown in FIG. **9**B, the pattern of difference pixels nicely shows the growth of size of the imaged cruciform object **908** along with several noise-induced differences **910** and **912**. Thus, in many cases in which computational digital-image comparison is used, the comparison may reveal meaningful patterns that are not apparent to human viewers. Such subtle patterns of intensity difference are often completely obscured by the presence of noise or systematic intensity variations, as discussed above with reference to FIGS. **7**A-D and **8**A-D. It

is to facilitate comparison of digital images that the normalization methods and systems disclosed in the current document were developed.

Implementations of the Currently Disclosed Methods and Systems

The current document is directed to normalization methods and systems that reduce or eliminate certain types of intensity variations among digital images prior to applying comparison operations to the digital images in order to detect meaningful differences in intensity between the digital images. The currently disclosed methods and systems seek to remove systematic intensity variation without exacerbating noise-induced intensity variations between images, which can lead to obscuring or eliminating the meaningful differences between digital images sought by digital-image comparison. The currently disclosed normalization methods and systems attempt to normalize digital images largely based on the intensity values of pixels or voxels within the images themselves rather than by using extrinsic information, and thus are useful in a wide variety of automated digital-image-processing and digital-image-analysis systems, including systems that identify and highlight meaningful differences in time sequences of medical images, systems that identify the time points of anomalies and events within long sequences of video frames, and systems that analyze images obtained by remote sensing.

FIGS. **10**A-B illustrate underlying concepts of the currently disclosed normalization methods and systems. As shown in FIG. **10**A, the currently disclosed normalization methods seek to generate a mapping model, such as a mapping function **1002** for two-dimensional images or a mapping function **1004** for three-dimensional images that, given the position and intensity of a pixel **1006** in a first image **1008**, generate a corresponding intensity **1010** for an equivalently located pixel in a second image **1012**. By applying the mapping model to each pixel in the first image, a normalized image is produced that can be compared to the second image by using any of many different types of comparison operations to reveal intensity differences of interest between the two images. Of course, the mapping model can also be applied in an opposite sense to the second image to normalize the intensities in the second image to those of the first image.

FIG. **10**B illustrates, for the two-dimensional-image case, a range of different types of analytical functions, that may be contemplated as mapping models for intensity normalization. A first class of mapping functions **1020** generates corresponding intensities j for intensities i without regard for the position of the pixel with that intensity in the first image. In other words, in this class of mapping functions, only the intensity i is provided as an argument. The mapping functions may be any of a variety of different types of expressions, including linear mapping functions **1021-1022** and quadratic mapping function **1024**. Note that, in FIG. **10**B, capital letters represent constant parameters in the example mapping functions.

In a second class of mapping functions **1030**, each mapping function takes both the intensity as well as the position of a pixel in the first image as arguments and generates a corresponding intensity for a pixel at that same position in the second image. However, as shown by example mapping function **1032**, the position arguments are used only to determine to which of several different subregions, or domains, the image any particular mapping function applies. In model **1032**, when the pixel is in an upper left triangular domain of the image, a first linear function **1033** is used while, when the input pixel is in a lower triangular region or domain of the image, a second linear function **1034** is used. Thus, the second class of mapping functions essentially divide or partition an image into multiple domains, for each of which a domain-specific mapping function is generated for normalization of the intensities within an image.

A third class of mapping functions **1040** specifically maps individual pixel intensities to corresponding individual pixel intensities. For these mapping functions, both the position and the intensity of a pixel are variables within the mapping function. As shown in the downward-pointing vertical arrow **1046** in FIG. **10**B, the specificity of the mapping functions significantly increase over the classes **1020**, **1030**, and **1040**. Were model functions of the final class **1040** obtainable, and were they accurate, such mapping functions may be reasonably expected to provide the most precise and accurate intensity normalization. However, the problem with this level of specificity is that there is insufficient data, when only the intensity values within the two images are considered, to try to determine parameter values for such functions in a single pass at parameter optimization. As the model functions become more specific, the danger of the functions being dominated by stochastic noise, rather than real intensity-difference variations between the images, greatly increases, as a result of which a normalization process that attempted to employ such mapping functions in an initial single-pass optimization would likely mask meaningful differences obtained by subsequent image comparison and would instead generate a large amount of unwanted and meaningless noise-induced differences. Thus, as indicated by arrow **1048** in FIG. **10**B, the currently disclosed normalization methods and systems initially use either models of the first class **1020** or the second class **1030**, with the additional caveat that the domains specified in the second class of mapping functions must be sufficiently large to provide a sound statistical basis for determining mapping-function parameters.

FIG. **11** provides a control-flow diagram for one implementation of the currently disclosed methods and systems. In step **1102**, the normalization procedure receives references to two images, refI and refJ, as well as image metadata that describes the types of images, their sizes, and other image parameters. In step **1104**, the routine "normalize" calls a routine "preprocess images" to prepare the images for normalization. The routine "preprocess images" registers the images, so that each positionally equivalent pair of pixels selected from the two images correspond to the same point within the imaged environment. Registration may involve rotation and translation of the two images, as well as cropping, and may also involve more complex operations when extrinsic information about the subject matter to which the content of the images pertains is available. Preprocessing may also identify domains with different intensity variations within the images and may compute minimum and maximum intensities to allow for selection of appropriate data structures used in the normalization process. In step **1106**, a set of possible mapping functions, or models, for normalization is selected. In many cases, normalization may use only a single intensity-mapping function when either multi-domain imaging is not supported or when multiple domains cannot be identified. However, in the general case, the normalization process may try numerous different mapping functions to determine which mapping function produces the best normalization. In that case, in step **1108** and the for-loop of steps **1110-1114**, normalization is attempted for each mapping function and the best mapping function is selected.

In step **1111**, the routine "fit model" is called to fit model parameters of a currently considered model, or mapping function, to the data, as discussed below, using the fitness function fitness 1, also discussed below. Note that the fitness function is passed to the routine "fit model" as an argument and is referred to internally within the routine "fit model" by the internal argument name "fitness." The best mapping function is then used to generate, as discussed below with reference to FIGS. **14**A-B, an image-adjustment model, in step **1118**, and the image-adjustment model is then applied, in step **1120**, to the image referenced by refI to normalize image i with respect to image j in preparation for an image-comparison operation.

The final three steps in FIG. **11**, shown within dashed rectangle **1122**, are applied, in certain implementations, to address the problem of inhomogeneities. Inhomogeneities of various different types are spatial artifacts in images, including, for example, spatial artifacts in medical magnetic-resonance images ("MRIs") as well as illumination changes in scenes imaged by surveillance cameras. Inhomogeneities may arise from characteristics of image-acquisition devices, including systematic spatial response differentials, from characteristics of the objects or scenes being imaged, including varying illumination intensities, varying illumination spectral characteristics, and temporal changes in the absorbance and reflectivity of imaged surfaces, and other such changes. These artifacts can be relatively continuous, large-scale intensity fluctuations across an image. Thus, amelioration of inhomogeneities involves an intensity model, such as mapping functions **1040** discussed above with reference to FIG. **10**B, that take into consideration the spatial locations of pixels within an image. In step **1124**, a spatial mapping function is selected for parameter fitting, in step **1126**, via a call to the above discussed function "fit model," called previously in step **1111**. In this call to the function "fit model," a different fitness function fitness 2, discussed below, is passed to the function "fit model." The model is then used, in step **1128**, to refine the normalization of the image referenced by refI. In certain implementations, the series of steps **1106** through **1120** may be alternated with steps **1124** through **1128** in multiple iterations to carry out multiple passes at normalization and refinement, with the iterations continuing until a convergence criterion is met or until a fixed number of iterations have been executed. In alternative implementations, amelioration of inhomogeneities may precede normalization, in one pass, or in each of multiple iterations. In yet additional implementations, various characteristics of the input images determine whether or not amelioration of inhomogeneities is attempted and, if attempted, whether or not amelioration of inhomogeneities precedes or follows normalization.

FIGS. **12**A-G illustrate tabulation of pixel-intensity mappings and generation of a difference metric value for a particular mapping model. FIGS. **12**A-E all use the same illustration conventions, next discussed with reference to FIG. **12**A. The examples are based on two-dimensional images, but the illustrated methods are equally applicable to three-dimensional images. In each figure, a first example image **1202** and a second example image **1204** are shown, similar to pairs of images shown in FIGS. **5**A, **6**A, **7**A, **8**A, and **9**A. Below the two images, a table **1206** is shown in each figure. The table represents a mapping of intensity values that occur in the first image **1202**, referred to as image "A," to intensity values in the second image **1204**, referred to as image "B." The population of this data table is illustrated in FIGS. **12**B-E. The illustrated mapping is a mapping for non-0 intensities in image A to corresponding intensities in image B, in the currently discussed example. In certain medical images, for example, areas or volumes of the image may be omitted from normalization, such as areas or volumes corresponding to air, or non-tissue volumes. These omitted areas or volumes may, of course, have non-zero intensities.

FIG. **12**B shows a first step in the population of data table **1206**. A pair of equivalently located pixels **1208** and **1209** are indicated by arrows **1210** and **1211** in images A and B. The intensity value 3 of pixel **1210** in image A is mapped to intensity value 9 of pixel **1211** in image B. Therefore, the cell **1212** in table **1206** corresponding to mapping of intensity value 3 to intensity value 9 from image A to image B is incremented to 1. FIG. **12**C shows consideration of a next pair of pixels represented by arrows **1214** and **1216**. In this case, the intensity value 3 in image A is mapped to the intensity value 7 in image B. Thus, the cell **1218** corresponding to a mapping of intensity value 3 to intensity value 7 is incremented to the value 1. FIG. **12**D shows a third step in table population. Arrows **1220** and **1222** indicate a third pair of pixels. In this case, intensity value 4 is mapped to intensity value 9, as a result of which cell **1224** in table **1206** is incremented to the value 1. This process proceeds through all of the shaded pixel pairs in images A and B to populate table **1206**, as shown in FIG. **12**E.

As shown in FIG. **12**F, table **1206**, produced by considering a sequence of positionally equivalent pixels in images A and B, as discussed above with reference to FIGS. **12**A-E, can be alternatively considered to be a set of histograms **1230-1234**, with each row in table **1206** providing the data for a single, corresponding histogram. Histogram **1230** shows the distribution of intensity values in image B for pixels in image B positionally corresponding to pixels in image A with intensity value 1. Similarly, histogram **1231** shows the distribution of intensities of pixels in image B positionally corresponding to pixels in image A with intensity value 2.

The currently disclosed methods and systems seek to use the tabulated intensity-mapping data, such as the data tabulated in example **1206** or, equivalently, tabulated in histograms **1230-1234** shown in FIG. **12**F, to generate parameters for a mapping function. FIG. **12**G shows a plot **1240** of the mapping function j=mi+b, where the values for the parameters m and b have been determined to be 2.2 and 1, respectively. The difference metric is used to evaluate how closely the mapping function fits the tabulated data. Computation of the difference metric is illustrated in the lower portion of FIG. **12**G. First, a table **1242** of differences is computed. Each row in this table corresponds to the mapping from a particular intensity value in image A to another intensity value in image B, and also corresponds to a particular bar within one of the histograms. The elements within a row, or the columns of the table, correspond to: (1) the intensity value in image A **1244**; (2) a corresponding intensity value computed using the mapping function **1245**; (3) the intensity value observed in image B **1246**; and (4) the absolute value of the difference between the observed intensity value and the intensity value computed by the mapping function **1247**. Thus, the first row **1248** in table **1242** corresponds to the first bar **1250** in histogram **1230**. This bar represents the number of pixels with intensity value 1 in image A whose positionally corresponding pixel in image B has the intensity value 3. According to the mapping function, the intensity value 1 (**1252** in FIG. **12**G) in image A is mapped to the intensity value 3.2 (**1254** in FIG. **12**G) in image B. The absolute value of the difference between the computed value 3.2 and the observed value 3 is 0.2.

In the central portion of FIG. **12**G, an example calculation of the difference metric D is shown **1256**. This difference metric is computed as a sum of terms, each term corresponding to a row in table **1242**. Each computed absolute-value difference in the final column of table **1242** is multiplied by the height of the histogram bar corresponding to the row in FIG. **1242** that contains the absolute-value difference to produce a numeric sum of terms **1258** that represents the sum of the absolute values of the differences between the observed pixel values in image B and the pixel values computed by the mapping function based on corresponding intensities in image A. The computation of the difference metric D is alternatively illustrated by two equations **1260** and **1262**. The first equation is equivalent to the computation shown in the example **1256**. The outer summation is over the distinct intensity values observed in image A. The inner summation is over the distinct intensity values observed in image B for a given intensity value observed in image A. The terms of the expression are the product of the number of pixels with a particular intensity value in image B times the absolute value of the difference between that intensity value and the computed intensity value. Alternatively, as shown by equation **1262**, the difference metric is the sum, over all corresponding pairs of pixels in images A and B, of the absolute value of the difference between the observed intensity value of each pixel in image B and the value computed by the mapping function for the intensity value of the corresponding pixel in image A.

FIGS. **13**A-F illustrate aspects of a genetic mapping-function-parameter-fitting method that is used to optimize parameter values for a mapping function that maps intensities from a first image to a second image within at least a pair of image domains. The genetic parameter-fitting method is used iteratively to produce successive generations of individuals, each corresponding to a set of mapping-function parameter values. The method simulates evolution of individuals to produce a most fit individual with the best model parameter values.

FIG. **13**A illustrates an individual. The individual **1302** can be thought of as a data structure that includes a set of mapping-function parameter values **1304**, a fitness value **1305**, and a timestamp **1306**. The fitness value is computed from the difference metric, computation of which is discussed above with reference to FIG. **12**G. The timestamp is, in the described implementation, an indication of the number of generations over which the particular individual has survived. Computation of the fitness value is shown by equation **1308** in FIG. **13**A. The fitness value is 1—the ratio of the difference metric for the set of parameter values contained in the individual divided by the maximum observed difference metric. Fitness values range from 0 to 1 **1310**, with 1 representing a maximally fit, or perfectly fit, individual. In alternative implementations, different computed fitness values with difference ranges and senses may be used. For example, the difference metric can be used as the fitness value, in which case a value of 0 would be best and increasing positive values would represent decreasing fitness. The parameter values β_1, β_2, . . . β_n are the constant parameter values for a mapping function. As discussed above, a linear mapping function may have two parameter values, in which case an individual would contain the two parameter values β_1 and β_2. There is a set of lowest-possible- and highest-possible values for each parameter value, so that the parameter values can be assumed to fall within the ranges specified by the lowest and highest values **1312**. In certain implementations, these ranges are empirically estimated. Thus, for example, the value of parameter β_1 **1314** is assumed to fall within the range $[B_{1,l}, B_{1,h}]$ **1315**. As discussed below with reference to FIG. **15**K, a modified fitness value is used for fitting spatial mapping functions to data.

FIG. **13**B illustrates construction of a first generation of individuals, generation 0. In this construction, used in certain implementations, a number q of different, evenly spaced, candidate parameter values within the range of values for each parameter is computed, as represented by the matrix-like set of nodes **1316** in FIG. **13**B. These candidate parameter values can be used to generate $(q+2)^n$ different sets of candidate parameters β_s. The value q is selected so that the number of candidate parameter-value sets β_s is approximately equal to, but equal to or greater than, the number of individuals used in the genetic optimization method. A unique set of candidate parameter values β_s is assigned to each individual, such as the candidate set of parameter values β_s^1 **1317** assigned to individual **1318**. The timestamp for each generation-0 individual is set to 0. Finally, a fitness value is computed for each candidate set of parameter values/individual and included in the individual data structure. Generation 0 is shown in FIG. **13**B as the individuals in the row of individuals **1319**.

FIG. **13**C illustrates production of a next generation n+1 of individuals **1320** from a generation n of individuals **1322**. In a first step, a set of combined or pairwise fitness values is computed for the possible combinations of two individuals selected from generation n **1324**. Computation of the pairwise fitness values may be simply addition of the fitness values of each individual in the pair of individuals, but may also be represented by a more complex function in alternative implementations. The set of pairwise fitness values is sorted **1325** in descending magnitude order. Then, a child individual is produced from the parent individuals in generation n corresponding to pairwise fitness values selected from the set of pairwise fitness values **1326** in magnitude-descending order. For example, a first child individual **1328** is obtained by breeding parent individuals **1330** and **1331** corresponding to the pairwise fitness value **1332**. A number of child individuals is produced in this manner equal to 90 percent of the total number of individuals in a generation. Then, the 10% most fit individuals from generation n are selected as the remaining 10% **1334** of the individuals in generation n+1. Thus, 90% of the individuals in a subsequent generation n+1 are children bred from the most fit pairs of individuals in generation n and 10% of the individuals in a subsequent generation n+1 are replicates of the 10% most fit individuals of generation n. Of course, the 90% death ratio and 10% survival ratios for successive generations are only one possible pair of ratios. In alternative implementations, different death and survival ratios may be used and, in certain implementations, the ratios may vary over parameter fitting through successive generations.

FIG. **13**D illustrates how two fit parents from generation n are bred to produce a child individual, such as the breeding of individuals **1330** and **1331** from generation n, in FIG. **13**C, to produce child **1328**. In FIG. **13**D, the two parents **1340** and **1341** are shown at the top of the figure. Pairs of corresponding parameter values of these two parents are sorted into pairs of parameter values that includes a first lower-valued parameter and a second higher-valued parameter **1342**. These sorted pairs of parameter values are then used to produce parameter-value ranges **1343**. In most cases, the range R_1-R_2 is equal to the range represented by ordered parameters β_1-β_2. However, when the difference between the highest value and lowest value in the range is less than a threshold value **1344**, the range values are adjusted to span

the minimum threshold range **1346**. This handles a case in which the difference between the highest value and lowest value is sufficiently small that the differences between adjacent parameter values for a parameter would be too small to produce meaningful changes in the overall fitness for the mapping function. Next, as indicated by matrix **1348**, a set of candidate parameter values, evenly spaced within the range for each parameter value, is generated. A number q of candidate values for each parameter value is generated, where q is a parameter of the genetic optimization method. A number q^n parameter combinations, each combination including a candidate value for each of the n model parameters, is selected from this set of candidate parameter values. Then, a corresponding fitness value is generated for each of the q^n combinations, as indicated by columns **1349** and **1350** in FIG. **13**D. The set of candidate parameter values with the highest fitness value is then selected as the set of parameter values for the child **1352**. The corresponding fitness metric is included in the child **1354** along with a new timestamp value of 0.

After producing children and copying fit individuals from a previous generation to produce individuals of the next generation, as discussed above with reference to FIG. **13**C, each of the individuals is mutated. FIG. **13**E illustrates the mutation operation. At the top of FIG. **13**E, a next-generation individual is shown **1360**. Two multipliers are computed for the individual. A first multiplier m_1 reflects the current optimality of the individual. The computed fitness for the individual **1361** is used to determine a range **1362** that is equal to the distance between the current fitness and the best-observed fitness **1363**. The first multiplier m_1 **1364** is computed as the ratio of that range to the difference between the best and worst observed fitnesses multiplied by a weight w_1 **1365**. A second multiplier m_2 is generated from an exponential decay curve **1366**. The current age, in generations of the individual, such as the age 2 (**1367** in FIG. **13**E), is used to compute a corresponding m_2 value **1368**. The more optimal the parameter set of the individual, as reflected by the smallness of the computed range **1362**, the smaller the multiplier m_1 **1364**. The older the individual, the smaller the multiplier m_2. The product of these two multipliers **1370** is used as a multiplier of the total possible range of parameter values **1372** to produce a mutation range **1373** for the parameter. Then, an evenly spaced set of candidate parameter values, shown within the dashed square **1374**, is generated within this range for each model parameter. Thus, the more fit the individual and the older the individual, the smaller the adjustments to the parameter values that are made during the mutation process. A set of combinations of candidate parameter values, one candidate parameter value selected from each row in the matrix **1374**, represents the set of possible parameter-value sets for the mutated individual. The fitness values for each candidate set of parameter values are then computed, as represented by columns **1376** and **1377** in FIG. **13**E, and the candidate set of parameter values corresponding to the highest-computed fitness is used as the set of parameter values for the mutant individual **1378**. The computed fitness value for the set of parameter values is inserted into the individual **1379** but the timestamp remains unchanged **1380**.

FIG. **13**F illustrates completion of construction of a next generation. As shown in FIG. **13**F, mutation **1382** of each individual in the pre-mutation set of individuals produces a complete subsequent generation n+1 **1384**. It should be noted that the currently disclosed genetic mapping-function-parameter-fitting method is fully deterministic, unlike commonly used genetic mapping-function-parameter-fitting methods. The term "deterministic," as used in the preceding sentence, means that the same parameter values would be obtained for a given data set each time the currently disclosed genetic mapping-function-parameter-fitting method is applied to the data set. Many stochastic genetic mapping-function-parameter-fitting methods employ pseudo-random-number generators to select parameter values during breeding and mutation, as a result of which generally different parameters are produced each time the commonly used genetic mapping-function-parameter-fitting methods are applied to a given data set. Determinism is a highly desirable characteristic for image normalization, particularly for medical images. However, stochastic parameter-fitting methods may also be used in alternative implementations. In fact, many other parameter-fitting methods may be used in alternative implementations, including least-squares, Gauss-Newton non-linear least squares, and various optimization methods.

FIGS. **14**A-B illustrate the final intensity-mapping model produced by the currently disclosed methods and system. Recall the data table **1206** in FIGS. **12**A-E. Each row in this data table corresponds to a histogram, as discussed above with reference to FIG. **12**F. As shown in FIG. **14**A, an intensity that occurs as a value of a pixel in the first image **1402** corresponds to a histogram of pixel intensities in the second image. When, as shown in histogram **1404**, there is a single prominent peak **1406** in the histogram, as determined either by the height of the peak or the relative height of the peak with respect to the next-highest peak, the final mapping model simply maps intensity **1402** to the intensity value j_{pk} corresponding to the prominent peak **1408**. Thus, in the prominent-peak case, the mapping function generated by the genetic parameter-fitting method is not used. By contrast, as shown in histogram **1410**, when there is no single prominent peak in the distribution of intensities, the mapping function $f(i)$ is used to generate the intensity value **1412** for normalizing intensity value i in the first image. Thus, final intensity-mapping model is a hybrid model, containing both observed intensity correspondences as well as computed intensity correspondences. A hybrid model can be thought of as a discontinuous model in relation to a model solely based on a mapping function.

The final intensity-mapping model for each image domain is a table of computed mappings, such as table **1420** in FIG. **14**B. An intensity value of a pixel in the image to be normalized is used as an index **1422** in the table **1420** to select a corresponding normalized value **1424** for the normalized image. However, in cases where there are far more possible intensity values than observed intensity values, in which case the table **1420** would be very large and sparse, a tree-like index **1426** can be developed to index a set of compact tables **1428-1430**. An intensity value from the original image is used to traverse the index **1426** to identify the appropriate compact table, and the intensity is then used as an index into that table, following subtraction of the intensity in the first entry of the table from the intensity value, in order to find a corresponding normalized image intensity. Many other types of model data structures are possible.

FIGS. **15**A-K provide control-flow diagrams that illustrate one implementation of the routine "fit model," called in step **1111** of FIG. **11**. The routine "fit model" carries out the parameter-fitting method discussed above with reference to FIGS. **12**A-**13**F. Note that, in certain cases, routines are shown with explicit input parameters, while, in other cases, it is assumed that a called routine can access variables within the scope of the calling routine. In FIG. **15**A, the routine "fit

model" receives references to the two images, a selected mapping function, or model, image metadata, and a reference to a fitness function, in step **1502***a*. In step **1502***b*, the number of m individuals to be used in each generation of the genetic method is determined based on the number of model parameters P. In step **1502***c*, the minimum and maximum intensity values in image I is determined from the metadata. In step **1502***d*, two arrays of individuals, referenced by reference variables genA and genB, are allocated to each contain m elements or individuals, each with storage for P parameter values. In step **1502***e*, a number of variables are initialized, including the variables bestF, worstF, bestβ, noChange, and maxNoChange. In step **1502***f*, the variable numIterations is set to 0 and the variable maxIter is set to the number of generations to produce during the genetic optimization method. In step **1502***g*, the routine "generation 0" is called to generate the first generation of individuals, as discussed above with reference to FIG. **13**B. Then, in the for-loop of steps **1502***h*-**1502***k*, the routine "next generation" is iteratively called, in step **1502***i*, until either no change in fitness has been observed for some number of preceding iterations, as represented by the value in the variable noChange, or until the maximum number of iterations maxIter has been carried out, as determined in step **1502***j*. In step **15021**, the parameters of the individual that produced the best fitness value are selected as the model parameters and are returned, in step **1502***m* along with the fitness value for those parameters.

FIG. **15**B provides a control-flow diagram for the routine "generation 0," called in step **1502***g* of FIG. **15**A. In step **1504***a*, the reference curGen is set to the value of the reference genA and the reference nextGen is set to the value of reference genB. In the for-loop of steps **1504***b*-**1504***d*, a set of candidate model parameter values is generated, as shown in matrix **1316** of FIG. **13**B. Then, in the for-loop of steps **1504***e*-**1504***j*, each of the individuals in generation 0 is initialized. A set of unique parameter values is selected from the candidate parameter values for the individual in step **1504***f*. The timestamp for the individual is set to 0 in step **1504***g*. In step **1504***h*, the routine referenced by the parameter fitness supplied to routine "fit model" is called in order to compute the metric value D for the selected set of parameter values, as discussed above with reference to FIG. **12**G. Initially, the metric value is inserted as the fitness value into the individual in step **1504***i*. In steps **1504***k* and **1504***l*, the variables bestF and worstF are initialized with a first fitness value for the first generation-0 individual, and then, in step **1504***m*, the routine "setFs" is called to transform the metric values in the individuals of generation 0 to fitness values, according to equation **1308** in FIG. **13**A while keeping track of the best and worst observed fitness values.

FIG. **15**C provides a control-flow diagram for the routine "fitness 1," one of the fitness routines called in step **1504***h* of FIG. **15**B. Again note that, in step **1504***h* of FIG. **15**B, the routine "fitness 1" is called via the internal argument name "fitness." This fitness function is used for normalization, as discussed above with reference to FIG. **11**. In step **1506***a*, the routine "fitness 1" receives a set of model parameters β_s and a reference to the variable maxD which contains the maximum metric value so far observed. In step **1506***b*, local variable D is set to 0. In the outer loop of steps **1506***c*-**1506***h*, each image domain is considered. In the inner loop of steps **1506***d*-**1506***g*, the difference metric value for the model is computed, as discussed above with reference to FIG. **12**G. When the computed difference metric D is greater than the value in maxD, as determined in step **1506***i*, maxD is set to the value of D in step **1506***j*.

FIG. **15**D provides a control-flow diagram for the routine "setFs," called in step **1504***m* of FIG. **15**B. In the for-loop of steps **1508***a*-**1508***g*, each individual in the array referenced by curGen is considered, and the difference metric stored as the fitness value in the individual is transformed, by equation **1308** in FIG. **13**A, into a fitness value. That is, in step **1504***i* of FIG. **15**B and step **1516***i* of FIG. **15**H, discussed below, a difference-metric value is initially inserted into the field F of each individual, and now, in the routine "setFs," the difference-metric value is changed to a fitness value using equation **1308** in FIG. **13**A. In addition, the computed fitness values are compared with the values stored in bestF and worstF and those values are updated when the currently computed fitness value is better or worse than the fitness values in bestF and worstF, respectively. The parameter set for the best fitness value is maintained in the variable best **13**.

FIG. **15**E provides a control-flow diagram for the routine "next generation," called in step **1502***i* in FIG. **15**A. This routine carries out the production of a next generation of individuals, as discussed above with reference to FIGS. **13**C-**13**F. In step **1510***a*, the variable v is set to 0.9 times the number of individuals m, the variable curBestF is set to the contents of variable bestF, and two arrays of model parameters lowβ_s and highβ_s are both initialized. As discussed above, the number 0.9 is one possible value for the death ratio for individuals in succeeding generation, but other death ratios may be used in alternative implementations. In step **1510***b*, the routine "generate pairwise fitness values" is called to generate the pairwise fitness values (**1324** in FIG. **13**C), as discussed above with reference to FIG. **13**C. In step **1510***c*, the pairwise fitness values, stored in an array pfv along with identifications of the individuals from which they were generated, are sorted, as discussed above with reference to sort operation **1325** in FIG. **13**C. In the for-loop of steps **1510***d*-**1510***h*, the most fit pairs of parents, selected based on the sorted pairwise fitness values in the array pfv, are bred, by a call to the routine "breed" in step **1510***f*, to produce a child individual for the next generation. Breeding is discussed above with reference to FIG. **13**D. In step **1510***i*, the individuals in the array referenced by curGen are sorted by fitness value and, in the for-loop of steps **1510***j*-**1510***n*, the most fit of the previous-generation individuals are transferred to the final 10% of individuals in the next generation, as discussed above with reference to FIG. **13**C. The routine "update," called in step **15101**, is used to update the parameter-value arrays lowβ_s and highβ_s to keep track of the lowest and highest values for each model parameter. In step **1510***o*, the routine "mutate" is called to mutate each individual in the next generation, as discussed above with reference to FIG. **13**F. In step **1510***p*, the reference curGen is set to point to the newly created next generation and the reference nextGen is set to point to the individuals of the previous generation, in preparation for another iteration of generation production. In step **1510***q*, the routine "setFs" is called to transform the difference metric values in the individuals of the next generation to fitness values, as discussed above with reference to FIG. **15**D. When the value stored in the local variable curBestF is less than bestF, indicating that a new best fitness value has been produced during production of the next generation of individuals, the value of the global variable noChange is set to 0 in step **1510***s*. Otherwise, the value in global variable noChange is incremented, in step **1510***t*. As discussed above, when the value stored in global variable noChange reaches a threshold

value, the genetic optimization method is terminated, since at least a very good local optimum for the model parameter values has been obtained.

FIG. **15**F provides a control-flow diagram for the routine "breed," called in step **1510***f* of FIG. **15**E. This routine carries out the generation of a child individual for a subsequent generation from two parent individuals in a current generation, as discussed above with reference to FIG. **13**D. In step **1512***a*, the routine "breed" receives references to the two parent individuals, parent1 and parent2, and the index w of the child individual in the subsequent generation. The variable best is set to the empty set. The variable localMax is set to a large number. In step **1512***b*, ranges of parameter values are determined, as discussed above with reference to tables **1342** and **1343** in FIG. **13**D. In the for-loop of steps **1512***c*-**1512***g*, the fitness of each of the combinations of parameter values selected from evenly spaced candidate parameter values within the ranges of values for each parameter, discussed above with reference to items **1348**-**1350** in FIG. **13**D, is evaluated by a call to the routine "fitness" in step **1512***d*. The most fit set of candidate parameter values is monitored in the for-loop of steps **1512***c*-**1512***g*, with the variables localMax and best set to the fitness value and candidate parameters of the best so-far-observed fitness, in step **1512***f*. In step **1512***h*, following termination of the for-loop of steps **1512***c*-**1512***g*, the child individual, indexed by index w, is updated with the best set of parameters and difference metric value obtained in the for-loop of steps **1512***c*-**1512***g*. The routine "update," called in step **1512***i*, updates the lowβ_s and highβ_s arrays to keep track of the smallest and greatest values for each model parameter.

FIG. **15**G provides a control-flow diagram for the routine "update," called in steps **15101** of FIG. **15**E and **1512***i* in FIG. **15**F. In step **1514***a*, the routine "update" receives a set of candidate parameter values. In the for-loop of steps **1514***b*-**1514***g*, each parameter value in the received set of parameter values is evaluated against the contents of the two arrays lowβ_s and highβ_s to ensure that these arrays contain the lowest and highest value for each model parameter so far observed during the genetic optimization of parameter values.

FIG. **15**H provides a control-flow diagram for the routine "mutate," called in step **1510***o* of FIG. **15**E. The routine "mutate" carries out the mutation of individuals in a next generation, as discussed above with reference to FIGS. **13**E and **13**F. In the for-loop of steps **1516***a*-**1516***h*, each individual in the next generation is considered. In step **1516***b*, local variables best and localMax are initialized, similarly to the initiation of local variables in step **1512***a* of FIG. **15**F of the same name. In step **1516***c*, sets of candidate parameter values are selected from a range of candidate values for each model parameter shown as array **1374** of candidate parameter values in FIG. **13**E. For each combination of a parameter-value set generated from these candidate parameter values, the routine "fitness" is called, in step **1516***e*, to generate a difference metric for the currently considered set of model parameter values. As in the for-loop of steps **1512***c*-**1512***g* in FIG. **15**F, the set of parameters that generates the lowest difference metric is determined in the for-loop of steps **1516***d*-**1516***h* of FIG. **15**H. In step **1516***i*, the currently considered individual is updated with the best determined set of candidate parameters obtained by parameter mutation in steps **1516***b*-**1516***h*.

FIG. **15**I provides a control-flow diagram for the routine "generate model," called in step **1118** of FIG. **11**. In step **1518***a*, one or more data structures for the intensity map discussed above with reference to FIG. **14**B are initialized. In the outer for-loop of steps **1518***b*-**1518***i*, each image domain is considered. In the inner for-loop of steps **1518***c*-**1518***h*, each discrete intensity value observed in the currently considered domain in image I is considered. In step **1518***d*, the distribution of intensities in image J for the currently considered intensity in image I is determined. When this distribution shows a single prominent peak, as determined in step **1518***e*, as discussed with reference to FIG. **14**A, then that peak intensity is entered into the intensity map for the currently considered intensity of the currently considered domain in step **1518***f*. Otherwise, in step **1518***g*, an intensity is generated using the mapping function fit to the data by the genetic optimization method, as discussed above with reference to FIG. **14**A.

FIG. **15**J provides a control-flow diagram for the routine "apply model" called in step **1120** of FIG. **11**. In step **1520***a*, the routine "apply model" receives a reference to image I and a reference to the intensity-map data structure generated in step **1118** of FIG. **11**. In the outer for-loop of steps **1520***b*-**1520***g*, each domain of the image is considered. In the inner for-loop of steps **1520***c*-**1520***f*, the intensity map for the currently considered domain is used to modify the intensity value of each pixel within that domain of image I.

FIG. **15**K provides a control-flow diagram for the routine "fitness 2," another of the fitness routines called in step **1504***h* of FIG. **15**B. As discussed above, with reference to FIG. **11**, this fitness function is called during amelioration of inhomogeneities. In step **1522***a*, the routine "fitness 2" receives a set of model parameters β_s and a reference to the variable maxD, which contains the maximum metric value so far observed. In step **1522***b*, local variable D is set to 0. In the outer for-loop of steps **1522***c*-**15061**, each image domain is considered. In the inner for-loop of steps **1522***d*-**1506***k*, each different intensity value in the currently considered domain of the image referenced by refI is considered. In the innermost for-loop of steps **1522***f*-**1506***j*, each intensity in the image referenced by refJ corresponding to the currently considered intensity in the image referenced by refI is considered. In step **1522***e*, the information referenced by the table **1242** or histograms, discussed above with reference to FIG. **12**G, is collected for the currently considered intensity in the image referenced by refI. In step **1522***g*, the local variable d is set to the metric value computed according to expression **1260** in FIG. **12**G. In step **1522***h*, the metric value stored in local variable d is multiplied by the number of pixels having the currently considered intensity value of the image referenced by refJ raised to the power w, where w is a parameter for the function "fitness 2." This multiplicative factor penalizes non-compact distributions of intensity values in the image referenced by refJ corresponding to an intensity value in the image referenced by refI. Thus, data fitting for spatial mapping functions used to ameliorate inhomogeneities seeks to produce compact distributions of intensity values in the image referenced by refJ corresponding to each intensity value the image referenced by refI. When the computed difference metric D is greater than the value in maxD, as determined in step **1506***i*, maxD is set to the value of D in step **1506***j*. Various other numeric values may be computed to penalize non-compact distributions.

Although the present invention has been described in terms of particular embodiments, it is not intended that the invention be limited to these embodiments. Modifications within the spirit of the invention will be apparent to those skilled in the art. For example, any of many different implementations may be generated by modifying any of

many different implementation and design parameters, including selection of hardware and computing platforms, programming languages, modular organization, control structures, data structures, and other such implementation and design parameters. Although a genetic approach to parameter optimization has proved to be efficient and robust, other types of optimization methods may be employed to generate the currently disclosed intensity map. The currently disclosed normalization method may be applied to color images as well as grayscale images, with each color channel of a color image separately normalized, in one approach, or a single-pass normalization may be used in which the intensity values for the color channels are combined.

It is appreciated that the previous description of the disclosed embodiments is provided to enable any person skilled in the art to make or use the present disclosure. Various modifications to these embodiments will be readily apparent to those skilled in the art, and the generic principles defined herein may be applied to other embodiments without departing from the spirit or scope of the disclosure. Thus, the present disclosure is not intended to be limited to the embodiments shown herein but is to be accorded the widest scope consistent with the principles and novel features disclosed herein.

The invention claimed is:

1. An image-normalization system comprising:

a computer system that includes one or more processors, one or memories, and one or more-storage devices; and

computer instructions, stored in the one or more memories, that, when executed on the one or more processors, control the computer system to

receive two digital images, including a first image and a second image, each having image units that are each associated with a position and an intensity,

identify one or more domains common to both images,

select one or more mapping functions,

determine parameters for the one or more mapping functions using genetic parameter fitting,

select a final mapping function, and

use the final mapping function to adjust intensities in one of the two images.

2. The image-normalization system of claim **1** wherein the two digital images are one of:

a pair of two-dimensional digital images in which domains are areas and units are pixels; and

a pair of three-dimensional digital images in which domains are volumes and units are voxels.

3. The image-normalization system of claim **1**

wherein the first and second images are registered with one another so that each equivalent pair of pixels selected from the two images correspond to the same point within the imaged environment;

wherein, when a first image unit is associated with a position in the first image that is equivalent to a position associated with a second image unit in the second image, the first and second image units are equivalent; and

wherein a mapping function is one of

a parameterized function that returns an intensity value associated with an image unit in one of two digital images based on the intensity value associated with an equivalent image unit in the other of the two digital images,

a parameterized function that returns an intensity value for an image unit in one of two digital images based on the domain of, and intensity value associated with, an equivalent image unit in the other of the two digital images; and

a parameterized function that returns an intensity value for an image unit in one of two digital images based on the intensity value and position of the equivalent image unit in the other of the two digital images.

4. The image-normalization system of claim **3** wherein determining parameters for the one or more mapping functions further comprises:

generating a fitness metric for the mapping function and a current set of mapping-function parameters.

5. The image-normalization system of claim **1** wherein selecting a final mapping function further comprises selecting a mapping function from the one or more selected mapping functions that produces an optimal fitness metric.

6. The image-normalization system of claim **1** further including:

after using the final mapping function to adjust intensities in one of the two images,

selecting a spatial mapping function,

determining parameters for the selected spatial mapping function, and

applying the spatial mapping function to the first image to ameliorate inhomogeneities.

* * * * *